UNIVERSIDADE DE SÃO PAULO
ESCOLA POLITÉCNICA

AHMAD ABUBAKAR

Sizing of battery energy storage systems in isolated photovoltaic plants using predicted solar radiation data

São Paulo
2020

AHMAD ABUBAKAR

Sizing of battery energy storage systems in isolated solar photovoltaic plants using predicted solar radiation data

Versão Corrigida

Dissertação apresentada à Escola Politécnica da Universidade de São Paulo para obtenção do título de Mestre em Ciências.

Área de concentração: Sistema de potência.

Orientador: Carlos Frederico Meschini Almeida.

São Paulo
2020

Este exemplar foi revisado e alterado em relação à versão original, sob responsabilidade única do autor e com anuência de seu orientador.

São Paulo, 12 de August de 2020

Assinatura do autor:

Assinatura do orientador:

Ficha catalográfica

Abubakar, Ahmad

O dimensionamento do sistema de armazenamento de energia da bateria em sistemas fotovoltaicos isoladas usando dados de radiação solar previstos / A. Abubakar – versão corrigida – São Paulo, 2020.

120 p.

Dissertação (Mestrado) – Escola Politécnica da Universidade de São Paulo. Departamento de Engenharia de Energia e Automação Elétricas.

1. Sistema de Armazenamento de Energia por Bateria, 2. Dimensionamento de Bateria, 3. Sistemas Fotovoltaicos, 4. Irradiância I.Universidade de São Paulo. Escola Politécnica. Departamento de Engenharia de Energia e Automação Elétricas II.t

I dedicate this work to everyone who played a part, major or minor, to the progress of this thesis.

ACKNOWLEDGEMENTS

To God Almighty, the sustainer of life, Who kept me alive and made it possible for me to achieve this research.

To Prof. Carlos Frederico Meschini Almeida, for his patience, guidance and immense contributions.

To Prof. Matheus Mingatos Fernandes Gemignani, for his support and knowledge sharing.

To Prof. Marco Roberto Gouvêa and Prof. André Luiz Veiga Gimenes, for their contributions in my qualification exam.

To PTDF – Petroleum Technology Development Fund, for their financial and moral support.

To ENERQ – Centro de Estudos em Regulação e Qualidade de Energia, da Escola Politécnica da USP for the support in realizing this work.

To my parents, Abubakar Musa Omar and Binta Muhammad Nashayya for their ever-presence and support throughout my life.

To my brother, Aminu Abubakar and my sisters, Amina and Aisha Abubakar for believing in me and supporting me.

To Forró and Forrever, for keeping focused throughout the period of this research without which it would have been much harder. “Forró é um movimento que leva muita gente e você pode conferir”

To all those that in one way or the other contributed in the success of this work.

Finally, to myself for believing in me and not giving up on me, through good and bad times and for having the mental strength to see the program through.

“God grant me the serenity to accept the things I cannot change: The courage to change the things I can: And the wisdom to know the difference.”

RESUMO

ABUBAKAR, Ahmad. **O dimensionamento do sistema de armazenamento de energia da bateria em sistemas fotovoltaicos isolados usando dados de radiação solar previstos.** 2020. 120 f. Tese (Mestrado) – Escola Politécnica, Universidade de São Paulo, São Paulo, 2020.

Este estudo apresenta uma metodologia para o dimensionamento de Sistemas para Armazenamento de Energia por Baterias (SAEB), gerada a partir de Sistemas Fotovoltaicos (FV) isolados, usando dados da radiação solar horária prevista. O método baseia-se em uma relação matemática estabelecida entre energia gerada por FV, demanda por carga horária e capacidade de armazenamento, permitindo determinar períodos de interrupção de energia e déficit de oferta. Para conseguir isso, o comportamento da radiação solar deve ser previsto através da aquisição e processamento de um conjunto de dados históricos de radiação solar horária, para que modelos autorregressivos (AR) e séries temporais sejam usados para gerar séries sintéticas horárias. As séries geradas, combinadas com a demanda de carga horária disponível, são usadas como entradas na simulação. O dimensionamento do SAEB é considerado ajustando as variáveis [na simulação para determinar a potência correspondente e a capacidade de energia até que sejam atingidas porcentagens aceitáveis de déficit de energia e interrupções de fornecimento. A análise de probabilidade também é realizada usando vários cenários de radiação de dados de radiação solar sintética, representados usando curvas de distribuição cumulativa e de probabilidade. O método proposto é aplicado em um local no Nordeste do Brasil, usando o método Box Jenkins AR, a fim de facilitar a avaliação do desempenho de vários possíveis SAEB, indicar o risco de déficit de energia e a possível frequência de interrupção de energia. A análise de custo é realizada para analisar os riscos e benefícios investidos na instalação do sistema de armazenamento de energia da bateria em plantas fotovoltaicas e mostra as contribuições da abordagem proposta. A metodologia foi aplicada a estudos de caso autossuficientes em escala não utilitária para fins de captação e redução de energia, resultados foram discutidos e conclusões tiradas.

Palavras-chave - Autorregressivo, Sistema de Armazenamento de Energia por Bateria, Dimensionamento de Bateria, Intermitência, Performance econômica, Sistemas Fotovoltaicos, Energia Renovável, Irradiância Solar, Série Sintética, Séries Temporais.

ABSTRACT

ABUBAKAR, Ahmad. **Sizing of battery energy storage systems in isolated photovoltaic plants using predicted solar radiation data**. 2020. 120 p. Thesis (Masters) – Escola Politécnica, Universidade de São Paulo, São Paulo, 2020.

This study presents a methodology for the sizing of Battery Energy Storage Systems (BESS) in isolated Photovoltaic Plants (PV) using predicted hourly solar radiation data. The method is based on a mathematical relationship that was established between PV generated energy, hourly load demand and storage capacity, allowing one to determine energy deficit and supply interruption periods. To achieve this, solar radiation behavior must be predicted through acquisition and processing sets of historical hourly solar radiation data so that autoregressive (AR) and time series models are used to generate hourly synthetic series. The generated series, combined with available hourly load demand, are used as inputs in the simulation. The sizing of BESS is considered by adjusting the variables in the simulation to determine the corresponding power output and energy capacity until acceptable percentages of energy deficit and supply interruptions are attained. Probability analysis is also carried out using multiple radiation scenarios of synthetic solar radiation data, represented using probability and cumulative distribution curves. The proposed method is applied to a location in Northeastern Brazil using the Box Jenkins AR method in order to facilitate the assessment of the performance of several possible BESS, indicate the risk of energy deficit and the possible frequency of energy interruption. A cost analysis is carried out to analyze the risks and benefits of investing in battery energy storage system installation in PV plants and shows the contributions of the proposed approach. The methodology was applied to self-sufficient non-utility scale case studies for purposes of energy harvesting and curtailment, results were presented, discussed and conclusions were drawn.

Keywords – Autoregressive, Battery Energy Storage System, Battery Sizing, Intermittency, Economic Performance, Photovoltaic Systems, Renewable Energy, Solar Irradiance, Synthetic Series, Time Series.

LIST OF FIGURES

LIST OF TABLES

LIST OF ABBREVIATIONS AND TERMS

ANEEL	Agência Nacional de Energia Elétrica
ANFIS	Adaptive Neuro-Fuzzy Inference System
ANN	Artificial Neural Network
AR	Auto Regressive
BESS	Battery Energy Storage System
BOS	Balance Of System
CWANN	Combination of Wavelet Artificial Neural Network
ECMWF	European Centre for Medium-Range Weather Forecasting
ESS	Energy Storage System
FV	Fotovoltaico
GHG	Greenhouse Gases
HESS	Hybrid Energy Storage System
MLP	Multi-Layer Perceptron
NPV	Net Present Value
NWF	Numerical Weather Forecasting
PBP	Payback Period
PV	Photovoltaic
RER	Recursos de Energia Renovaveis
RES	Renewable Energy Sources
SAEB	Sistemas de Armazenamento de Energia por Bateria
SAM	System Advisor Model
SVM	Support Vector Machines
UC	Ultracapacitor

TABLE OF CONTENTS

1.0 INTRODUCTION

1.1 PREAMBLE

Renewable energy sources (RES) also referred to as clean energy sources, and especially solar photovoltaics (PV) are becoming increasingly popular in the electricity sector for providing electric power to residential, commercial and industrial consumers mainly due to growing environmental concerns, fuel price dependency and operational complexity associated with fossil fuel generation (ABUBAKAR; GEMIGNANI; MESCHINI ALMEIDA, 2019; DULOUT et al., 2017). This has motivated several countries around the world to formulate and adopt renewable energy and sustainable development policies to provide favorable conditions for further development of renewable energy technologies (YANG et al., 2018a) and have set targets for more renewable energy production and less of the more conventional fossil fuel dependent generation. PV systems have an edge over other renewable energy sources (RES) such as wind, hydro and nuclear systems because they are less restricted by resource availability, manufacturing material, transmission distance and geography as compared to the others (WANG et al., 2015) and their rapid development around the world attributed to the advancements in the technology which has led to decreasing costs of the system components and general installations, and its ability to be used in the electrification of isolated systems where connection to public grid is difficult or practically impossible.

However, the intermittent nature of solar resource and other RESs is a major concern because generation output of these resources are mostly random (ZHOU et al., 2016) with unpredictable variation (DULOUT et al., 2017) which can adversely affect electric systems and result in damages. Issues of voltage and frequency regulations might also be experienced as a result of high penetration levels of RES systems.

In this scenario, the use of Energy Storage Systems (ESS) as possible solutions to coping with increasing penetration of renewable energy has been extensively studied. As the penetration of RES is on a steady increase, Battery Energy Storage System (BESS) has proven to be an effective solution to the various problems associated with RES power production. BESS has attracted much attention due to its geographical independence, project flexibility sustained power delivery and fast response (YANG et al., 2018a), however, high cost has limited its development over the years (LIAO et al., 2018). This has led several researchers to focus on

the search for cost effective BESS in the quest to improving their reliability, efficiency and general performance in RES based electric networks. Optimal sizing of BESS is an important step in PV system design to balance peak and off-peak demand periods, improve quality management, reduce operational and maintenance costs (DAS; KUMAR, 2018; DAS et al., 2018) and prevent unnecessarily oversizing of BESS which leads to system complexity and unnecessarily high expenses (WHOLESALE SOLAR, 2020).

In isolated systems, incorporating BESS into solar PV systems guarantees that excess generated energy is stored and used later when there is no sufficient sun for generation. It is also important to adequately size the BESS as it can reduce the operational cost of microgrids (MGs) (ZOLFAGHARI; GHAFFARZADEH; ARDAKANI, 2019) and helps avoid shortage is supply. Several studies have developed sizing BESS methods for isolated PV systems, either by considering overloading characteristics and limitations of the state of charge (SOC) of battery (AGHAMOHAMMADI; ABDOLAHINIA, 2014), frequency control (KERDPHOL et al., 2016), capacity distribution (ABBASSI; DAMI; JEMLI, 2017) and so on. All these methods are limited owing to the fact that the behavior of the energy source is not adequately taken into account. Considering time-series generated synthetic series of solar irradiance data in the sizing of BESS helps solve this limitation issue.

This paper presents a novel BESS sizing methodology for PV systems using predicted solar radiation synthetic series data. Hourly solar radiation data of a location in northeastern Brazil is studied and processed using Box-Jenkins method, and autoregressive (AR) model and time-series model are used to generate synthetic series. These models are first validated using the confident interval method and the comparison indices method to determine if they are adequate enough to be used in predicting the behavior of solar irradiance. One year hourly synthetic series solar radiation data is then generated and converted to PV generated energy using details of a PV system determined based on consumer load profile. The generated energy combined with hourly load demand and battery storage capacity are used in running a typical PV system simulation. The outcomes of the simulation are hourly energy deficit and supply interruptions which shows the behavior of the PV–battery combination. Power and battery storage capacity are adjusted until acceptable percentages of energy deficit and supply interruptions are attained. Probability analysis is carried out with a set of 1000 scenarios of synthetic solar radiation data from the same simulation protocol. This provides a clearer

picture and allows us to further analyze the risks and certainties of the choice of BESS size in the PV system. Cost analysis considering net present value (NPV) and payback period (PBP) financial metrics is also performed to optimal selection of suitable BESS in isolated PV systems and to determine the economic implications of battery size on the overall system. The methodology was applied to self-sufficient non-utility scale case studies for purposes of energy harvesting and curtailment, results were presented, discussed and conclusions were drawn. Results of the study shows that the methodology is adequate for sizing of BESS in PV system design with higher accuracy than conventional sizing methodologies.

1.2 MOTIVATION

The main motivation for carrying out this research is to contribute to improving power supply using renewable energy resources, especially in countries like Nigeria. Nigeria has faced a lot of developmental problems in recent years and this is in part due to the fact that the country has struggled to meet power generation requirements. It is estimated that its per capita electricity consumption is about 100kWh per annum (OGUNLEYE, 2017). The electricity supply of the country is characterized by long periods of power outages in most parts of the country which has resulted in serious negative implications on the standard of life as well as industrial development.

Furthermore, electricity harvesting from renewable sources is relatively poor given the abundance of solar irradiance, wind speed and biomass (WORLD BANK GROUP, 2019).

Another motivation is to encourage efficient generation of clean energy especially in Nigeria and Africa in general. This is particularly important so as to protect the environment from GHG emissions and other emissions associated with generation of energy using fossil fuels and other unclean methods.

1.3 OBJECTIVES

The objective of this research in its entity is to contribute to the adoption of solar PV systems through the improvement of BESS sizing methods. To achieve this, practical applications of BESS sizing methodology using predicted solar radiation data and cost analysis for optimal selection of BESS were studied.

Long-term meteorological data were collected, analyzed and models were proposed for the prediction of solar synthetic series using auto-regressive (AR) and time series models. The predicted solar data was then used in BESS sizing and probability analysis.

Sizing of the BESS made it possible for practical real-life applications to be achieved and cost analysis for BESS size selection was made possible

1.4 DOCUMENT STRUCTURE

This document is organized as follows: Apart from chapter 1 which presented the introduction, motivation and the objectives of the research, chapter 2 presented the bibliographical review of past studies on synthetic series, solar irradiance and energy storage systems. Chapter 3 presented the introduction of solar photovoltaic systems, Chapter 4 presented the methods used for data acquisition, data filtering and processing, time series modeling, sizing of battery, probability analysis and cost analysis. Chapter 5 presented the case study and discussed obtained results which is the optimal sizing of BESS in isolated PV systems. The final chapter which is chapter 6 presented the conclusion of the research.

2.0 BIBLIOGRAPHICAL REVIEW

The evolution of ESS over time is triggering opportunities to building as many self-sufficient communities as possible, therefore, to understand how researchers have been utilizing synthetic series data in the study of sizing BESS and to understand the evolution of PV systems in isolated areas, the state of the art chapter of this research presents past literatures on solar radiation prediction, sizing of battery storage systems and cost analysis of BESS, to contextualize the information relevant to the research.

The chapter was developed to discuss the most relevant works in the context of methods used in this research, which include: the use of synthetic series data, the acquisition and forecast of solar irradiance for PV systems and the evolution of energy storage systems, which are the focus of this dissertation, highlighting its main characteristics and contributions.

2.1 SOLAR IRRADIANCE

The fact that solar photovoltaics and other clean energy sources are perceived to be the future of the energy sector has been categorically ascertained. For this reason, many literatures have studied and carried out experiments on solar photovoltaics and many more are ongoing. This research reviewed and compiled some of the available literatures. GEMIGNANI, ROSTEGUI and KAGAN (2017) proposed a periodic autoregressive model for solar radiation to generate synthetic sequences and the results used for practical application in defining bidding strategies for energy auctions. BRACALE et al. (2013) proposed a new short-term probabilistic forecasting method for predicting the probability density function of hourly active power generated by solar photovoltaic systems. The research carried out by FILIPE et al. (2015) described a hybrid solar power forecasting tool that uses the combination of physical and statistical models to improve short-term forecasting skills. CARLOS and CORVACHO (2013) discussed the possibility of the estimation of solar irradiance on non-horizontal surfaces for a specific location using data values of global solar radiation on horizontal surface. MEYBODI, RAMIREZ SANTIGOSA and BEATH (2017) studied the impact of time resolution in solar data on the performance modeling of concentrating solar power plant. This was done through systematic analysis of the influence of multi-year data sets with different time step sizes and thermal storage capacities using physical parabolic trough with molten salt storage model in NREL's System Advisor Model (SAM). LILIENTHAL (2007)

defines the penetration of renewables using four separate metrics with two simplest metrics being; the ratios of the renewable power systems' aggregate capacity either to the peak load or to the systems total installed capacity. Table 1 presents the penetration levels of wind and solar resources in small island utilities without external interconnections based on the four metrics.

Table 1 – Penetration by various metrics

Penetration by various Metrics	Wind	Solar
Peak Instantaneous Penetration	25%	15%
Penetration based on Peak Load	10%	10%
Penetration based on System Capacity	6.67%	6.67%
Penetration based on Energy	5%	3%

Source: (LILIENTHAL, 2007)

RAMEDANI, OMID and KEYHANI (2012) developed an artificial neural network base model that could estimate solar radiation on horizontal surfaces for locations in Karaj and other cities with similar climate and terrain. MORA-LÓPEZ, MARTÍNEZ-MARCHENA and PILIOUGINE (2011) presented in their paper a model capable of forecasting production of a photovoltaic solar plant for the next-day using the information obtained from the plant itself and the global solar radiation values for previous operation days (machine learning tool). ALMEIDA, LAMIGUEIRO and FERNÁNDEZ (2015) proposed a methodology to forecast one day ahead hourly AC power produced by a PV plant using a nonparametric PV model, its input being several forecasts of meteorological variables from NWF model and actual AC power measurements of PV plants. The methodology was built on R environment and uses quantile regression forests as machine learning tool to forecast AC power with a confidence interval. HASSAN et al. (2017) studied the potential of four different machine learning algorithm (Multi-layer Perceptron MLP, Adaptive Neuro-fuzzy Inference System ANFIS, Support Vector Machines SVM and Decision trees) in modeling global horizontal solar irradiance. All models were trained, optimized, validated and compared with each other using high-resolution, high quality accurate measured data. MLP model produced a result with the lowest root mean square error. Decision trees despite their simplicity also demonstrated their ability to model solar radiation. ROYER et al. (2016) also proposed an iterative combination of Wavelet ANN (CWAN) which produced short-term solar radiation time series forecasting. An iterative algorithm was proposed for iteratively searching for optimal values of CWANN parameters. On another dimension, EHNBERG and BOLLEN (2005) suggested a model that

can account for local meteorological conditions using cloud cover observation as input for the simulation. This is particularly useful in developing countries where solar radiation data is not readily available or is hard to obtain. VOYANT et al. (2014) used geostationary satellites data to generate 2-D time series of solar radiation for the next hour. To validate results obtained, an error metric called gamma index which is a criterion for comparing data from two matrices in medical physics was introduced. On the other hand, GHIMIRE et al. (2019) proposed an alternative method to forecast solar energy and assist with energy modelling for solar-rich sites that have diverse climatic conditions to further support clean energy utilization. The method involves the integration of ANN with ECMWF (European Centre for Medium Range Weather Forecasting) fields, incorporating physical interactions of incident solar radiation with atmospheric data. CORNEJO-BUENO et al. (2019) evaluated the performance of machine learning regression techniques in a problem of global solar radiation estimation from geostationary data. The research used one year hourly global solar radiation data from a radiometric station of Toledo in Spain to train the regression techniques considered and different input variables were considered. The research concluded that machine learning regressors have the capacity to obtain reliable global solar radiation estimation using measured satellite data. GOUDA et al. (2019) calibrated and evaluated nine-day of the year-based models to estimate the daily global solar radiation on a horizontal surface using long-term data of some stations across China.

2.2 SYNTHETIC SERIES

Synthetic series is any data that is applicable to a given situation or location that are not obtained by direct measurement but by observation and analysis of measured historical data. Many areas of the electric sector use synthetic series data which is crucial for the planning and operation of solar PV power plants. For example, in Brazil, synthetic series data is used in the planning and operation of wind farms. It is also used in the field of hydrology. The generation of synthetic series can be achieved using time series analysis which involves obtaining time-series models that can predict future series from historical series with minimal error (LOURENÇO et al., 2017).

Time series can simply be defined as a series of data points ordered in time (e.g. $L = \{l_1, l_2, \ldots l_t\}$) and time series prediction is the prediction of future data values l_{t+1} based on measured or observed historical data using time-series models (YUAN et al., 2020). Time

series analysis are carried out on collected/observed weather data which are collected over a long period of time (e.g. 15 to 20 years) and time series models are generated which are able to reproduce the registered series (LOURENÇO et al., 2017). The models obtained are responsible for the generation of synthetic series. Different time series models are obtained for different locations around the world as the weather characteristics of every location is different.

2.3 ENERGY STORAGE SYSTEM

There are also many literatures concerning energy storage systems and especially battery energy storage system because of its various advantages such as fast response and geographical independence. YANG et al. (2018a) presented a review based on the energy application type of the renewable energy source. The paper reviewed BESS sizing as applied to various renewable energy systems. As against previous assumptions and notions, BESS size determination is dependent on the specific renewable energy system size and application. This is especially important to the design process as the type of renewable energy system requirements and applications ultimately determines the BESS sizing methodology. Figure 1 is a BESS-incorporated hybrid standalone RES consisting of solar and wind renewable resources. CARPINELLI et al. (2014) used a four-step procedure based on decision theory to address the problem of determining the optimal size of a battery storage system to be installed in an industrial facility to reduce the facility's electricity bill. The sizing was done considering unavoidable uncertainties in electricity bill cost coefficients and the profile of the industrial facility's load demand. PERALTA and SALLES (2017) explored a method of increasing the penetration of renewable energies in isolated systems by combining several power sources and storage systems. BUCCIARELLI, PAOLETTI and VICINO (2018) proposed a two-stage stochastic programming formulation to accommodate uncertainties on future demand and generation with the aim of addressing the problem of finding the optimal sizes of energy storage systems in distribution networks. The first stage involves storage size decision while the second stage has to do with the storage control policy for a particular demand and generation profiles.

Figure 1 – A Hybrid Standalone Renewable Energy System

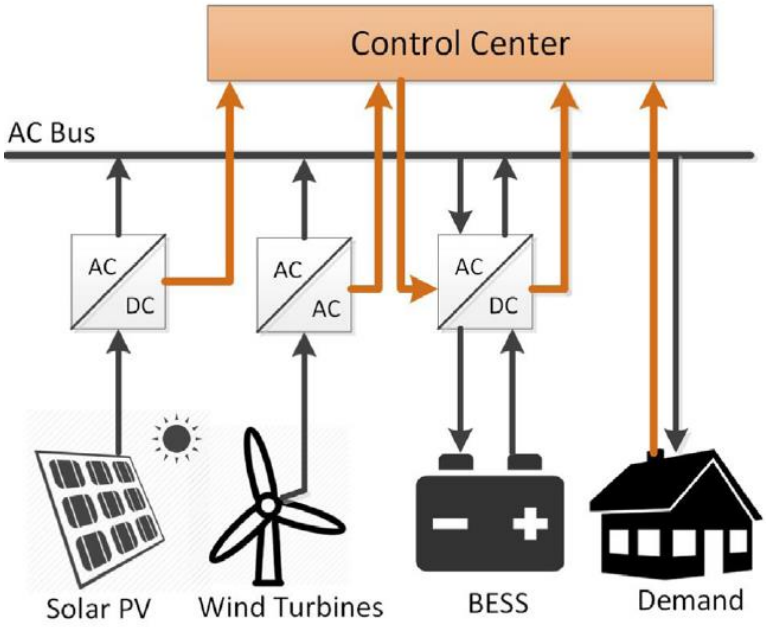

Source: (YANG et al., 2018a)

SAENGER et al. (2017) used a sizing tool based on the simulated annealing method to minimize global storage system weight which is an essential requirement in aeronautics. The study deals with the optimal sizing of secondary batteries and supercapacitors for aircrafts by developing a tool which sets parameters such as the cut-off frequency of the low-pass filter, the discharge ratio for storage components and temperature. WONG et al. (2019) carried out extensive reviews of issues related to the use of ESS in electricity networks with emphasis on optimal ESS placement, sizing and control methods of ESS. Three categories of methods were reviewed which are the mathematical optimization method, the analytical method and the artificial intelligence method. ÁLVARO, ARRANZ and AGUADO (2019) experimented on the sizing of a HESS (combination of ultracapacitors (UC) and batteries) to control ramp rate solar power plants. The study found the hybrid solution helps reduce cost by reducing unused storage capacity in the batteries that is only needed to not surpass C-rate limitation during short and sharp power oscillations. Hybridization of battery and ultra-capacitors also prolongs battery life because UCs reduce the amount and depth of cycles the battery performs. The figure below is the ramp-rate control scheme used in the study. A sizing methodology using pinch analysis and design space for hybrid ESS in solar PV-based isolated power system is presented in (JACOB; BANERJEE; GHOSH, 2018). The time series simulation used in the pinch analysis is such that the generation should always be larger than the load. In the

methodology, short, medium- and long-term storage sizes and PV array ratings for a the load are defined as feasible combinations for the design space which are then approximated using quadratic equations and the correlations used as constraints for determining the optimal supply mix and storage that minimizes the lifecycle cost. An innovative analytical sizing methodology was studied in (WU et al., 2017) where key factors that affect the optimal sizing of BESS were identified using an objective quantitative analysis of the costs and benefits for customer-side BSS, then developed a guideline for determining the most cost-effective battery size. LI (2019) presented algorithms for sizing of BESS in grid-connected PV systems for residential buildings with the aim of minimizing total annual cost of electricity. Figure 2 is a pictoral representation of typical charge/discharge characteristics of lead-acid batteries as presented in (LI, 2019).

Figure 2 – Typical charge/discharge characteristics of lead-acid batteries

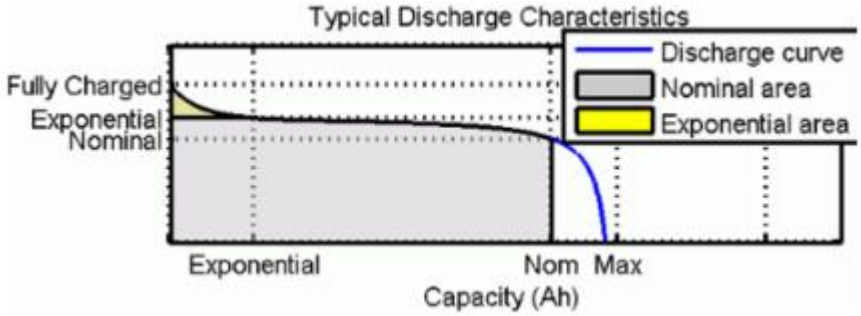

Source: (LI, 2019)

WENIGER, TJADEN and QUASCHNING (2014) also analyses PV BESS for residential building to gain insight into their sizing. XU, SHANG and ZHANG (2019) concentrates on sizing BESS for industrial customers with PV power by proposing a bi-level stochastic programming model to determine the power capacity and operation of BESS. The study also involves the careful assessment of the economic benefits of optimally sizing a BESS for industrial purposes. CARPINELLI, MOTTOLA and PROTO (2016) proposed a probabilistic approach for sizing BESS when time-of-use pricing is applied. It takes into account various uncertainties that unavoidably affect evaluation of cost incurred by customer such as load demand, energy prices and other economic factors. MEJÍA-GIRALDO et al. (2019) presented a strategy for sizing BESS that supports primary frequency regulation services of solar PV plants. An optimization model which includes investment cost and a novel penalty function depending on the state of charge was used. The graph in Figure 3 shows the investment and replacement cost of BESS while Figure 4 shows state of charge deviation penalty function.

Figure 3 – Figure: BESS investment and replacement costs

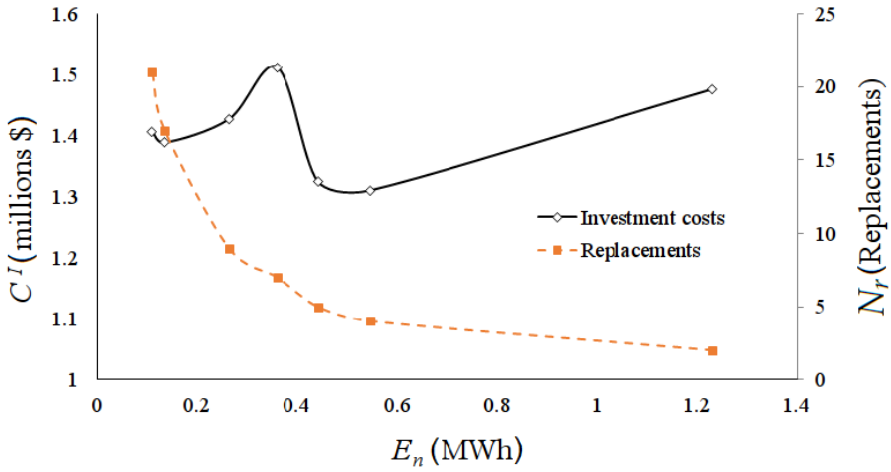

Source: (MEJÍA-GIRALDO et al., 2019)

Figure 4 – Figure: State of charge deviation penalty function

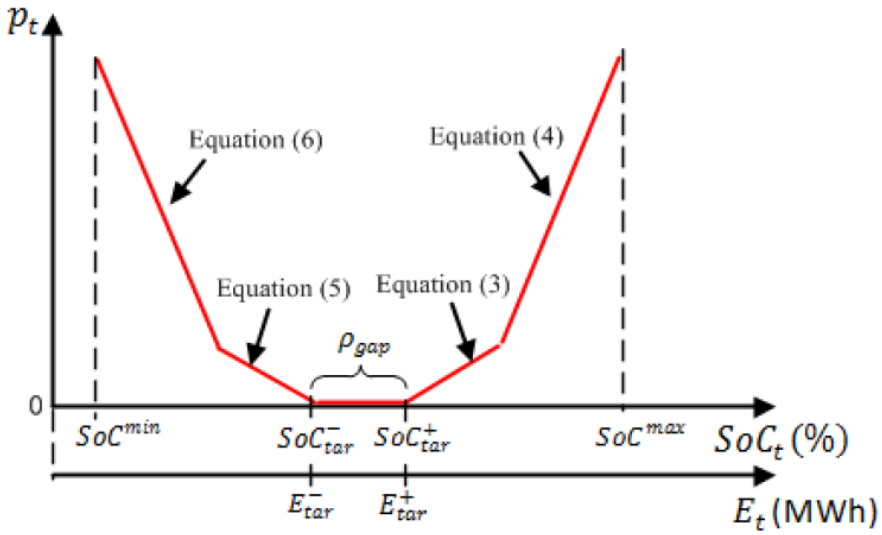

Source: (MEJÍA-GIRALDO et al., 2019)

YANG et al. (2018b) aimed at achieving maximum operating profit of hybrid PV and wind power plant by an analytical sizing of BESS strategy. The idea in the study is compensating for forecasting errors using batteries, introducing an optimization methodology which converts nonlinear programming to linear programming problem. LIAO et al. (2018) investigated an optimization method that sizes and schedules BESS and smart inverter for PV systems. The proposed methodology assists both PV system owners and distribution system operators (DSOs) in the sense that it ensures investment returns to PV system owners and helps adjust voltages for DSOs by taking into account scheduling optimization of related facilities. This encourages PV owners to invest BESS without causing any problems to the

DSOs which leads to rise in operational profits to PV system owners and an improved power supply quality of distribution systems. The diagram below illustrates the proposed voltage control architecture in a distributed network topology. QUINTERO PULIDO et al. (2018) studied sizing of BESS in residential off-grid PV systems using distributed energy management methodology (DEMkit model). Results showed that the DEMkit model was able to find an optimal value for the BESS size to half the initial battery capacity and still sufficiently cover the load. MÜLLER et al., (2019) presented a BESS sizing strategy that gives insight to both energy and power requirements of a system. In order to provide the ESS energy and power sizing strategy, three PV modeling techniques were used to estimate the non-measured and non-harnessed PV power. A control strategy to store or release power from the DC-link without modifying the MPPT strategy was also presented in the study. Figure 5 presents different classifications of energy storage system technologies. CHO, KIM and KIM (2014) proposed a BESS sizing methodology with the aim of managing minimizing the consumer's electricity cost by managing electricity demand. A BESS sizing optimization methodology in typical household microgrid connected PV system was presented in (WANG et al., 2015) while DULOUT et al. (2017) focused on sizing lithium BESS and its optimal operating conditions. LAI et al. (2019) proposed an algorithm-based BESS sizing for microgrids to limit load shedding when energy sources are attacked.

Figure 5 – Figure: Energy storage technologies classification

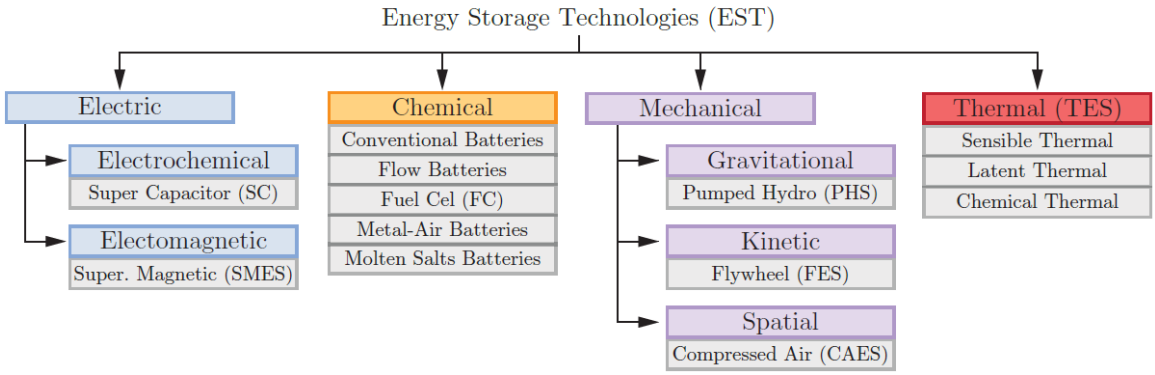

Source: (MÜLLER et al., 2019)

CHEDID and SAWWAS (2019) presented a two-step optimization approach to determining the effect of BESS addition to a PV system incorporated distribution network where a generic algorithm technique is used in order to reach the optimal configuration in both steps. The first step of the study examines the sizing and placement of the PV arrays while the second step examines the sizing and placement of the BESS all with the objective of finding the lowest

possible losses, cost and voltage deviation from the reference bus. In study (ABBASSI; DAMI; JEMLI, 2017), modeling of an autonomous DC-coupled wind-solar power generation system connected with a super capacitor-batteries hybrid energy storage system (HESS) was presented. A statistical approach was used in the description of the distribution capacity of the HESS. This was done in order to smoothen the wind-solar power production variation and ensure a controllable output power. FOSSATI et al. (2015) proposed a genetic algorithm-based method for sizing energy storage system in microgrids. The method aimed at minimizing the operating cost of microgrids by identifying the energy power and capacities of the storage system. VENU et al. (2009) presented a method of BESS sizing to help shave peak demand of residential power distribution feeder. They also studied the impact of distributed PV systems on the BESS sizing and discovered that there is little impact on the BESS but assists in downsizing of energy storage rating of the BESS while achieving the same level of peak load shaving. The work carried out by (OH; SON, 2018) investigated the discrete Fourier transform based two-step energy storage system sizing and operation strategy in order to enhance wind power generation reliability. This strategy enhances performance of RMSE by cutting-off the high frequency component of the wind power generation. BUCCIARELLI et al. (2017) presented the deployment of energy storage system (ESS) for voltage support applications in low voltage networks was discussed. Sizing of the ESS was assessed taking into consideration the uncertainty of demand and supply through a stochastic programming formulation. CABELLO et al. (2018) proposed a method of energy storage system sizing based on Energy-Power plane where it separates the energy storage device characterization, the demanded profile synthesis and the sizing stage. This way, it is easier to change the energy management strategy or add a new device to the analysis. MARTINS et al. (2018) formulated a model for sizing the most cost-effective BESS for a variety of industrial load profiles and multiple billing schemes. It does so by minimizing the storage degradation cost and the maximum power peak in the billing period. The work however, is limited to the optimization of storage systems using historical data on specific industrial load profile. In their paper titled “Optimal sizing of battery storage systems for industrial applications when uncertainties exist”. XIA et al. (2018) proposed a general stochastic cost-benefit analysis model which accounted for expected generation fuel cost and ESS daily capital cost to optimize ESS size for power system planning with uncertain wind generation. MICHIORRI et al. (2018) studied the influence of wind prediction errors autocorrelation on the sizing of

energy storage for wind power network integration. ZHANG et al. (2017) investigated battery sizing and rule-based operation of grid-connected PV-battery systems. The study opined that optimal components design should be determined with consideration of system operation. The methodology involved the design and evaluation of three rule-based operation strategies including the conventional operation strategy, the dynamic price load shifting strategy and the hybrid operation strategy. DAS and KUMAR (2018) considered a battery storage and a hydro storage to examine a proposed model for the sizing of energy storage systems connected to a renewable energy generation farm and the effectiveness of the model was tested using data of electricity generation and load demand for 24 hours.

3.0 SOLAR PHOTOVOLTAIC SYSTEMS

The main components of a typical BESS incorporated solar photovoltaic system which are PV modules and battery storage systems are presented and discussed in this chapter to give an insight around the workings of solar PV systems.

The chapter discusses different PV and battery technology types, characteristics, costs, system applications as well as their advantages and disadvantages, in order to understand how and where these technologies can be efficiently utilized.

3.1 PHOTOVOLTAICS (PV)

Photovoltaics (PV) consist of small rectangular cells made of semiconductor materials that eject electrons when photons (sunlight) hit the surface, producing a few watts of direct current (DC) electricity. These cells have electrical conductors which allow the flow of electrons to external loads and surface coatings to reduce light reflection. (CENTRE FOR SUSTAINABLE SYSTEMS UNIVERSITY OF MICHIGAN, 2019).

PV modules are a rectangular grid of about 60 to 72 cells connected in parallel circuits and laminated between a transparent front surface and a protective back surface. They also have metal frames to strengthen them.

There are three major types of PV modules (monocrystalline, polycrystalline or multi-crystalline and thin-film) and most of the solar panel options currently available in the market today fit into one of the three, each type with its own unique advantages and disadvantages. These panels vary based on how they are made, performance, appearance, costs and what installation each is suited for.

The advantages of monocrystalline panels include high performance efficiency and aesthetics and its disadvantage is higher cost. Polycrystalline panels cost much less than monocrystalline panels but also have lower performance efficiency. Thin-film panels have the lowest performance efficiency of the three types but they are portable, flexible, light weighted and have aesthetics.

Of the three types of PV panel modules, polycrystalline panels are the most commonly used because they are cheaper and easier to manufacture among other reasons.

3.1.1 PV Cost

Since 2008, there has been a drastic drop of solar electricity cost by over 85% (CENTRE FOR SUSTAINABLE SYSTEMS UNIVERSITY OF MICHIGAN, 2019). This is due to rapid deployment rate of solar PV and high learning rates (decline in PV module cost). PV module has seen their prices reduced continuously in recent years starting 2010, by about 15% for Crystalline silicon (ci-Si) PV modules and by 4% for thin-film modules (IRENA, 2016). Analysis have shown that in 2018, the average retail cost of solar power for all sectors is about 10.58 cents/kWh and 12.89cents/kWh for residential consumers, global investments in solar power also dropped to about $130.8 billion and it is likely partially due to the decline in capital costs of PV systems. (CENTRE FOR SUSTAINABLE SYSTEMS UNIVERSITY OF MICHIGAN, 2019).

The cost of deploying a solar PV plant depends on the size of the system, the cost of PV module and the balance of system (BOS) cost. PV module cost is determined by the cost of raw materials, cell manufacturing cost and module assembly cost. BOS cost on the other hand is the cumulative costs of the structural system (site acquisition, site preparation, structural installation, racks) and the electrical system (inverters, wiring, transformers and in the case of off-grid systems, battery and other storage system costs) (IRENA, 2012).

Large-scale utility PV systems operate as a centralized power system supplying power to the grid. The average price of utility-scale ci-Si PV systems in 2010 was about USD 5.03/W and plants with capacity above 2MW do not offer significant economy of scale i.e. there is no significant difference in price between a 20MW plant and a 2MW plant (IRENA, 2012). For thin-film technology, the prices have stayed at around USD 0.5/W in early 2016 (IRENA, 2016).

Figure 6 shows the cost benchmark for utility-scale PV plants between 2010 and 2017. It can be observed that a significant chunk of reduction is overall cost is due to reduction in PV module prices (FU et al., 2017). (GAETAN; SINEAD; MANOEL, 2018) provides a comprehensive outlook of the future of the global solar market between 2018 and 2022.

Figure 6 – Utility-scale PV plant cost benchmark 2010-2017

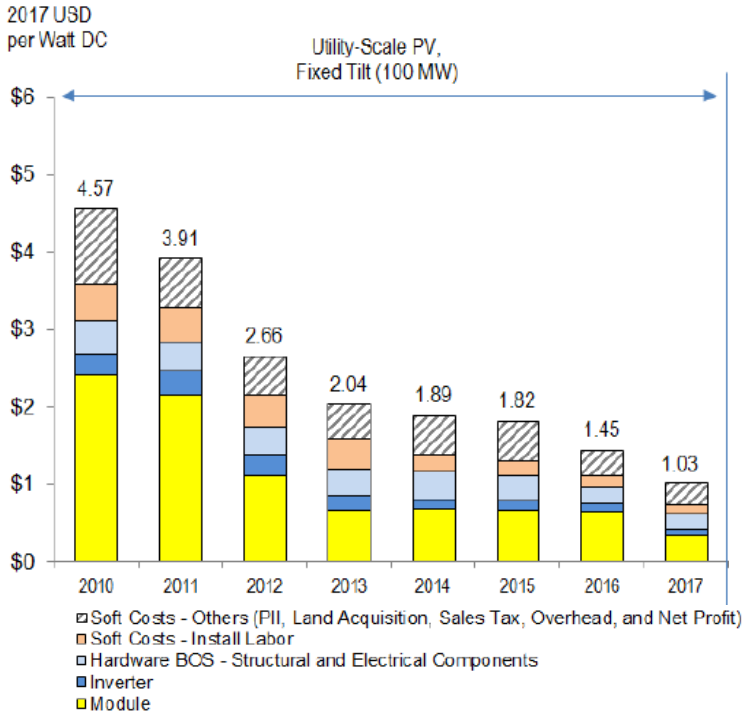

Source: (FU et al., 2017)

3.2 BATTERY

Battery is one of the components of a solar PV system's BOS (Balance of system). The main purpose of incorporating batteries in PV systems is to store the energy produced by the PV array during periods of high solar energy, and then supply the stored energy to electric loads and other end-users during periods of low or no solar energy (BERNABÉ; MARTÍNEZ, [s.d.]). Other reasons or functions of batteries in PV systems include (BERNABÉ; MARTÍNEZ, [s.d.])

- To supply surge currents to inverters and electric loads
- To provide stable voltages to electric loads
- To help the PV array to operate at near maximum power potential.

Batteries also need protection from overcharging and over-discharging. It is for this reason that it is common practice to install battery charge controllers alongside battery storage systems.

No one type of battery is ideal for all PV system applications (LACHO, 2019). Knowledge of operational requirements, design features and performance characteristics is important in the optimal selection of battery storage system to be used in a PV system depending on the particular PV system's applications. Price, capacity, lifespan, maintenance requirements,

battery mobility and size should all be considered before choosing the battery storage type to be used in a PV application (LACHO, 2019).

Selecting the appropriate solar battery for your PV system requires careful consideration. This study provides a review of the basic battery storage system features and characteristics, and how they influence battery applications in PV systems. Costs of different battery storage technologies are also reviewed to aid system designers in efficient and practical decision-making (BERNABÉ; MARTÍNEZ, [s.d.]).

3.2.1 Types of Batteries and Their Classifications

Primary batteries: The batteries in this classification can store and deliver electrical energy but cannot be recharged. Their inability to be recharged is the reason they are not used in PV system applications (BERNABÉ; MARTÍNEZ, [s.d.]).

Secondary batteries: These batteries can store and deliver electrical energy and can be recharged by passing current in opposite direction to the discharge current. Their ability to be recharged makes them ideal for PV system applications (BERNABÉ; MARTÍNEZ, [s.d.]).

3.2.2 Types of Batteries Used in PV System Applications

The most common types of batteries used in solar PV applications include lead-acid batteries, lithium-ion batteries, flow batteries, nickel-cadmium batteries and flooded type batteries. Others include; sodium batteries, Aquion hybrid (salt water) battery, molten salt batteries (CHOICE, 2020), Nickel Chloride batteries, Sodium-sulfur batteries, and Aluminum-ion batteries. Each battery type has its own unique characteristics and is suitable for certain PV applications.

1. ***Lead-acid Battery****:*

These are deep-cycle batteries popular within off-grid PV applications (MOZAW, 2019). Their low cost makes them ideal for small-scale solar PV applications e.g. household installations (SOLAR QUOTES, 2019a). They contain large amounts of electrical energy which are capable of discharging very quickly if any form of conductor is placed across their terminal. They are characterized by low energy and power densities, long charge time and have between 1000 to 3000 cycle-life (2-8 years) at 60-70% depth of discharge. Their capacity tend to decrease significantly in case of deep and rapid discharge rates (SOLAR QUOTES, 2019a).

2. Lithium Ion Batteries

These are the same types of batteries found in IPhone and laptops and in Tesla Powerwall and their popularity is growing by the day (SOLAR QUOTES, 2019b). It is also a deep-cycle battery and although, it has high initial capital cost which is about 50% more expensive than lead-acid batteries for the same amount of storage, its advantages over lead-acid include lighter weight, decreased maintenance, deeper discharge, longer lifetime (13-18 years) and has 6000-8000 cycle-life at 80% depth of discharge (SOLAR QUOTES, 2019b). Its operating temperature is between 0^0 and 40^0C and its temperature increases when overcharged (NORTHERN ARIZON WIND AND SUN, 2019). This type of battery is extensively applied in renewable energy grid systems and micro-grid systems and it is deal for large-scale EV and residential applications (SOLAR QUOTES, 2019b).

3. Nickel-Cadmium Batteries:

These batteries have long life in chronological terms but not in cycle terms and are not recommended for most solar systems because they are very expensive and have low efficiency of between 65% and 80%. Some of the advantages of Nickel-cadmium batteries over lead-acid batteries include; longer life, lower maintenance requirement, ability to withstand excess discharge, excellent low temperature capacity retention, non-critical voltage regulation requirements. Some of its disadvantages are higher cost and limited ability (BERNABÉ; MARTÍNEZ, [s.d.]).

3.2.3 Cost of Batteries

Cost of battery vary depending on the amount of energy storage capacity (in kWh), type of battery technology, type of installed inverter, backup power requirements and the installation location. Table 2 presents the costs of some battery technologies in the market.

Table 2 – Cost of some battery technologies popular in the market

Product name	Manufacturer	Battery Chemistry	Usable storage capacity (kWh)	Total warranted kWh	Cost per warranted kWh (unlimited cycles per day) ($)	Estimated price ($)
Powerwall 2 (AC)	Tesla	Lithium ion	13.20	38,261	0.23 (1 cycle per day)	8,800
Powerwall 2 (DC)	Tesla	Lithium ion	13.50	38,095	0.21 (1 cycle per day)	8,000
Aspen 48S-2.2	Aquion Energy	Aquion Hybrid ion	2.20	4,000	0.55 (1 cycle per day)	2,200
Fronius Solar Battery	Fronius International	Lithium ion	9.60	17,472	0.89 (1 cycle per day)	15,550
SolaX Lead Carbon	SolaX	Lead Carbon	4.50	3,282	2.13 (1 cycle per day)	6,990
Zcell	Redflow	Flow (Zinc-Bromide)	10.00	36,000	0.35 (1 cycle per day)	12,600
Apollion Cube	Lelanche	Li-ion	5.40	19,575	0.47 (1 cycle per day)	9,200
GridEdge Quantum	GridEdge	Sodium Nickel Chloride	7.68	13,986	1.43 (1 cycle per day)	20,000

Source: (ECOWHO, 2020)

3.2.4 Comparisons, Advantages and Disadvantages of Different Battery Technologies

Table 3 presents comparisons of different popular battery technologies used in PV systems based on rated power, energy density, discharge duration, energy efficiency, lifecycle and storage costs. Table 4 on the other hand presents the advantages and disadvantages of battery technologies used in PV systems.

Considering the Table 3 and Table 4, it can be concluded that lithium-ion battery technology has an overall advantage over the other technologies.

Table 3 – Comparison of different battery technologies

Battery Technology	Rated Power (MW)	Energy Density (Wh/kg)	Discharge duration (h)	Energy Efficiency (%)	Lifetime/Cycles	Storage costs (USD/Kwh)
Lead-acid	< 36	< 50	< 8	75-85	3-12 years/500-1200	300-600
Lithium-ion	< 102	< 200	< 6	90-94	5-15 years/1000-10,000	1200-4000
Vanadium-based flow battery	< 28	< 30	< 10	70-85	5-15 years/12,000-18,000	600-1500
Sodium-sulfur	< 50	< 240	< 8	75-86	5-10 years/2500-4000	1000-3000
Aluminum-ion (estimated)	N/A	< 60	< 6	90-94	5-15 years/1000-10,000	300-600

Source: (ZHANG et al., 2018)

Table 4 – Advantages and disadvantages of different battery technologies

Battery Technology	Advantages	Disadvantages	Energy storage applications
Lead-acid	Low capital cost	Limited life cycle, long charging time and high self-discharge rate	Hot spare, frequency control and load adjustment
Lithium-ion	High energy densities, high efficiency, long life cycle	High production cost, requires Battery Management System	Frequency control, load shifting and power quality
Vanadium based flow battery	High power, long life cycle, fast charge and discharge	High production cost, large area	Load shifting, emergency standby and power quality
Sodium-sulfur	High power and energy densities, high efficiency	Production cost and safety concerns	Load adjustment and standby power
Aluminum-ion (estimated)	Low capital cost, fast charge and discharge, high efficiency	Under development, low energy densities	N/A

Source: (ZHANG et al., 2018)

4.0 METHODOLOGY

In this chapter, the step by step method process of the research is presented from data acquisition, data filtering and processing, time-series modeling, synthetic series generation, to battery sizing, probability analysis and cost analysis.

This study is focused on the optimal sizing of BESS in solar PV systems and this is achieved by first, developing time-series models for synthetic series generation from historical solar irradiance data, and then utilizing the generated synthetic series in the sizing of the BESS. Then, a cost analysis of the sized BESS is carried out to evaluate its economic performance.

The method proposed starts with the acquisition and processing of historical solar irradiance, generation of synthetic series using time-series models and ends with cost analysis of severally sized BESSs.

4.1 DATA ACQUISITION

A program for satellite data estimation systems called Vortex Solar Series (VSS) was used in the acquisition of the solar irradiance data used in this research. The program makes it possible to obtain irradiance data for onshore and offshore locations, providing data such as global horizontal irradiance (GHI), direct normal irradiance (DNI), diffuse horizontal irradiance (DHI), temperature, wind speed, etc., for different time steps. The program has a resolution of about 3km around specified coordinates. 20 years hourly solar irradiance data used for the prediction of hourly solar irradiance synthetic series data.

4.2 DATA FILTERING AND PROCESSING

There are several methods used for data filtering and data processing and a number of these methods have been proven to be effective. The method chosen for data processing in this research is the Box-Jenkins method. This method applies autoregressive moving average and autoregressive integrated moving average models to find the best fit of a time-series model to past values of a time series.

The mean (μ), standard deviation (σ), covariance (γ) and correlation (ρ) of the obtained data were calculated for the days of the corresponding years. Mean and standard deviation operations represent the average sample value and degree of dispersion of the sample around the mean respectively. These properties are the foundation of the entire time series analyses.

The covariance is calculated to identify the time dependence between two variables spaced by a fixed order (time interval). The correlation is the standardization of the covariance order with a base of 1. Correlation of 1 indicates that the annual flow is totally dependent on the previous year while correlation of zero connotes total independence between flows of consecutive years (GEMIGNANI, 2018).

The equations (1), (2), (3) and (4) represent the statistical properties mentioned;

$$\mu = \frac{1}{n}\sum_{i=1}^{n} Z_i \tag{1}$$

$$\sigma = \sqrt{\frac{1}{n}\sum_{i=1}^{n}(Z_i - \mu)^2} \tag{2}$$

$$\Upsilon(j) = \frac{1}{n}\sum_{i=1+j}^{n}(Z_i - \mu)(Z_{i-j} - \mu) \tag{3}$$

$$\rho(j) = \frac{\Upsilon(j)}{\sigma^2} \tag{4}$$

Where;

μ = mean,
Z_i= sample value
n = amount of sample data
σ = standard deviation
$\Upsilon(j)$= covariance of order (j)
$\rho(j)$= correlation of order (j)

To make the series stationary it is necessary to remove the seasonal component (trend) applying equation (5)

$$Z_i = \frac{x_t - \mu_h}{\sigma_h} \tag{5}$$

Where;

μ_h = hourly average
σ_h = hourly standard deviation

The average of the series Z_i is approximately zero (0) and its standard deviation is unity (1).

The series has N number of observations (20 years x 8760 hours = 175200).

4.3 TIME SERIES MODELING

4.3.1 Box-Jenkins Method

The Box-Jenkins method is a common name and is frequently used in the fields of econometrics, system modeling and control, finance and meteorology to obtain time series models (GEMIGNANI, 2018). The goal of this method is to obtain parsimonious models with adequate and finite parameters, to represent a time series after the validation phase by an iterative method of obtaining stochastic models for the time series from predefined model structure. The method is represented graphically by Figure 7.

Figure 7 – Flow diagram representing Box-Jenkins method

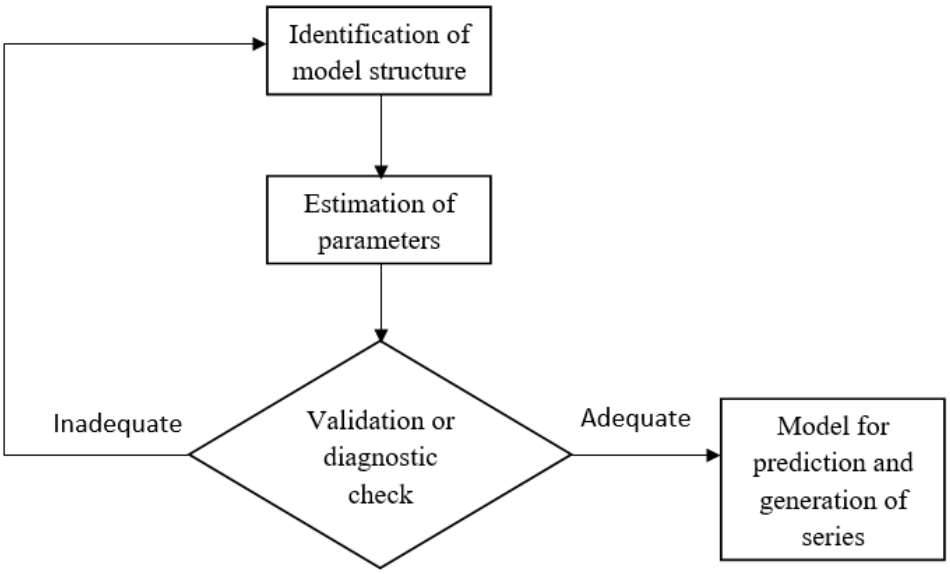

Source: (GEMIGNANI, 2018)

Choice of model is the first step of the method, starting with as few parameters as possible. These parameters are then estimated using methods such as the least square method or minimum variables likelihood ratio method. The model is then validated using statistical properties process. The model can also be simulated to verify if the scenario generated by the model is consistent with reality. If the model is considered fit, the process ends otherwise the process is repeated with addition of parameters until validation is achieved. It is basically a trial and error process.

4.3.2 Autoregressive Model (AR)

An autoregressive process of order p, AR(p), is defined as a model where the current value of the process z_t is expressed as a linear combination of the past p values z_{t-1}, z_{t-2},..., z_{t-p} and a white noise a_t (Box, G. E. P. and Jenkins, G. M. 1976), where a_t is a sequence of random variables with normal distribution, zero mean and variance σ_a^2, i.e. $N(0, \sigma_a^2)$. An AR model can be of any order from 1 to p. It is represented mathematically by the equation (6)

$$z_t = a_t + \phi_1 z_{t-1} + \phi_2 z_{t-2} + \cdots + \phi_p z_{t-p} \tag{6}$$

Where;

z_t= autoregressive process of order p
a_t= white noise

For the purpose of this research, AR model of up to order 5, i.e., AR(5) was investigated and AR model of order 2, i.e., AR (2) was chosen. This is because the error difference between orders 2, 3, 4 and 5 were observed to be negligible. The results obtained from this equation was used to calculate the values of autocovariance $c_k$and autocorrelation r_k using equations (7) and (8).

$$c_k = \frac{1}{N-k}\sum_{t=1}^{N-k}(z_t - \bar{z})(z_{t+k} - \bar{z}),\ k = 0, 1, \ldots, K \tag{7}$$

Where;

c_k= autocovariance
N = amount of sample data
K = interval in which the data correlations are analyzed
$\bar{z}$ = mean
z_t = current value

$$r_k = \frac{c_k}{c_0} \tag{8}$$

Where;

r_k = autocorrelation
c_k = autocovariance of order k
c_0 = autocovariance of the 1st order 0

The AR(5) model is expressed by equation (9)

$$z_t = a_t + \phi_1 z_{t-1} + \phi_2 z_{t-2} + \phi_3 z_{t-3} + \phi_4 z_{t-4} + \phi_5 z_{t-5} \tag{9}$$

Where $\phi_5 = \hat{\phi}_{55}$

The coefficient ϕ_1 is given by the estimation of the partial autocorrelation coefficient $\hat{\phi}_{51}$ and the coefficient ϕ_5 is given by $\hat{\phi}_{55}$. These coefficients are estimated by means of the Yule-Walker equation

$$r_j = \hat{\phi}_{51} r_{j-1} + \hat{\phi}_{52} r_{j-2} + \hat{\phi}_{53} r_{j-3} + \hat{\phi}_{54} r_{j-4} + \hat{\phi}_{55} r_{j-5} \tag{10}$$

$j = 1, 2, 3,4,5$ and $r_j = r_{-j}$

For an AR model of order 5, the equation can be represented as follows;

$$r_1 = \hat{\phi}_{51} r_0 + \hat{\phi}_{52} r_{-1} + \hat{\phi}_{53} r_{-2} + \hat{\phi}_{54} r_{-3} + \hat{\phi}_{55} r_{-4}$$

$$r_2 = \hat{\phi}_{51} r_1 + \hat{\phi}_{52} r_0 + \hat{\phi}_{53} r_{-1} + \hat{\phi}_{54} r_{-2} + \hat{\phi}_{55} r_{-3}$$

$$r_3 = \hat{\phi}_{51} r_2 + \hat{\phi}_{52} r_1 + \hat{\phi}_{53} r_0 + \hat{\phi}_{54} r_{-1} + \hat{\phi}_{55} r_{-2}$$

$$r_4 = \hat{\phi}_{51} r_3 + \hat{\phi}_{52} r_2 + \hat{\phi}_{53} r_1 + \hat{\phi}_{54} r_0 + \hat{\phi}_{55} r_{-1}$$

$$r_5 = \hat{\phi}_{51} r_4 + \hat{\phi}_{52} r_3 + \hat{\phi}_{53} r_2 + \hat{\phi}_{54} r_1 + \hat{\phi}_{55} r_0$$

Also, from the Yule-Walker equation, the ϕ parameters are obtained for the desired order of model (in this case $p = 5$) as in equation (11)

$$\begin{bmatrix} 1 & r_1 & r_2 & r_3 & r_4 \\ r_1 & 1 & r_1 & r_2 & r_3 \\ r_2 & r_1 & 1 & r_1 & r_2 \\ r_3 & r_2 & r_1 & 1 & r_1 \\ r_4 & r_3 & r_2 & r_1 & 1 \end{bmatrix} \text{x} \begin{bmatrix} \phi_1 \\ \phi_2 \\ \phi_3 \\ \phi_4 \\ \phi_5 \end{bmatrix} = \begin{bmatrix} r_1 \\ r_2 \\ r_3 \\ r_4 \\ r_5 \end{bmatrix} \tag{11}$$

The residue or error is calculated by making a_t in equation 9 the subject of the formula as shown in equation (12), checking that $a_t \sim N(0, \sigma_a^2)$;

$$a_t = z_t - \phi_1 z_{t-1} - \phi_2 z_{t-2} - \phi_3 z_{t-3} - \cdots \tag{12}$$

For the chosen AR model of order 2, the equations are represented by equations (13) and (14)

$$r_1 = \hat{\phi}_{21} r_0 + \hat{\phi}_{22} r_{-1} \tag{13}$$

$$r_2 = \hat{\phi}_{21} r_1 + \hat{\phi}_{22} r_0 \tag{14}$$

4.3.3 Validation

a. Comparison indices method

For the validation/testing phase of this research, a comparison was made between the forecasts generated and the forecasts observed using four error comparison indices; root mean square error, mean absolute error, mean relative percentage error and maximum relative percentage error.

- Root Mean Square Error (RMSE) represents the quadratic mean of the differences between predicted values and the observed values. It is represented mathematically by equation (15)

$$RMSE = \sqrt{\frac{1}{n}\sum_{j=1}^{n}\left(y_j - \hat{y}_j\right)^2} \tag{15}$$

- Mean Absolute Error (MAE) is the measure of the average magnitude or absolute difference between predicted and observed values where all individual differences have equal weight. It is represented mathematically by equation (16)

$$MAE = \frac{1}{n}\sum_{j=1}^{n}\left|y_j - \hat{y}_j\right| \tag{16}$$

- Mean Relative Error (MRE) is the mean ratio of the absolute error to the observed value expressed in percentage. It indicates the average of the quotient between the error and observed value. It is represented mathematically by equation (17)

$$MRE = \frac{100}{n}\sum_{j=1}^{n}\frac{\left|y_j - \hat{y}_j\right|}{y_j} \tag{17}$$

- Maximum Relative Percentage Error (PE_{max}) is the maximum absolute ration of error to observed value and is represented mathematically by equation (18)

$$PE_{max} = \max 100\left|\frac{y_j - \widehat{y_j}}{y_j}\right| \tag{18}$$

Where, y_j is the real value and $\hat{y}_j$ is the forecast value.

b. Confidence interval method

The confidence interval (CI) method is also used in the verification of obtained models. The 95% confidence interval is the likely range of the true unknown parameter (HIPEL;

MCLEOD, 1994). It does not reflect the variability of the unknown parameter but reflects the amount of random error in the sample and provides a range of values that are likely to include the unknown parameter. Thus, confidence interval is a range of likely values of the parameter with a specified level of confidence. It can be represented mathematically by equation (19)

$$CI = \pm 1.96\sqrt{\frac{1}{n}} \tag{19}$$

Where n is number of sample space

The order selection process of the AR model has three common strategies:

- The order of the AR model is given by the last coefficient autoregressive outside the boundary of the confidence interval boundary.
- The order of the AR model is given by the first coefficient autoregressive outside the confidence interval boundary.
- The order of the AR model is chosen by observing, from the first coefficient, the quantity of consecutive coefficient that exceed the confidence limit, i.e., the last coefficient outside the confidence interval before the next coefficient within the interval.

Figure 8 is an example of a 95% confidence interval graph. The red lines represent the 95% confidence interval.

Figure 8 – Confidence interval graph

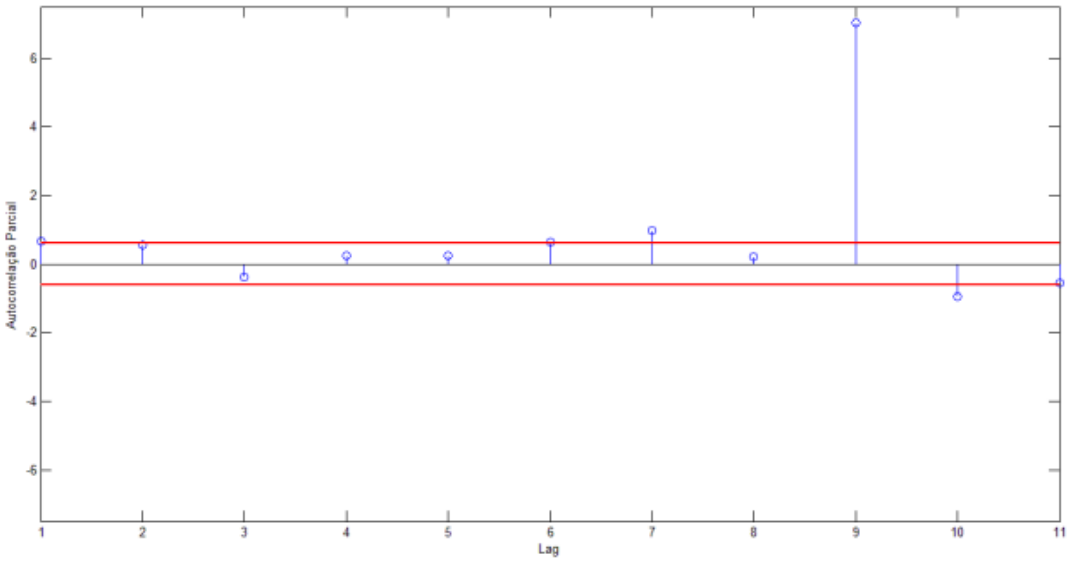

Source: (HIPEL; MCLEOD, 1994)

Following the descriptions of the strategies above, the order of the AR model in this example is;

i. The last lag outside the CI is number 10, therefore the order of the model is 10.
ii. The first lag outside the CI is number 1, therefore the order of the model is 1.
iii. The last lag outside the CI before the next lag within the CI is number 1, therefore the order of the model is 1.

4.3.4 Synthetic Series Generation

After the generated model has been validated and found to be adequate, the residual a_t(error) was calculated for each month using equations derived from the generated AR model. In this study, one equation was generated for each month of the year. The synthetic series was then generated using the mean and standard deviation of the calculated residue.

4.4 TREND REINTRODUCTION

After the generated model has been validated, the removed trend is then reintroduced to obtain the synthetic series. Equation (20) was used to reintroduce the trend;

$$x_t = (z_t \,.\, \sigma_h) + \mu_h \tag{20}$$

4.5 ELECTRIC COMPONENT

The synthetic series irradiance data obtained was then converted to electrical values (generated electricity) by multiplying the synthetic series components (x_t) by plant efficiency (η) and plant power at Standard Test Condition (STC), as represented in equation (21).

$$E = \eta \,.\, P_{stc} \,.\, x_t \tag{21}$$

4.6 BATTERY SIZING IN ISOLATED PV PLANTS

BESS sizing otherwise known as battery bank sizing is a crucial step in PV system applications. It is important to ensure that loads are being supplied in the absence of solar PV generation. Having the right battery size in a PV system is important to handle the load coming from the PV panel and to serve as a reliable backup to the system without having to discharge the battery to an unhealthy level (ALTERNATIVE ENERGY, 2020). Unnecessarily oversizing BESS leads to unnecessary expenses to the system while also making the system more complex which leads to high maintenance costs (WHOLESALE SOLAR, 2020). The

basic idea of BESS sizing is to select a battery that is compatible with the PV system while also meeting the load requirements without the risk of power outage or damage to the system.

4.6.1 BESS Sizing Based on Panel Manufacturers' Recommended Methodology

Depending on system requirements, there are several factors that panel manufacturers recommend to be considered when sizing BESS. Panel manufacturers currently size batteries considering factors such as the daily load demand, battery depth of discharge, system losses, days of autonomy, battery rated capacity, aging, specified limits of operation, nominal battery voltage, operating temperature, rate of discharge and other engineering design factors (ALTE STORE, [s.d.]; ALTERNATIVE ENERGY, 2020; BERNSTEIN, 1988; CRUZ, 2013; HEIDER, 2012; IEEE 485, 2019; IEEE STANDARDS COORDINATING COMMITTEE, 2019; LEONICS, 2013; LOADS, 2009; OPEN ELECTRICAL, 2017; SKH ARCHITECTS, 2017; SOLAR STIK, 2020; SOLAR TOWN, 2020; TEITELBAUM, 2016; TROJAN BATTERY COMPANY, [s.d.]; WEBB, [s.d.]; WHOLESALE SOLAR, 2020). Some other manufacturers like (CRUZ, 2013) also consider spill containment and seismic zone when sizing BESS for PV systems. Reference (ALTERNATIVE ENERGY, 2020) also considers the amount of money available to be spent on the solar project. The IEEE standards association has a board that provides recommended practices for sizing batteries for PV systems which is updated periodically. Some of these factors are explained.

a. Daily energy consumption

The total daily energy consumption in kWh is calculated. The load analysis is determined by the complexity of the load profile (TROJAN BATTERY COMPANY, [s.d.]). To calculate the load, multiply the power rating of each appliance (kW) by its running time (Hours) and the sum the values for each appliance. For example; If you have a 10kW load that runs for 3 hours and a 15kW load that runs for 5 hours, the total energy consumption will be;

Energy consumption = $(10kW * 3hrs) + (15kW * 5hrs) = 30kWh + 75kWh = 105kWh$

b. Days of Autonomy

Days of autonomy refers to the number of days that a fully charged battery can meet the energy consumption without being recharged (ALTERNATIVE ENERGY, 2020; BERNSTEIN, 1988). It can also be defined as the number of cloudy days in a row (days without sun) that might occur for which the battery will have to supply the load without being

recharged (LEONICS, 2013; SKH ARCHITECTS, 2017). The number of days is determined by analyzing and evaluating the peak hours of sun per day for the lowest insolation month of the year (LOADS, 2009). It is a factor that is considered when designing standalone PV systems. Autonomy is usually between two to five days (OPEN ELECTRICAL, 2017).

c. Depth of Discharge (DoD)

This defines the maximum usable capacity of the battery (amount of energy that can be used in a fully charged battery) as specified by the manufacturer (BERNSTEIN, 1988). Lead-acid batteries have about 50% DoD while lithium-ion batteries generally have about 80% DoD. It is advisable to limit the depth of discharge in cold climates in order to protect the battery from freezing (BERNSTEIN, 1988). Reference (TROJAN BATTERY COMPANY, [s.d.]) suggests that a shallow daily depth of discharge (max 20%) should be considered and a maximum of 80% on cloudy days.

d. System losses and operating temperature

System losses are included in BESS sizing calculations due to efficiencies of power conditioning (TROJAN BATTERY COMPANY, [s.d.]). The standard battery capacity rated temperature is 25^0C (WEBB, [s.d.]). High operating temperatures also affects the effective capacity of the battery bank (ALTE STORE, [s.d.]) and therefore is factored in BESS sizing calculations. Temperature change in batteries is much slower than ambient temperature change due to the mass of the batteries, therefore, the temperature of batteries is usually the average temperature for the past 24 hours plus or minus a few degrees (LOADS, 2009).

For example, a battery that operates in a very cold climate providing about 80% of its capacity may lose more than half of its expected life if it is required to operate in a very hot climate.

e. Aging

Battery capacity degrades with age. The older the battery, the lower it capacity. IEEE recommendation is that batteries be replaced at 80% of initial value (WEBB, [s.d.])(IEEE STANDARDS COORDINATING COMMITTEE, 2019).

For example, a battery capacity requirement of 240Ah should be adjusted by 80% to ensure adequate capacity at end of lifetime. This means that if the requirement is 240Ah, a battery capacity of 300Ah should be installed.

f. Battery capacity and Rate of discharge

When sizing a battery, rate of discharge has to be taken into consideration as the higher the rate of discharge, the higher the losses which leads to a decrease in the battery capacity. With the battery capacity in ampere-hour, the battery size in kWh can be calculated by multiplying the capacity by the nominal battery voltage.

To size BESS using the recommended methodology of panel manufacturers, this study used the most common factors considered for general analysis; daily load demand as presented in Figure 10 and Figure 11, 3 days of autonomy, 80% lithium-ion battery depth of discharge and system losses. Equation (22) represents the mathematical relationship between battery size in kWh and the factors considered in this research.

$$\text{Battery size (kWh)} = \frac{\text{Total daily load} \times \text{days of autonomy}}{\text{Depth of discharge} \times \text{system losses}} \tag{22}$$

4.6.2 BESS sizing Based on Proposed Methodology

To size the battery system using the proposed methodology, one year hourly synthetic series solar radiation data is generated and used in simulating a PV system in relation to the load demand and storage capacity for each of the case studies. The simulation enables one to observe the amount of hourly energy shortage and duration of interruption in the system.

The simulation setup is such that generated power is supplied directly to the load demand and excess power is stored in the BESS, and when the generation is less than demand, the BESS supplies the deficit. It is worthy to note that the BESS is fully charged at the beginning of the simulation.

The mathematical relationship between the simulation variables is such that, when generated power satisfies the load demand or when generated power combined with BESS satisfy the load demand, the output parameters (energy deficit and supply interruption) return null values. If there is shortage is any combination of the simulation input, the energy deficit output returns the amount of energy not supplied while the supply interruption output returns a unity value for each hour with deficit. Total interruption and deficit for the year are then used in calculating the percentage supply interruption and energy deficit for the year in relation to the total number of hours in the year and total load demand for the year respectively.

The battery size is continuously adjusted until acceptable energy deficit and supply interruptions are obtained. It is possible to attain battery sizing that ensures no energy deficit or supply interruption. The battery behavior for the whole year can also be observed in the simulation to have an insight on the charging and discharging cycle of the battery.

Total energy deficit for each series were calculated by summing up the hourly energy deficit for each series. The hourly energy deficit is the amount of hourly energy demand not supplied. The total supply interruptions for each series were also calculated which is the sum of the hourly interruptions for each series. In this study, it was assumed that there is a possibility of only one supply interruption per hour.

The percentage energy deficit as calculated, is defined as the ratio of total energy deficit in a series to the total demand multiplied by a hundred. The percentage supply interruptions is defined as the ratio of the sum of supply interruptions in a series to the total number of hours in the series.

This approach considers how much energy was supplied and the energy deficit for each hour. Plant power in STC and storage size were continuously altered to determine the energy deficit and the frequency of supply interruption for each combination.

This method is more adequate for the sizing of BESS as compared to the methodology recommended by panel manufacturers because future solar irradiance is considered in the proposed methodology as against the use of days of autonomy in the panel manufacturers method.

4.7 COST ANALYSIS

This study economically evaluated the BESS using two financial metrics; Net present value (NPV) and payback period (PBP).

Present value (PV) is the current value of a future sum of money or cash flow given a specific interest rate and is mathematically represented by equation (23).

$$PV = \frac{FV}{(1+i)^t} \tag{23}$$

Where:

FV is future value

i is interest rate

t is number of time periods

Figure 9 represents cash flow over the lifecycle of the battery. It is a way to evaluate the financial implications (cost and benefit) of investing in BESS and at the same time accounting for the current value of money. The total cost equivalent of the energy supplied (energy benefit) is the total arithmetic sum of individual years' present values of the cost equivalent of energy supplied for that year. Cost equivalent is the monetary value of the expected energy supplied per year. Total investment on the other hand is the total cash outflow which is the sum of initial investment, and the present value of the sum of O&M cost and cost equivalent of yearly expected energy deficit. Investment cost is the cost of installing the BESS while O&M cost of yearly maintenance of the BESS and equivalent cost of energy deficit in the monetary value of energy deficit or cost of interruption. The arithmetic difference between the total cost equivalent of expected energy supplied and total cost of investment determines the lifecycle cost of the system otherwise known as the net present value (NPV). The higher the NPV, the better the investment i.e. the greater the total cost equivalent of expected energy benefit over the total investment cost, the better.

Figure 9 – Cash flow diagram

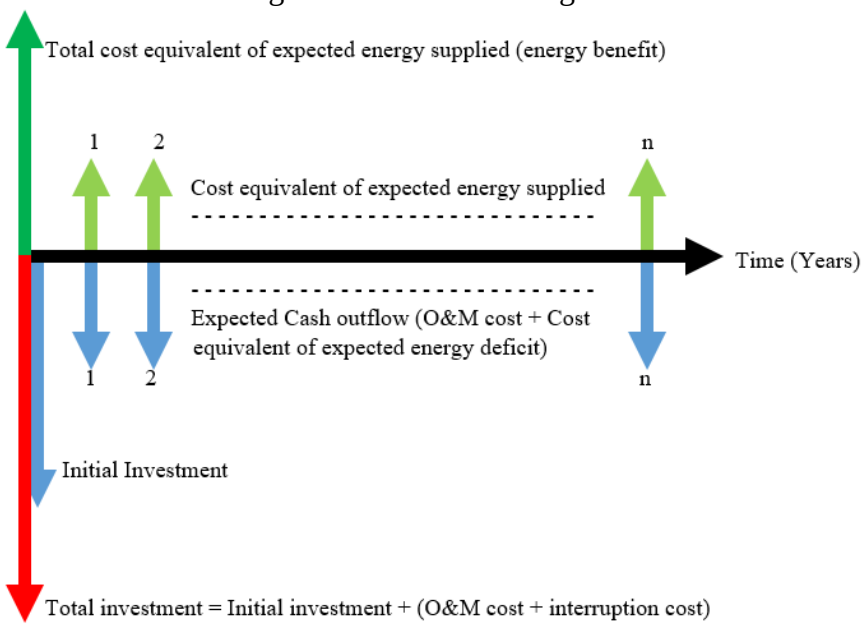

Source: Author

4.7.1 Net Present Value

The net present value (NPV) is a way to evaluate the lifecycle costs and benefits of BESS in PV systems while accounting for the time value of money. Lifecycle costs of BESS include BESS installation costs, O&M costs and cost of load demand energy not supplied by the system (energy deficit). Lifecycle benefit of BESS on the other hand is the cost equivalent of the energy supplied to the load by the system. A positive NPV signifies that the investment is predicted to yield greater returns or benefits than the summation of initial and future expenditures associated with the system and the higher the NPV, the better the benefit. A negative NPV however signifies that the benefits to be enjoyed from the investment is predicted to be less than the initial and future expenditures associated with the system. NPV is a useful financial metric to utilize when evaluating the economic performance of BESS in PV systems as it accounts for all expenditures including O&M and energy deficit or interruption costs over the lifecycle of the BESS. Equation (24) represents the mathematical expression of NPV.

$$NPV = \sum_{t=0}^{n} \frac{R_t}{(1+i)^t} \tag{24}$$

Where; R_t net cash flow during a single period t

i interest rate

t number of time periods

4.7.2 Payback Period

Payback period (PBP) represents the number of periods required for the flow of benefits to exceed capital invested. (PBP) quantifies the number of years it takes for the benefits in years two and later of the project to equal or exceed the initial cost. PBP is the financial metric with the ability to quickly communicate tangible value of a project. A system with low PBP is regarded as a profitable one as subsequent years of the system results in benefits for the system owner. However, a system with high PBP or a system that cannot be paid back over its lifecycle period is regarded as a poor investment because at the end of the systems' lifetime, more money will have been spent than the benefit enjoyed. In calculating the PBP, care must be taken to consider all expenditures in later years. The mathematical expression of PBP is presented in equation (25).

$$\text{PBP} = \frac{Initial\ Investment}{Net\ cash\ flow\ per\ period} \tag{25}$$

5.0 RESULTS AND DISCUSSION

In this chapter, the case study is presented and obtained results are analyzed and discussed. Two case studies were considered in the application and testing of the various steps of the methodology described in the previous chapter.

5.1 CASE STUDY

5.1.1 Load

Load profiles for two case studies were considered in this research as presented in Figure 10 and Figure 11. The first case study considered residential consumers located in the city of Abuja in Nigeria. The daily average load profile for these consumers in Figure 10 was obtained from (ECN, 2013). The second case study considered a commercial consumer located in the city of Campinas, Sao Paulo – Brazil and the daily load profile for the consumer in Figure 11 was obtained from (MARTINEZ-BOLANOS et al., 2020) and (ABRADEE, 2019).

Solar PV systems intended to supply power to consumers with similar daily average load profiles as in Figure 10 and Figure 11 were simulated. Yearly consumption profiles were simulated from the daily average load curves using regression models similar to those used in the prediction of solar radiation data presented in (ABUBAKAR; GEMIGNANI; MESCHINI ALMEIDA, 2019). It is worth noting that variations in hourly and daily consumption were duly accounted for in the simulation. Figure 12 and Figure 13 present the simulated hourly consumption profiles for a year for the residential and commercial consumers respectively.

Figure 10 – Daily load profile (Residential)

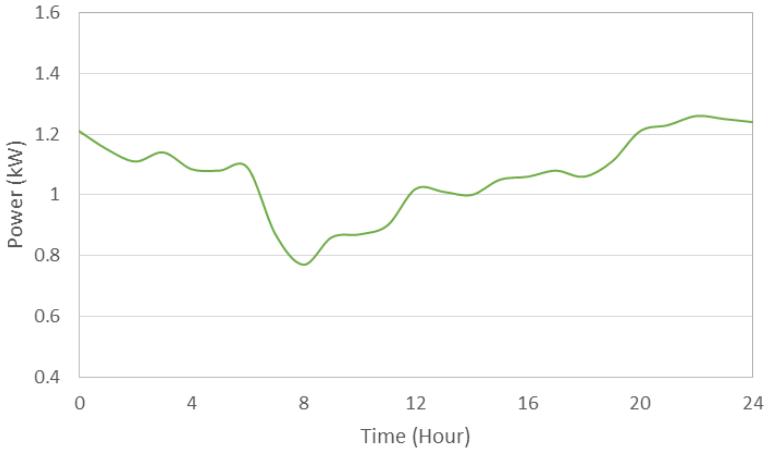

Source: (ECN, 2013)

Figure 11 – Daily load profile (Commercial)

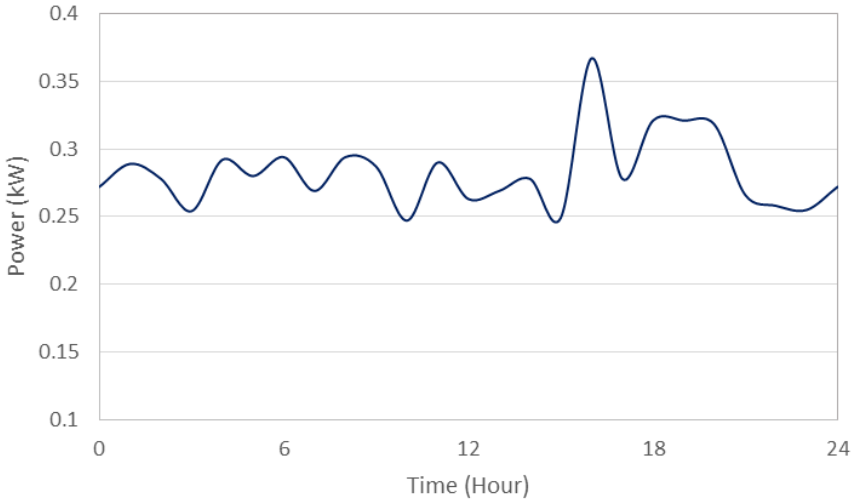

Source: (ABRADEE, 2019; MARTINEZ-BOLANOS et al., 2020)

Figure 12 – Simulated hourly power consumption profile for a year (Residential)

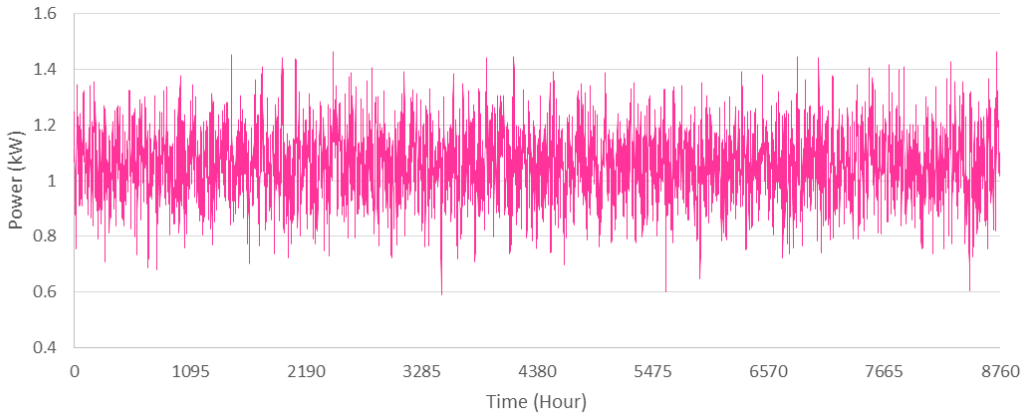

Source: Author

Figure 13 – Simulated hourly power consumption profile for a year (Commercial)

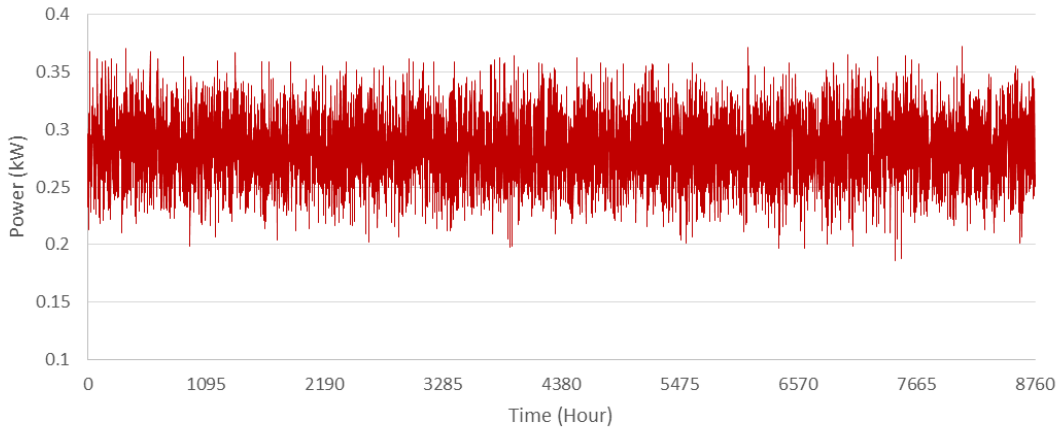

Source: Author

5.1.2 System Configuration

PV systems of 1.3kWdc and 0.4kWdc nameplate capacities were considered to serve the residential and commercial consumers respectively. Lithium ion battery chemistry was selected for the systems because of its superiority in energy efficiency, depth of discharge and lifecycle. For the cost evaluation, an analysis period of 15 years (lithium ion battery lifecycle (MONGIRD et al., 2019)) and interest rate of 7.5% (DIORIO; DOBOS; JANZOU, 2015) were considered. Interruption cost of 5.36 USD/kWh_{int} and tariff peak/off-peak cost of 0.4/0.14 USD/kWh were obtained from (SINAPSIS, 2016) and (MARTINEZ-BOLANOS et al., 2020) respectively. Other financial values used are presented in Table 5.

Table 5 – System cost

Variable	Cost
Module cost	0.71 $/Wdc (DIORIO; DOBOS; JANZOU, 2015)
Inverter cost	0.21 $/Wdc (DIORIO; DOBOS; JANZOU, 2015)
Battery cost	850 /kWh (MARTINEZ-BOLANOS et al., 2020)
Balance of System	0.57 $/Wdc (DIORIO; DOBOS; JANZOU, 2015)
Labor	0.15 $/Wdc (DIORIO; DOBOS; JANZOU, 2015)
Margin and overhead	0.75 $/Wdc (DIORIO; DOBOS; JANZOU, 2015)
Permit	0.06 $/Wdc (DIORIO; DOBOS; JANZOU, 2015)
O&M	20 $/kW-yr (DIORIO; DOBOS; JANZOU, 2015)

Source: (DIORIO; DOBOS; JANZOU, 2015)

5.2 RESULTS

For the sake of analysis, a set of one-hour estimated global solar irradiance data for the city of Petrolina in the northeastern part of Brazil was obtained from vortex website and used for this research. In total, a set of 175,200 entries (approximately twenty years) were recorded between 1996 and 2015. The data was obtained from satellite data estimation systems and

have resolution of three kilometers (3km) around the specific coordinates. For each month, there is a total of 720 measured points for a 30-day month, 744 measured points for 31-day month and 672 measured points for February. The data was then arranged in such a way that similar hour of each corresponding year were aligned.

In order to identify the states and relationships between the obtained sample data, the equations for the statistical properties presented in the previous chapter were used to obtain the results. Table 6 shows the hourly irradiance mean and standard deviation for ten (10) hours of January of the 20 years (1996-2015). Note that the first 6 hours have zero values due to insufficient solar irradiance to be converted to electricity, therefore were excluded from the table. Figure 14 and Figure 15 respectively show the mean solar irradiance and moving average of mean solar irradiance for the data used.

Table 6 – Mean and standard deviation for ten hours of January (1996-2015)

	7	**8**	**9**	**10**	**11**	**12**	**13**	**14**	**15**	**16**
1996	58.4	223.6	411.2	614.2	772.4	872	903.4	870.3	763.6	593.6
1997	28.9	170.6	339.7	531.9	693.3	790.9	840.2	786.7	657.9	501.2
1998	67.6	199	345.9	573.9	606.4	686.9	703.3	764.6	714.7	561.3
1999	68.7	250.3	458.5	674.3	822.6	912.8	921.3	846.9	734.7	542
2000	49.4	189.7	400.4	564.8	707.3	814.9	862.2	857.4	764.7	573.3
2001	72.3	258.2	461.2	653.7	785.5	872.8	900.1	836.1	703.8	499.7
2002	57	179	306.2	464.9	584.9	656.8	665	614.1	524.8	425.5
2003	86.9	300.4	499.7	680.4	836	925.1	899.4	839	793.2	600.1
2004	86.3	308.1	534.3	732.4	875.3	954.5	970.6	926.9	793.6	601.8
2005	72.2	291.5	519.2	722.5	866.3	955.4	989.3	945.2	814.1	614.9
2006	51.4	198.8	371.9	555.2	692.8	808.1	866	886.2	766.8	574.4
2007	88.8	301.6	529.3	753.9	910.6	993	1019.3	967	829.1	630.8
2008	79	268.2	451.4	633.8	754.4	872.2	906.1	876.4	779.3	582.5
2009	63	233.8	460.9	617.4	758.2	840.4	928	877.8	776.3	612.3
2010	26.8	164.4	112.7	84.2	151.3	388.3	517.1	409.9	376.2	265.9
2011	53.1	335.1	587.7	794.8	802.7	887	929.4	937.8	803.7	614.5
2012	44.5	336.9	585.8	630.7	889.7	979.5	978.3	966.3	858.5	670.6
2013	44.1	256.6	450.7	648.4	908.8	1017.5	1012.3	951	829	664.5
2014	89	345.6	597.6	812.1	955.5	1006.8	1029.8	987	864	658.6
2015	88	338.9	568.3	738.8	904.7	936.9	893.6	672.8	587	630.9
Mean	63.77	257.515	449.63	624.115	763.935	858.59	886.735	840.97	736.75	570.92
SD	18.969	59.135	114.38	151.567	172.33	143.889	124.125	136.537	117.442	91.276

Source: Author

Figure 14 – Mean hourly solar radiation

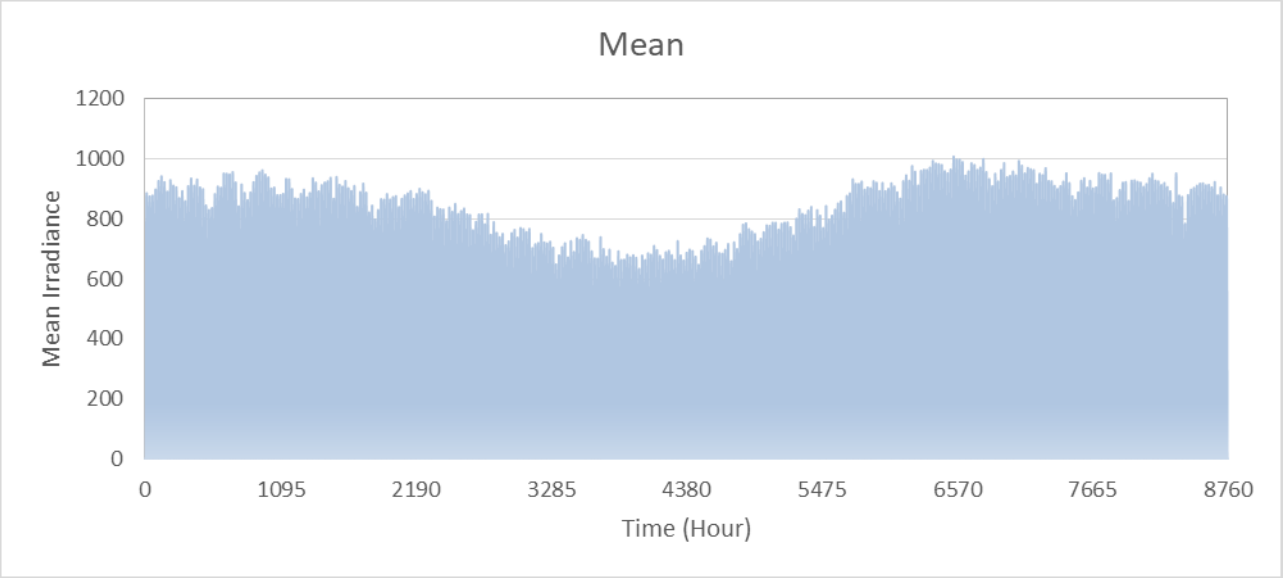

Source: Author

Figure 15 – Mean hourly solar radiation moving average

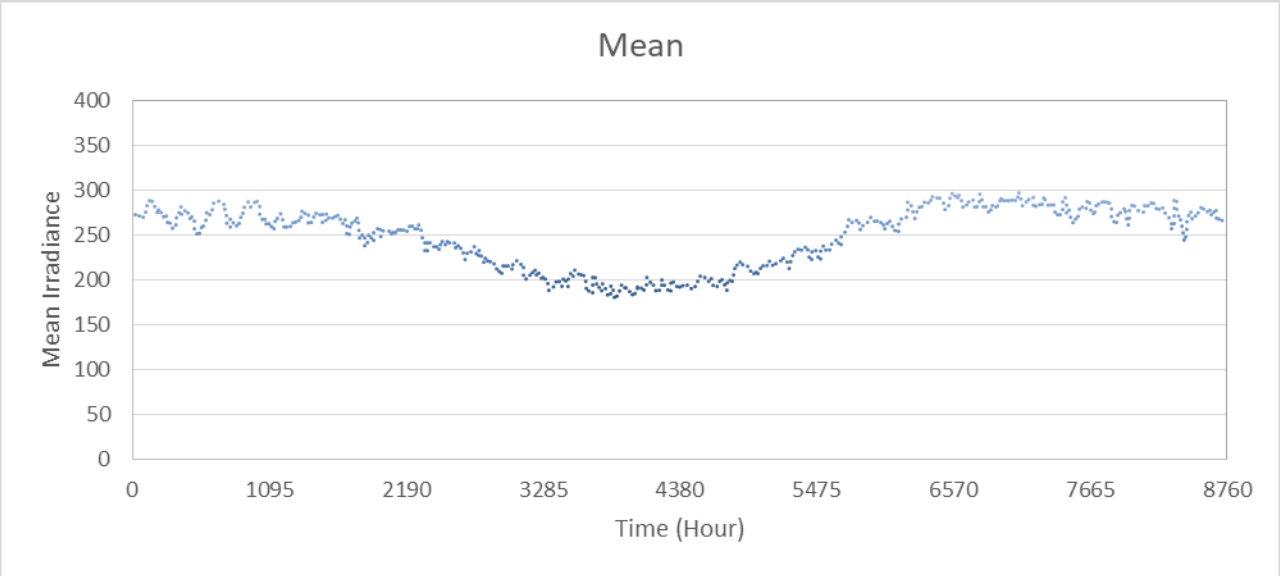

Source: Author

It can be seen from the Table 7 that when the seasonal component (trend) is removed, the standard deviation of each series becomes 1 except for the hours where zero (0) was recorded in which case the standard deviation is zero (0). The first 6 hours of the month were excluded here as well, due to insufficient solar irradiance returning zero (0) values.

Table 7 – Hourly radiation series pre-treated for trend removal

	7	8	9	10	11	12	13	14	15	16
1996	-0.283	-0.574	-0.336	-0.065	0.049	0.093	0.134	0.215	0.229	0.248
1997	-1.838	-1.470	-0.961	-0.608	-0.410	-0.470	-0.375	-0.397	-0.671	-0.764
1998	0.202	-0.990	-0.907	-0.331	-0.914	-1.193	-1.478	-0.559	-0.188	-0.105
1999	0.260	-0.122	0.078	0.331	0.340	0.377	0.278	0.043	-0.017	-0.317
2000	-0.758	-1.147	-0.430	-0.391	-0.329	-0.304	-0.198	0.120	0.238	0.026
2001	0.450	0.012	0.101	0.195	0.125	0.099	0.108	-0.036	-0.281	-0.780
2002	-0.357	-1.328	-1.254	-1.050	-1.039	-1.402	-1.786	-1.662	-1.805	-1.593
2003	1.219	0.725	0.438	0.371	0.418	0.462	0.102	-0.014	0.481	0.320
2004	1.188	0.855	0.740	0.714	0.646	0.667	0.676	0.629	0.484	0.338
2005	0.444	0.575	0.608	0.649	0.594	0.673	0.826	0.763	0.659	0.482
2006	-0.652	-0.993	-0.680	-0.455	-0.413	-0.351	-0.167	0.331	0.256	0.038
2007	1.319	0.745	0.697	0.856	0.851	0.934	1.068	0.923	0.786	0.656
2008	0.803	0.181	0.015	0.064	-0.055	0.095	0.156	0.259	0.362	0.127
2009	-0.041	-0.401	0.099	-0.044	-0.033	-0.126	0.332	0.270	0.337	0.453
2010	-1.949	-1.575	-2.946	-3.562	-3.555	-3.268	-2.978	-3.157	-3.070	-3.342
2011	-0.562	1.312	1.207	1.126	0.225	0.197	0.344	0.709	0.570	0.477
2012	-1.016	1.342	1.190	0.043	0.730	0.840	0.738	0.918	1.037	1.092
2013	-1.037	-0.015	0.009	0.160	0.841	1.104	1.012	0.806	0.785	1.025
2014	1.330	1.490	1.294	1.240	1.112	1.030	1.153	1.070	1.084	0.961
2015	1.277	1.376	1.037	0.757	0.817	0.544	0.055	-1.232	-1.275	0.657
SD	1	1	1	1	1	1	1	1	1	1

Source: Author

From the treated data, the autocorrelation and autocovariance functions were calculated for each month using equations (7) and (8) and the following results were obtained

Table 8 – Autocorrelation and autocovariance values

January		**February**		**March**		**April**	
$C_0 = 1.0000$	$r_0 = 1.0000$	$C_0 = 1.0000$	$r_0 = 1.0000$	$C_0 = 1.0000$	$r_0 = 1.0000$	$C_0 = 1.0000$	$r_0 = 1.0000$
$C_1 = 0.8006$	$r_1 = 0.8006$	$C_1 = 0.7182$	$r_1 = 0.7182$	$C_1 = 0.7624$	$r_1 = 0.7624$	$C_1 = 0.7540$	$r_1 = 0.7540$
$C_2 = 0.6506$	$r_2 = 0.6506$	$C_2 = 0.5406$	$r_2 = 0.5406$	$C_2 = 0.6176$	$r_2 = 0.6176$	$C_2 = 0.6104$	$r_2 = 0.6104$
$C_3 = 0.5568$	$r_3 = 0.5568$	$C_3 = 0.4558$	$r_3 = 0.4558$	$C_3 = 0.5317$	$r_3 = 0.5317$	$C_3 = 0.5257$	$r_3 = 0.5257$
$C_4 = 0.4891$	$r_4 = 0.4891$	$C_4 = 0.4112$	$r_4 = 0.4112$	$C_4 = 0.4695$	$r_4 = 0.4695$	$C_4 = 0.4714$	$r_4 = 0.4714$
$C_5 = 0.4496$	$r_5 = 0.4496$	$C_5 = 0.3880$	$r_5 = 0.3880$	$C_5 = 0.4312$	$r_5 = 0.4312$	$C_5 = 0.4267$	$r_5 = 0.4267$
May		**June**		**July**		**August**	
$C_0 = 1.0000$	$r_0 = 1.0000$	$C_0 = 1.0000$	$r_0 = 1.0000$	$C_0 = 1.0000$	$r_0 = 1.0000$	$C_0 = 1.0000$	$r_0 = 1.0000$
$C_1 = 0.7737$	$r_1 = 0.7737$	$C_1 = 0.7988$	$r_1 = 0.7988$	$C_1 = 0.7872$	$r_1 = 0.7872$	$C_1 = 0.7767$	$r_1 = 0.7767$
$C_2 = 0.6113$	$r_2 = 0.6113$	$C_2 = 0.6421$	$r_2 = 0.6421$	$C_2 = 0.6137$	$r_2 = 0.6137$	$C_2 = 0.6157$	$r_2 = 0.6157$
$C_3 = 0.5097$	$r_3 = 0.5097$	$C_3 = 0.5395$	$r_3 = 0.5395$	$C_3 = 0.5027$	$r_3 = 0.5027$	$C_3 = 0.5140$	$r_3 = 0.5140$
$C_4 = 0.4414$	$r_4 = 0.4414$	$C_4 = 0.4659$	$r_4 = 0.4659$	$C_4 = 0.4198$	$r_4 = 0.4198$	$C_4 = 0.4416$	$r_4 = 0.4416$
$C_5 = 0.3956$	$r_5 = 0.3956$	$C_5 = 0.4042$	$r_5 = 0.4042$	$C_5 = -0.3639$	$r_5 = -0.3639$	$C_5 = 0.3899$	$r_5 = 0.3899$
September		**October**		**November**		**December**	
$C_0 = 1.0000$	$r_0 = 1.0000$	$C_0 = 1.0000$	$r_0 = 1.0000$	$C_0 = 1.0000$	$r_0 = 1.0000$	$C_0 = 1.0000$	$r_0 = 1.0000$
$C_1 = 0.8162$	$r_1 = 0.8162$	$C_1 = 0.8155$	$r_1 = 0.8155$	$C_1 = 0.8376$	$r_1 = 0.8376$	$C_1 = 0.8181$	$r_1 = 0.8181$
$C_2 = 0.6675$	$r_2 = 0.6675$	$C_2 = 0.6638$	$r_2 = 0.6638$	$C_2 = 0.7050$	$r_2 = 0.7050$	$C_2 = 0.7001$	$r_2 = 0.7001$
$C_3 = 0.5755$	$r_3 = 0.5755$	$C_3 = 0.5703$	$r_3 = 0.5703$	$C_3 = 0.6112$	$r_3 = 0.6112$	$C_3 = 0.6286$	$r_3 = 0.6286$
$C_4 = 0.5011$	$r_4 = 0.5011$	$C_4 = 0.4958$	$r_4 = 0.4958$	$C_4 = 0.5438$	$r_4 = 0.5438$	$C_4 = 0.5795$	$r_4 = 0.5795$
$C_5 = 0.4498$	$r_5 = 0.4498$	$C_5 = 0.4503$	$r_5 = 0.4503$	$C_5 = 0.4975$	$r_5 = 0.4975$	$C_5 = 0.5399$	$r_5 = 0.5399$

Source: Author

Application of the Yule-Walker equation yielded the values of $\hat{\phi}_1$ to $\hat{\phi}_n$. The values are presented in Table 9

Table 9 – Yule-walker equation values

January	February	March	April	May	June
$\hat{\phi}_1$ = **0.8006**	$\hat{\phi}_1$ = 0.7182	$\hat{\phi}_1$ = 0.7624	$\hat{\phi}_1$ = 0.7539	$\hat{\phi}_1$ = 0.7737	$\hat{\phi}_1$ = 0.7988
$\hat{\phi}_2$ = **0.0268**	$\hat{\phi}_2$ = 0.0512	$\hat{\phi}_2$ = 0.0870	$\hat{\phi}_2$ = 0.0974	$\hat{\phi}_2$ = 0.0316	$\hat{\phi}_2$ = 0.0114
$\hat{\phi}_3$ = **0.0792**	$\hat{\phi}_3$ = 0.1049	$\hat{\phi}_3$ = 0.0852	$\hat{\phi}_3$ = 0.0866	$\hat{\phi}_3$ = 0.0679	$\hat{\phi}_3$ = 0.0643
$\hat{\phi}_4$ = **0.0442**	$\hat{\phi}_4$ = 0.0810	$\hat{\phi}_4$ = 0.0516	$\hat{\phi}_4$ = 0.0692	$\hat{\phi}_4$ = 0.0497	$\hat{\phi}_4$ = 0.0394
$\hat{\phi}_5$ = **0.0710**	$\hat{\phi}_5$ = 0.0774	$\hat{\phi}_5$ = 0.0631	$\hat{\phi}_5$ = 0.0407	$\hat{\phi}_5$ = 0.0487	$\hat{\phi}_5$ = 0.0151
July	**August**	**September**	**October**	**November**	**December**
$\hat{\phi}_1$ = **0.7872**	$\hat{\phi}_1$ = 0.7767	$\hat{\phi}_1$ = 0.8162	$\hat{\phi}_1$ = 0.8155	$\hat{\phi}_1$ = 0.8376	$\hat{\phi}_1$ = 0.8181
$\hat{\phi}_2$ = **-0.0157**	$\hat{\phi}_2$ = 0.0313	$\hat{\phi}_2$ = 0.0039	$\hat{\phi}_2$ = -0.0037	$\hat{\phi}_2$ = 0.0115	$\hat{\phi}_2$ = 0.0932
$\hat{\phi}_3$ = **0.0641**	$\hat{\phi}_3$ = 0.0667	$\hat{\phi}_3$ = 0.0890	$\hat{\phi}_3$ = 0.0895	$\hat{\phi}_3$ = 0.0598	$\hat{\phi}_3$ = 0.1006
$\hat{\phi}_4$ = **0.0211**	$\hat{\phi}_4$ = 0.0399	$\hat{\phi}_4$ = 0.0192	$\hat{\phi}_4$ = 0.0208	$\hat{\phi}_4$ = 0.0500	$\hat{\phi}_4$ = 0.0732
$\hat{\phi}_5$ = **0.0416**	$\hat{\phi}_5$ = 0.0394	$\hat{\phi}_5$ = 0.0525	$\hat{\phi}_5$ = 0.0697	$\hat{\phi}_5$ = 0.0554	$\hat{\phi}_5$ = 0.0499

Source: Author

Thus, solving the linear system of the AR (5) model for the data series, the equation for each month can be written as:

January

$$z_t = 0.8006\, z_{t-1} + 0.0268\, z_{t-2} + 0.0792\, z_{t-3} + 0.0442\, z_{t-4} + 0.0710\, z_{t-5} + a_t$$

February

$$z_t = 0.7182\, z_{t-1} + 0.0512\, z_{t-2} + 0.1049\, z_{t-3} + 0.08102\, z_{t-4} + 0.0774\, z_{t-5} + a_t$$

March

$$z_t = 0.7624\, z_{t-1} + 0.0870\, z_{t-2} + 0.0852\, z_{t-3} + 0.0516\, z_{t-4} + 0.0631\, z_{t-5} + a_t$$

April

$$z_t = 0.7539\, z_{t-1} + 0.0974\, z_{t-2} + 0.0866\, z_{t-3} + 0.0692\, z_{t-4} + 0.0407\, z_{t-5} + a_t$$

May

$$z_t = 0.7737\, z_{t-1} + 0.0316\, z_{t-2} + 0.0679\, z_{t-3} + 0.0497\, z_{t-4} + 0.0487\, z_{t-5} + a_t$$

June

$$z_t = 0.7988\, z_{t-1} + 0.0114\, z_{t-2} + 0.0643\, z_{t-3} + 0.0394\, z_{t-4} + 0.0151\, z_{t-5} + a_t$$

July

$$z_t = 0.7872\, z_{t-1} - 0.0157\, z_{t-2} + 0.0641\, z_{t-3} + 0.0211\, z_{t-4} + 0.0416\, z_{t-5} + a_t$$

August

$$z_t = 0.7767\, z_{t-1} + 0.0313\, z_{t-2} + 0.0667\, z_{t-3} + 0.0399\, z_{t-4} + 0.0394\, z_{t-5} + a_t$$

September

$$z_t = 0.8162\, z_{t-1} + 0.0039\, z_{t-2} + 0.0890\, z_{t-3} + 0.0192\, z_{t-4} + 0.0525\, z_{t-5} + a_t$$

October

$$z_t = 0.8155\, z_{t-1} - 0.0037\, z_{t-2} + 0.0895\, z_{t-3} + 0.0208\, z_{t-4} + 0.0697\, z_{t-5} + a_t$$

November

$$z_t = 0.8376\, z_{t-1} + 0.0115\, z_{t-2} + 0.0598\, z_{t-3} + 0.0500\, z_{t-4} + 0.0554\, z_{t-5} + a_t$$

December

$$z_t = 0.8181\, z_{t-1} + 0.0932\, z_{t-2} + 0.1006\, z_{t-3} + 0.0732\, z_{t-4} + 0.0499\, z_{t-5} + a_t$$

Where t = 1...N

The residual a_t calculated using equation (12) for AR (1), AR (2), AR (3), AR (4) and AR (5) are represented using histograms. The histograms representing the equation for January are presented in Figure 16. The histogram for the months of February to December are presented in ANNEX I.

Figure 16 – Residual a_t for January

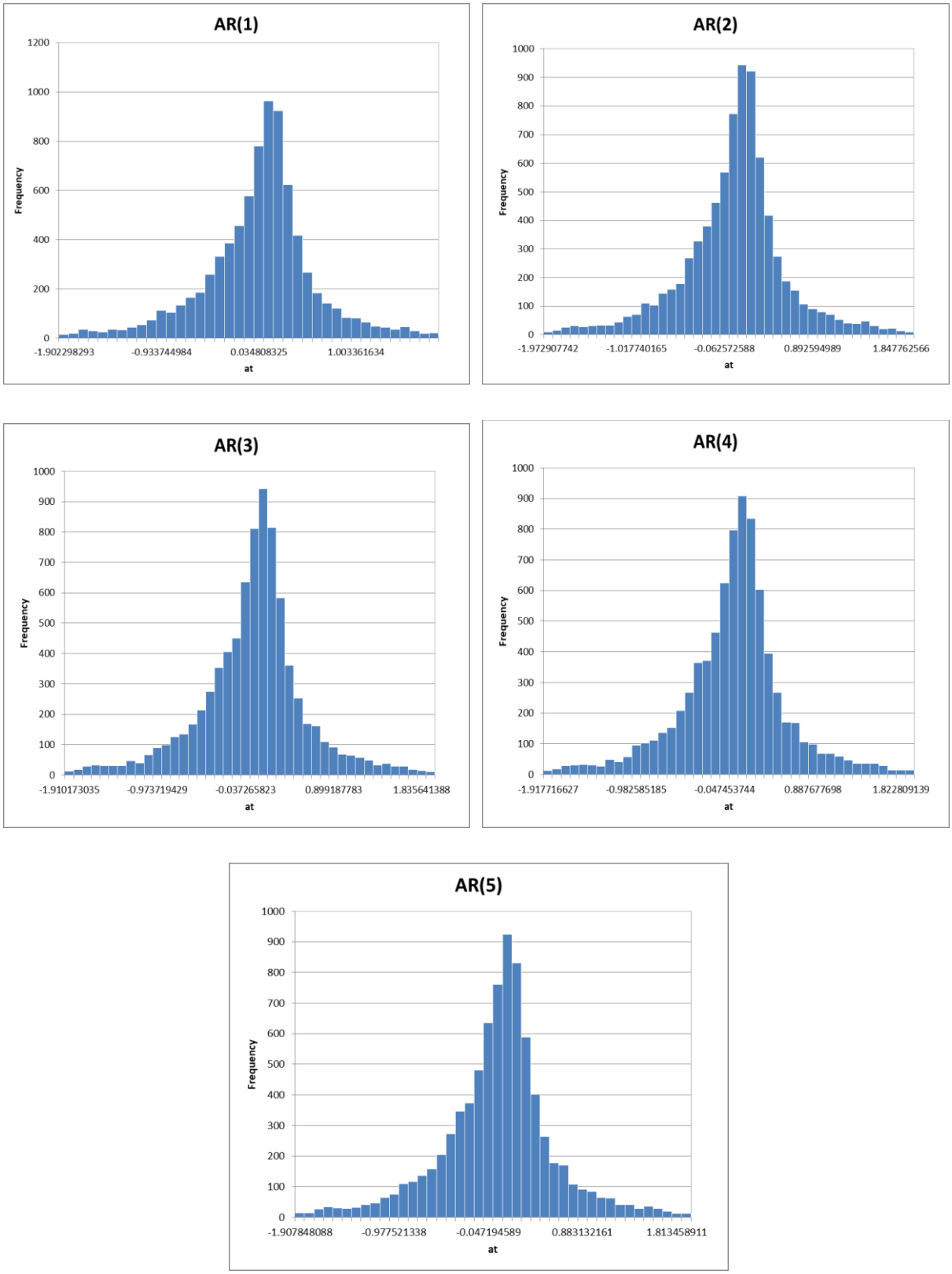

Source: Author

The models obtained were verified by comparative method between the observed forecasts and the generated forecasts. Comparison indices (root mean square error, absolute mean error, relative mean error and maximum relative percentage error) represented by equations (15), (16), (17) and (18) were used to achieve this. A set of forecasts were produced per month for one year ahead with the residue. The predictions were then applied to the error calculation formulas and results were obtained. It was observed that the error results for the hourly data have better resolutions than the daily data. The results for January are presented by Table 10 and Figure 17. The results for February to December are presented in ANNEX II

Table 10 – Error values by comparative method for January

	Error (pu)			
Models	**RMSE**	**AME**	**RMPE**	**PEmax**
AR(1)	1.0000	1.0000	0.9373	0.8760
AR(2)	0.9997	0.9996	0.9624	0.9266
AR(3)	0.9966	0.9980	1.0000	1.0000
AR(4)	0.9957	0.9971	0.9763	0.9432
AR(5)	0.9933	0.9955	0.8595	0.6903

Source: Author

Figure 17 – Graphical representation of errors for January

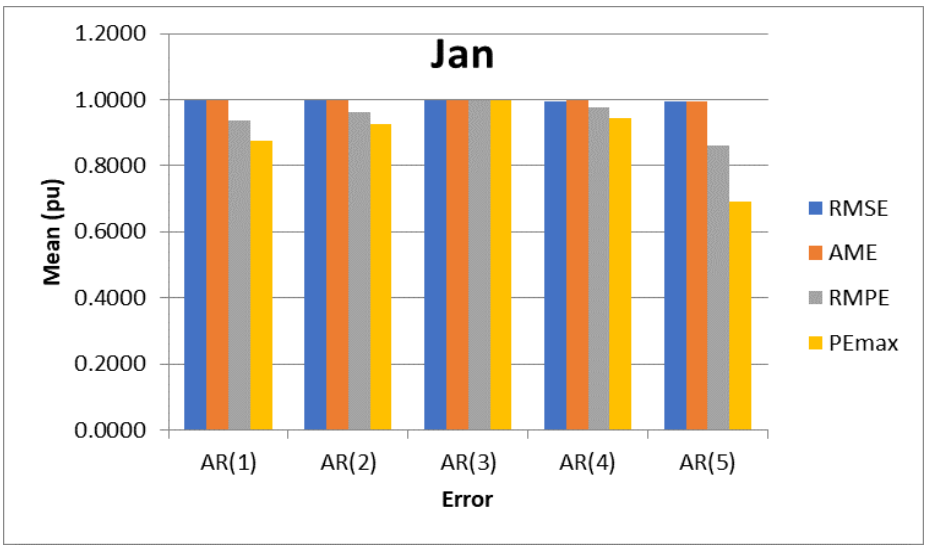

Source: Author

Another method used to validate the models is the confidence interval method. This was achieved using equation (19). The results of the 95% confidence intervals for January are presented in Figure 18. The confidence interval of February to December can be seen in ANNEX III.

Figure 18 – Confidence interval graph for January

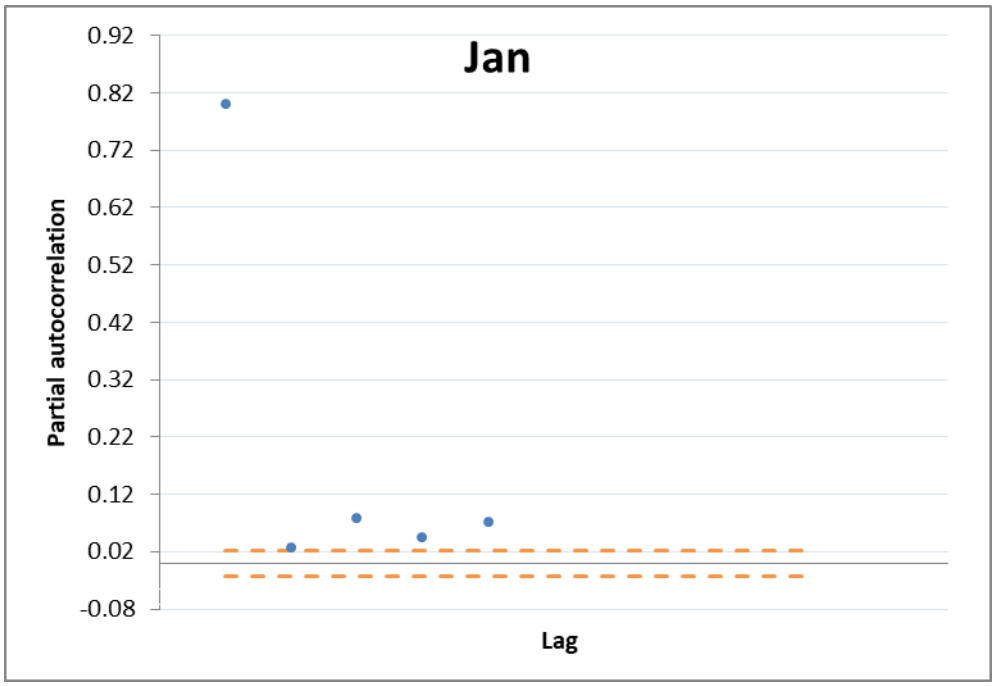

Source: Author

Both validation methods showed that the model is adequate thus, we can proceed to the next step which is the prediction and generation of synthetic series.

Table 11 presents a sample of the generated synthetic series using the obtained AR models. It is worthy of note that these generated series are without the trend component.

Table 12 shows the synthetic series after the reintroduction of the trend component. It can be observed that after the reintroduction of the trend. The first 6 hours with zero values were excluded from the table.

Table 13 represents a sample of electric component obtained using the generated synthetic series data.

Table 11 – Sample of the generated synthetic series

1	2	3	4	5	6	7	8	9	10
-0.543	-0.880	0.850	0.908	0.765	1.001	-0.828	-1.227	0.147	0.553
1.252	1.013	1.442	1.610	1.429	1.937	1.958	1.866	1.933	0.386
-0.589	-0.666	-1.215	-0.811	-0.975	-1.341	-2.494	-1.516	-2.402	-1.797
0.509	0.166	-1.019	-0.716	-0.217	-1.565	-1.182	-1.554	-0.533	-0.343
0.275	0.588	0.383	-0.848	-0.152	0.483	1.530	0.854	2.385	1.975
1.312	0.974	2.186	2.238	2.373	0.982	1.538	-0.111	0.544	0.917
-0.764	-0.095	0.508	1.027	2.226	1.689	1.688	1.215	-0.195	0.685
0.024	-1.187	-0.019	0.077	-1.078	-0.361	-1.039	-2.298	-2.169	-0.843
-0.392	-0.071	-0.248	-0.879	-1.222	-1.286	-1.114	-1.700	-1.291	-0.851
1.535	1.659	0.462	0.888	-0.056	0.300	-0.652	-1.744	-1.574	-0.873
0.165	0.618	0.326	-0.126	0.394	0.539	0.373	0.452	-0.417	-0.791
-1.067	-0.526	0.553	0.817	1.450	2.480	2.356	1.890	0.904	2.014
-0.747	-0.671	0.432	0.834	0.328	-0.289	2.053	2.260	1.545	1.449
-0.343	-0.484	0.262	-0.001	1.302	1.336	2.862	2.633	1.349	0.809
-0.417	-1.044	-0.259	0.159	1.058	2.349	1.272	0.598	1.138	1.026
-0.635	0.184	0.146	-0.948	-1.249	0.226	-0.918	-1.775	-1.497	-1.888
0.033	-0.507	-0.743	-0.290	0.440	-0.059	1.008	0.643	0.373	-0.408
0.731	0.813	-0.273	-0.321	1.125	1.812	1.815	1.399	1.323	1.554
1.392	1.019	0.819	0.814	0.370	1.927	2.736	2.624	0.726	0.941

Source: Author

Table 12 – Synthetic series sample after trend component reintroduction

7	8	9	10	11	12	13	14	15	16
107.70	324.48	563.02	735.79	915.82	1150.16	989.83	992.26	983.82	751.07
82.10	368.69	583.84	778.79	824.01	996.29	970.69	953.74	989.84	777.25
103.50	365.09	618.86	794.02	886.51	1097.33	1187.91	1074.97	1032.71	722.87
42.59	241.81	462.82	709.03	663.40	922.09	836.93	722.84	596.14	392.41
63.97	279.97	559.05	730.01	994.77	1026.40	932.58	1085.00	1167.97	904.59
82.93	305.24	640.90	594.36	857.42	855.01	879.98	843.46	666.44	532.36
68.03	197.64	264.30	351.77	812.98	827.75	965.35	893.33	720.79	632.43
72.87	299.62	546.45	629.43	715.71	923.11	898.33	952.66	759.95	531.68
115.93	396.78	653.90	710.50	828.85	768.30	832.48	835.86	712.50	544.95
98.50	362.54	665.31	935.09	1222.54	1330.63	1202.63	1167.89	874.06	728.61
88.11	207.57	252.38	408.71	752.91	896.61	909.72	919.87	826.02	673.05
86.63	285.72	369.93	435.25	748.74	967.78	890.10	770.67	850.93	646.82
87.06	329.47	422.91	724.80	853.71	960.21	1035.41	1053.59	842.78	691.84
46.80	263.33	427.45	751.27	936.04	1100.03	1060.60	1076.51	934.81	749.03
40.49	169.52	277.44	516.83	658.99	873.65	800.38	729.33	554.81	643.74
74.07	254.13	327.81	394.04	577.42	773.40	1001.16	985.47	948.32	682.15
109.36	390.62	663.38	831.40	837.30	977.92	791.64	721.16	621.58	418.71
59.16	302.41	620.85	836.26	1024.45	1067.78	941.39	835.88	905.76	826.41

Source: Author

Table 13 – Sample of electric component of the synthetic series

7	8	9	10	11	12	13	14	15	16
130.05	391.80	679.85	888.47	1105.85	1388.82	1195.22	1198.15	1187.97	906.91
99.13	445.20	704.99	940.39	994.99	1203.02	1172.11	1151.64	1195.23	938.52
124.97	440.84	747.27	958.78	1070.46	1325.02	1434.40	1298.02	1247.00	872.86
51.43	291.99	558.86	856.16	801.06	1113.42	1010.59	872.83	719.84	473.84
77.24	338.06	675.06	881.49	1201.18	1239.38	1126.09	1310.14	1410.32	1092.29
100.14	368.57	773.89	717.69	1035.34	1032.42	1062.57	1018.47	804.73	642.83
82.15	238.65	319.15	424.76	981.67	999.50	1165.66	1078.70	870.35	763.66
87.99	361.79	659.84	760.04	864.22	1114.66	1084.73	1150.34	917.64	642.01
139.98	479.11	789.59	857.93	1000.84	927.72	1005.22	1009.30	860.35	658.03
118.94	437.77	803.36	1129.12	1476.22	1606.74	1452.18	1410.23	1055.43	879.80
106.39	250.64	304.75	493.52	909.14	1082.66	1098.49	1110.74	997.41	812.71
104.61	345.01	446.69	525.56	904.11	1168.59	1074.80	930.59	1027.49	781.04
105.13	397.84	510.67	875.20	1030.86	1159.46	1250.26	1272.21	1017.66	835.40
56.51	317.97	516.14	907.16	1130.26	1328.29	1280.67	1299.88	1128.79	904.45
48.89	204.70	335.01	624.07	795.73	1054.93	966.46	880.67	669.93	777.31
89.44	306.87	395.83	475.81	697.23	933.88	1208.90	1189.96	1145.09	823.69
132.05	471.68	801.03	1003.91	1011.04	1180.84	955.91	870.80	750.56	505.59
71.44	365.17	749.68	1009.79	1237.02	1289.34	1136.73	1009.33	1093.71	997.89
128.98	455.18	811.82	952.78	989.47	961.59	933.25	967.05	1055.45	802.14
76.36	344.99	651.10	1143.37	1328.56	1299.72	1212.06	1253.00	1198.37	976.56
91.16	293.45	490.46	560.29	922.90	986.53	859.04	864.93	933.81	774.85
80.34	329.60	361.53	453.09	569.56	923.68	881.11	893.64	658.11	626.35
99.32	293.15	501.49	533.61	788.55	862.69	1039.42	1051.90	921.18	603.15
92.38	377.97	603.44	795.53	952.08	1282.26	1176.84	1051.58	960.02	641.25
86.87	299.38	643.76	952.06	1322.10	1398.96	1349.51	1194.46	1133.34	896.28
120.09	442.40	710.08	914.79	1170.47	1314.39	1324.25	1023.79	956.78	930.87
63.17	346.48	548.10	814.47	1258.37	1346.77	1372.46	1247.09	1086.32	784.81
79.39	296.22	506.22	829.35	1150.58	1059.74	1112.84	857.83	858.47	811.39

Source: Author

After successfully predicting the solar radiation behavior, the data was then used in the sizing of BESS with regards to the two case studies introduced in the previous chapter.

Table 14 and Table 15 present the proposed method's simulation results for the residential consumers considering synthetic and measured solar radiation data respectively. Simulations for different battery sizes were carried out with respect to the load profile and percentages of energy deficits and supply interruptions were calculated. Percentage energy deficit is the ratio of the total hourly deficit for the year to the total energy demand for the year and percentage interruption is the ratio of the total hourly interruptions for the year to the total number of hours in the year.

Table 14 – Simulation results for the residential consumers (synthetic)

BESS size (kWh)	Residential Consumer (Synthetic)		
	Number of Interruptions	Percentage Interruptions (%)	Percentage Deficit (%)
19.2	0	0.0	0.0
16	38	0.4	0.2
14.9	166	1.9	1.0
14.7	217	2.5	1.3
14.5	260	3.0	1.7
14.2	319	3.6	2.1
14	378	4.3	2.6
13.8	476	5.4	3.3

Source: Author

Table 15 – Simulation results for the residential consumers (Measured)

BESS size (kWh)	Residential Consumer (Measured)		
	Number of Interruptions	Percentage Interruptions (%)	Percentage Deficit (%)
17.7	0	0.0	0.0
16.7	13	0.1	0.1
15.7	52	0.6	0.3
14.7	199	2.3	1.2
14.5	240	2.7	1.5
14.3	296	3.4	1.9
13.9	415	4.7	2.9
13.7	482	5.5	3.4

Source: Author

Graphs of percentage interruption and percentage deficit were plotted for synthetic series data and measured data. In Figure 19 and Figure 20, it can be observed that there is only a slight difference between the results of the synthetic and the measured data.

It can also be observed from the graphs that as the battery size increases, the difference in energy deficit and supply interruption between battery sizes decreases. Therefore, one has to consider available BESS budget to decide between spending more money on battery and accepting a certain percentage of energy loss. This methodology provides flexibility and options in deciding the BESS size to use in a particular system. Decision can be made based on budget, physical size of battery or desired energy quality.

Figure 19 – Percentage interruption (Residential consumer)

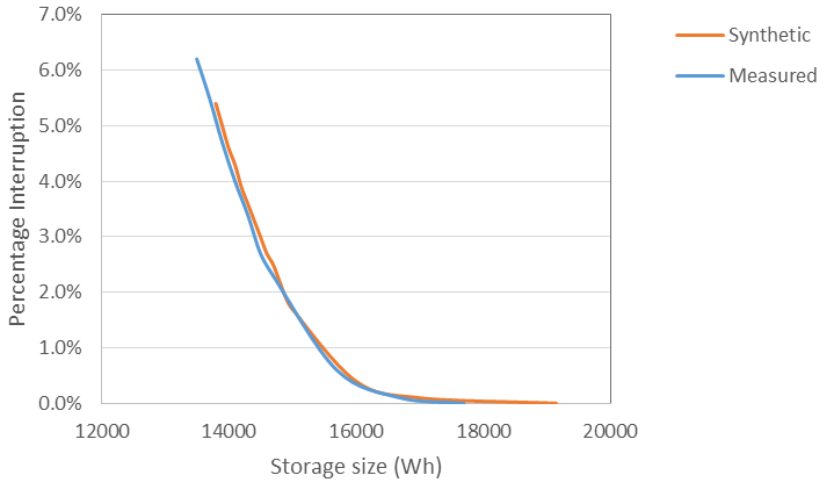

Source: Author

Figure 20 – Percentage deficit (Residential consumer)

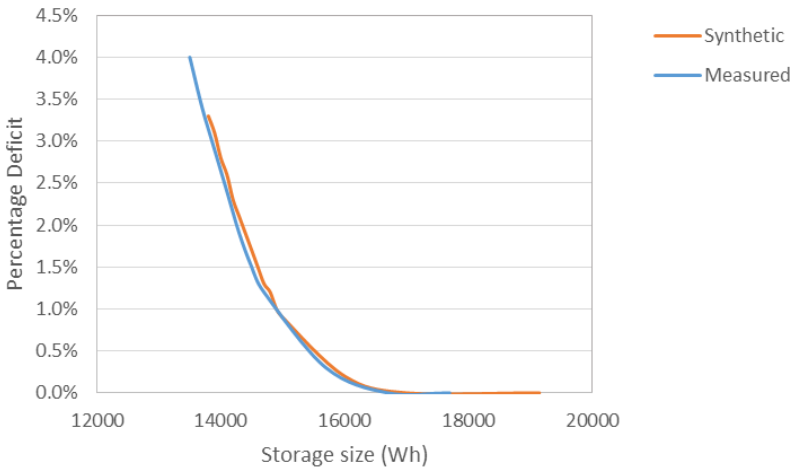

Source: Author

The proposed method's simulation results of different battery sizes for the commercial consumer are presented in Table 16 and Table 17. As in the residential consumer case study, simulations were carried out for both the synthetic series data and the measured data and percentage energy deficit and percentage supply interruptions were calculated. It can be observed here also that there is only a slight difference between the results of the synthetic and the measured data. Figure 21 and Figure 22 represent the graphs of the simulation results.

Table 16 – Simulation results for the commercial consumers (synthetic)

BESS size (kWh)	**Commercial Consumer (Synthetic)**		
	Number of Interruptions	**Percentage Interruptions (%)**	**Percentage Deficit (%)**
6.5	0	0.0	0.0
4.5	27	0.3	0.1
4.3	66	0.8	0.3
4.1	181	2.1	0.8
4.0	311	3.6	1.4
3.9	449	5.1	2.4
3.8	599	6.8	3.6
3.7	758	8.7	5.0

Source: Author

Figure 21 – Percentage interruption (commercial consumer)

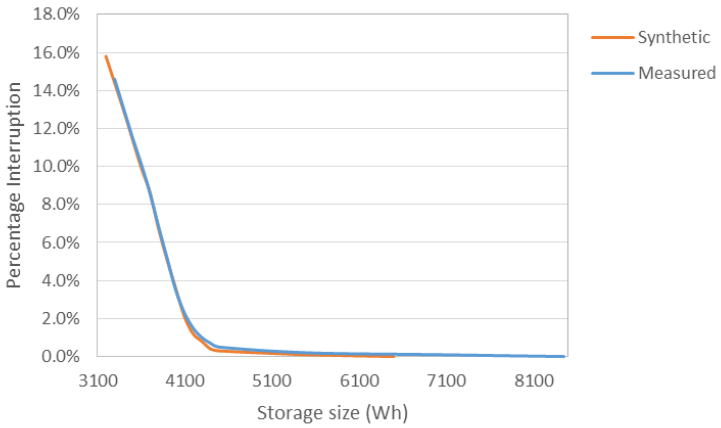

Source: Author

Table 17 – Simulation results for the commercial consumers (Measured)

BESS size (kWh)	Commercial Consumer (Measured)		
	Number of Interruptions	Percentage Interruptions (%)	Percentage Deficit (%)
7.0	6	0.1	0.1
4.5	44	0.5	0.3
4.4	58	0.7	0.4
4.1	199	2.3	1.0
4.0	304	3.5	1.6
3.9	455	5.2	2.5
3.8	602	6.9	3.6
3.7	760	8.7	4.9

Source: Author

Figure 22 – Percentage deficit (commercial consumer)

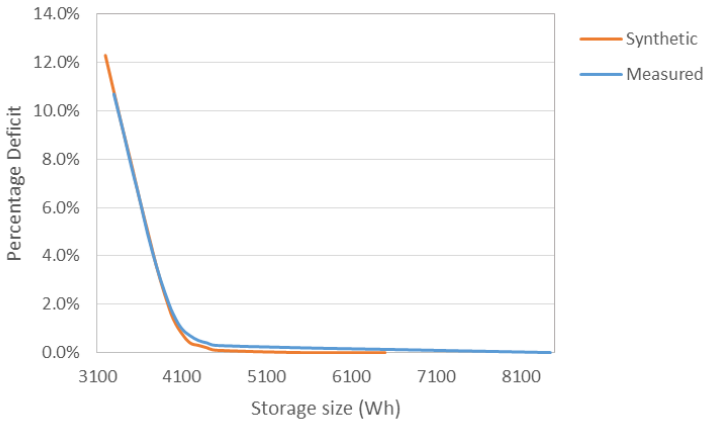

Source: Author

Figure 23 and Figure 24 present closer examination of the behavior of the residential consumers' PV system with change in simulation variables for one synthetic scenario (a set of 1-year hourly data). Depending on the requirement of the system, appropriate percentage of energy deficit and supply interruption can be achieved. Both graphs suggest that the best combination to attain better energy supply falls within the light blue area due to low

percentage supply interruption and energy deficit of storage and power combinations that fall with the area.

Figure 23 – Percentage hourly supply interruption (Residential consumer).

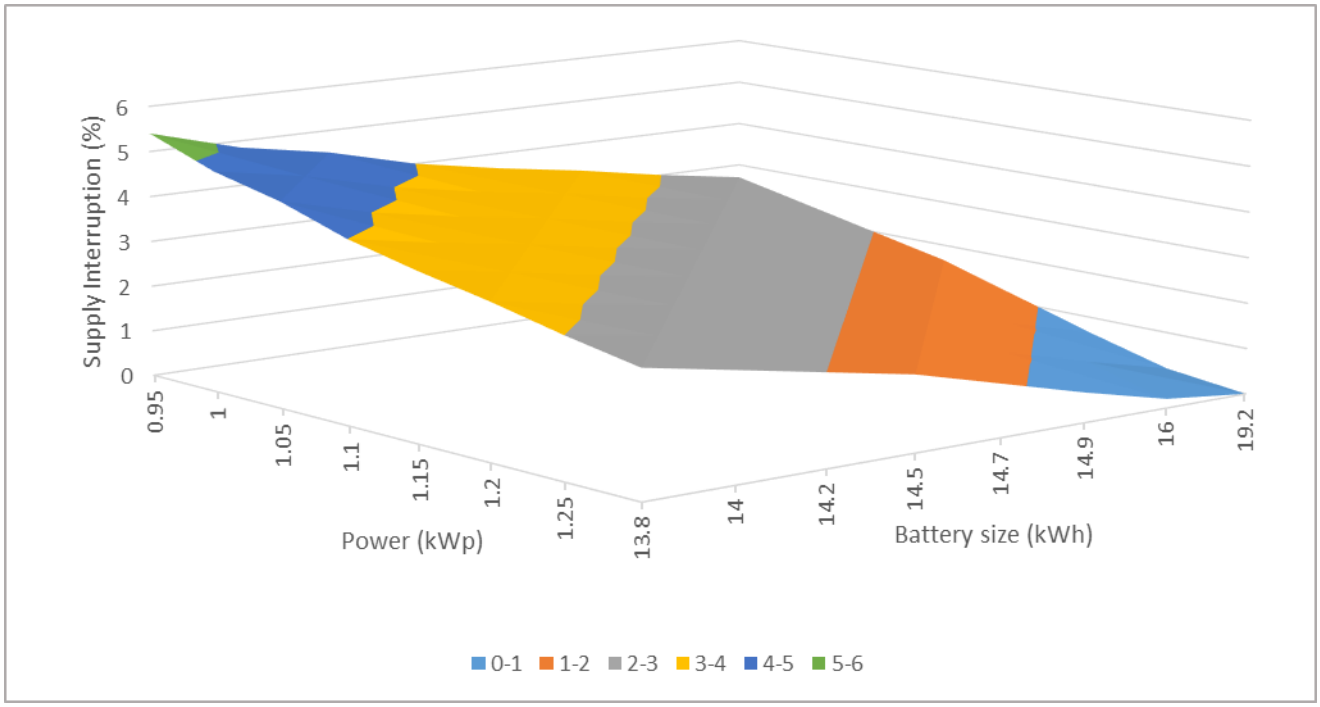

Source: Author

Figure 24 – Percentage hourly energy deficit (Residential consumer).

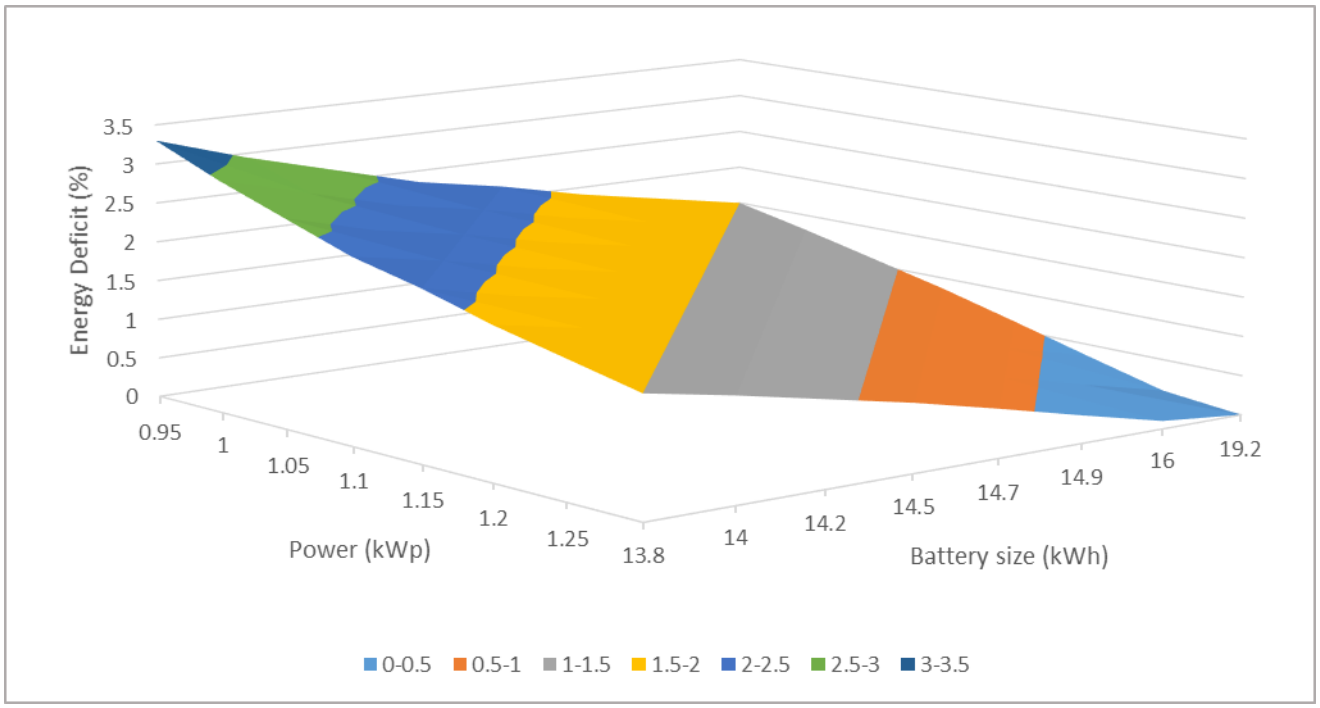

Source: Author

Figure 25 and Figure 26 present closer examination of the behavior of the commercial consumers' PV system with change in simulation variables for one synthetic scenario (a set of 1-year hourly data). As in the case of the residential consumers' graphs, the best combination to attain better energy supply falls within the light blue area also due to low percentage supply interruption and energy deficit of storage and power combinations that fall with the area.

Figure 25 – Percentage hourly supply interruption (Commercial consumer).

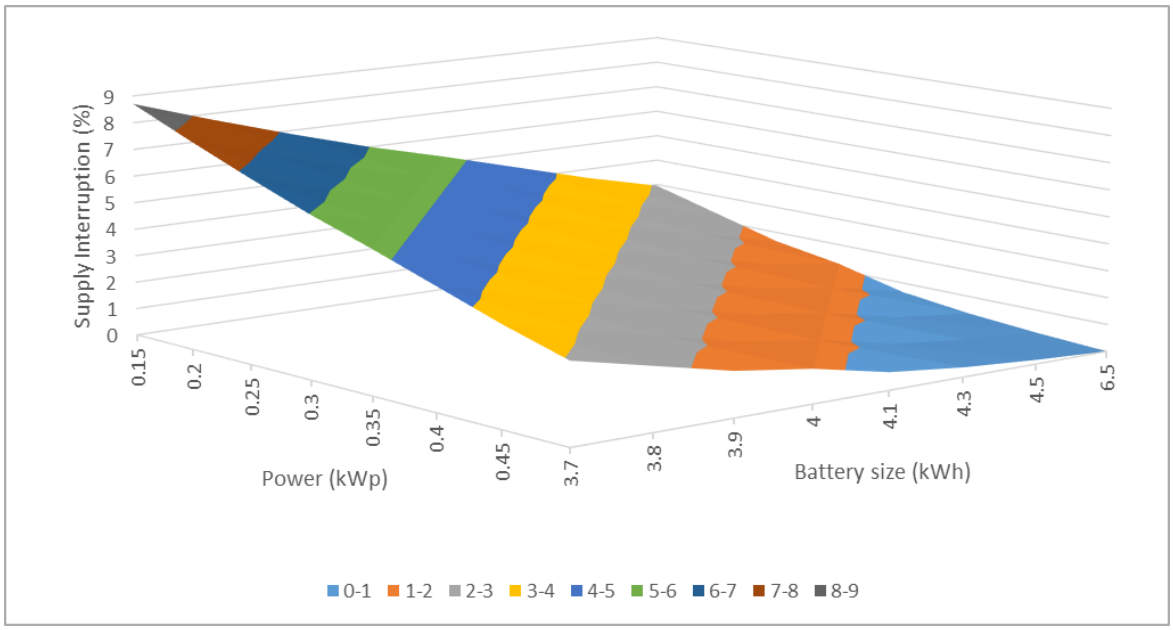

Source: Author

Figure 26 – Percentage hourly energy deficit (Commercial consumer).

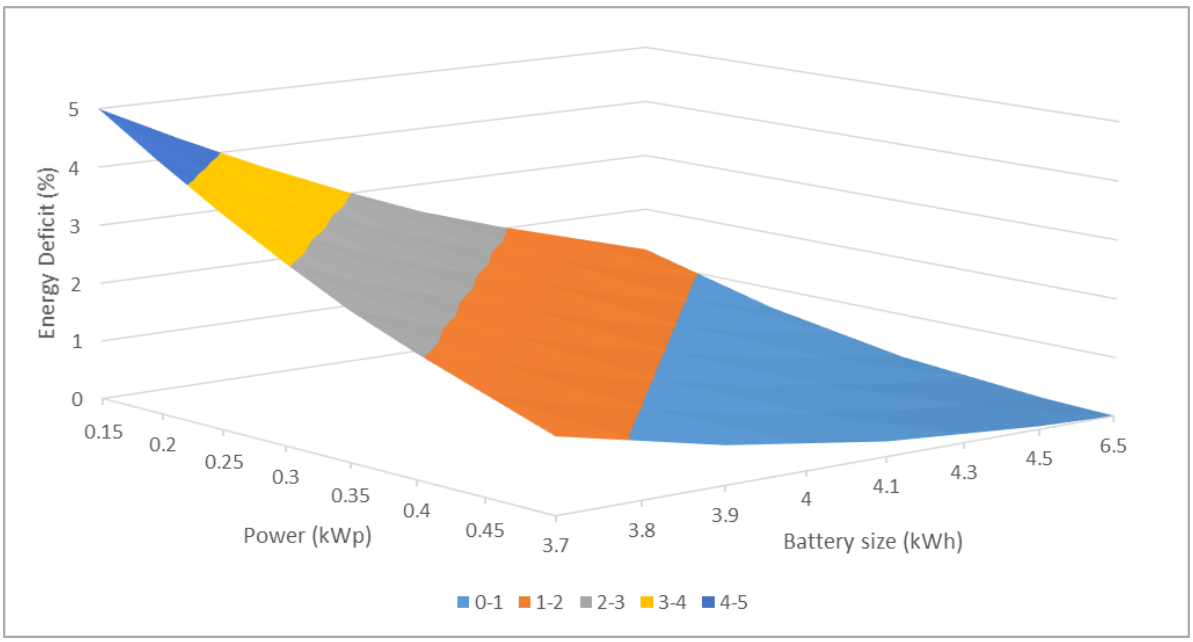

Source: Author

Probability analysis was carried out using 1000 generated scenarios of one year hourly synthetic series data each with equal probability of occurrence. The method of battery sizing proposed in this study was applied to the generated scenarios to obtain 1000 outcomes of energy deficit and supply interruptions. Normal curves were plotted for several battery sizes for the two case studies. Each battery size is represented by one probability distribution curve presenting the probability of attaining percentages of energy deficit and supply interruptions. This analysis provides a clearer picture of the possible outcomes of the simulation with greater accuracy. This graphical representation gives the decision maker the freedom to choose the battery size that suits the project in question.

The graphs of probability and cumulative distributions of this study are presented in Figure 27-42. Figure 27 and Figure 28 are percentage supply interruption probability and cumulative distribution curves respectively of 8 different battery sizes for the residential consumers (First case study).

Figure 27 – Supply interruption probability distribution curves (Residential consumer).

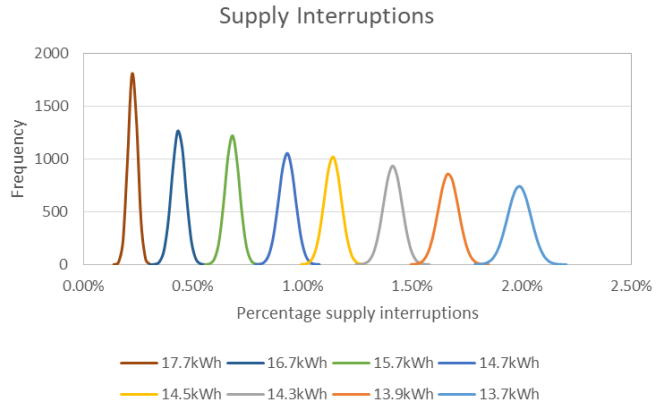

Source: Author

Figure 28 – Supply interruption cumulative distribution curves (Residential consumer).

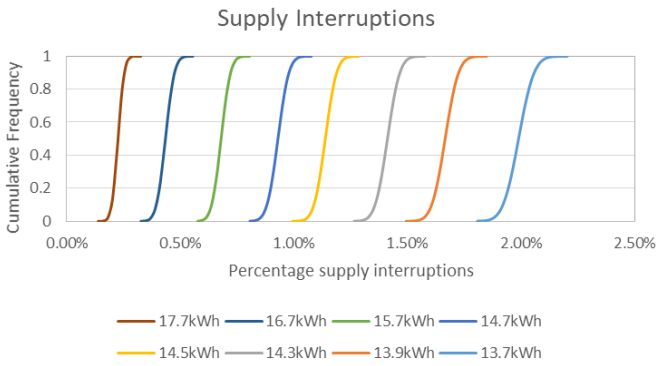

Source: Author

Each normal curve represents the possibility distribution and cumulative distribution of achieving a certain percentage supply interruption for one battery size. In Figure 29 for example, the curve represents the probability distribution curve for a 13.7kWh battery with a 50% probability of achieving about 2% supply interruption for the whole year and Figure 30 is its cumulative distribution curve.

Figure 29 – Supply interruption probability distribution curve (Residential consumer).

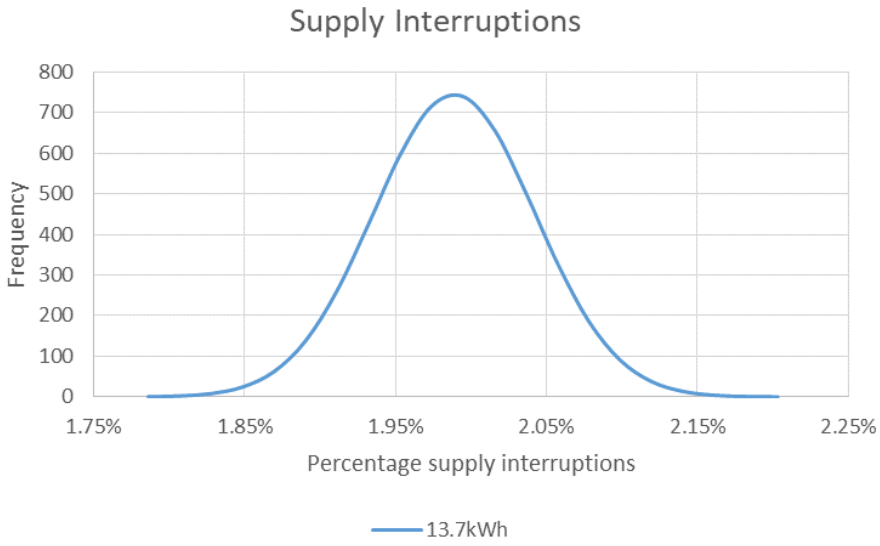

Source: Author

Figure 30 – Supply interruption cumulative distribution curve (Residential consumer)

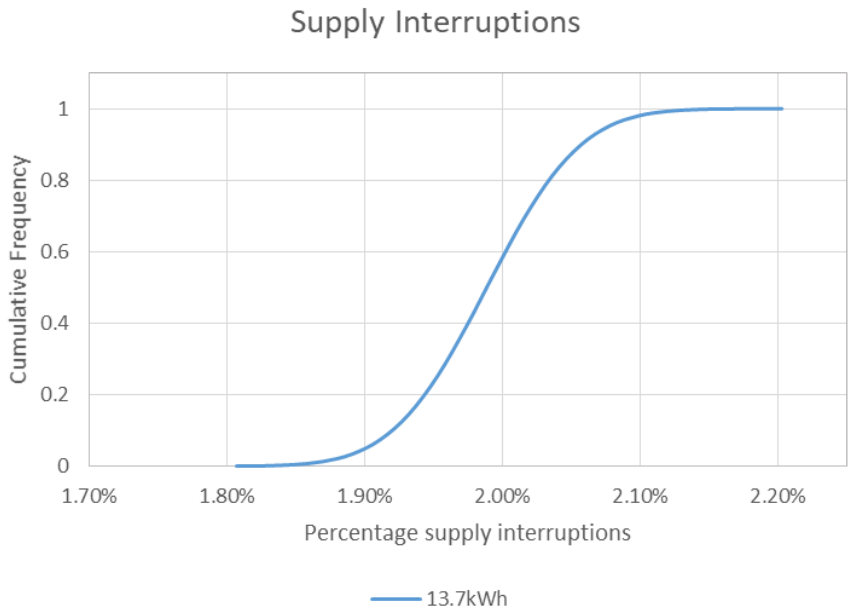

Source: Author

Figure 31 and Figure 32 represent the percentage energy deficit probability and cumulative distribution curves respectively of 8 different battery sizes for the residential consumers (First case study).

Figure 31 – Energy deficit probability distribution curves (Residential consumer)

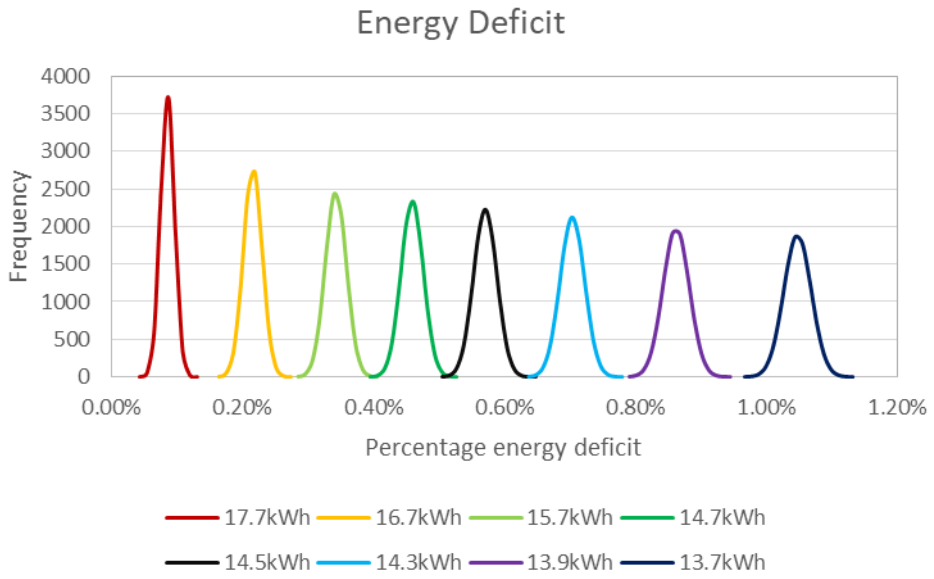

Source: Author

Figure 32 – Energy deficit cumulative distribution curves (Residential consumer)

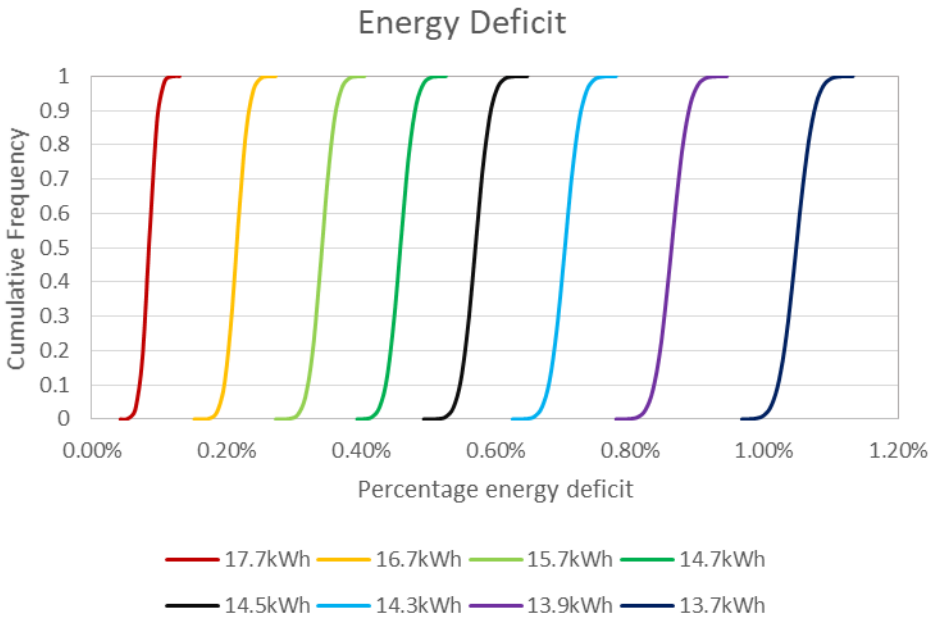

Source: Author

Each normal curve represents the possibility distribution and cumulative distribution of achieving a certain percentage energy deficit for one battery size. In Figure 33 for example, the curve represents the probability distribution curve for a 14.5kWh battery with a 50% probability of achieving 0.5% energy deficit across the year and Figure 34 is its cumulative distribution curve.

Figure 33 – Energy deficit probability distribution curve (Residential consumer)

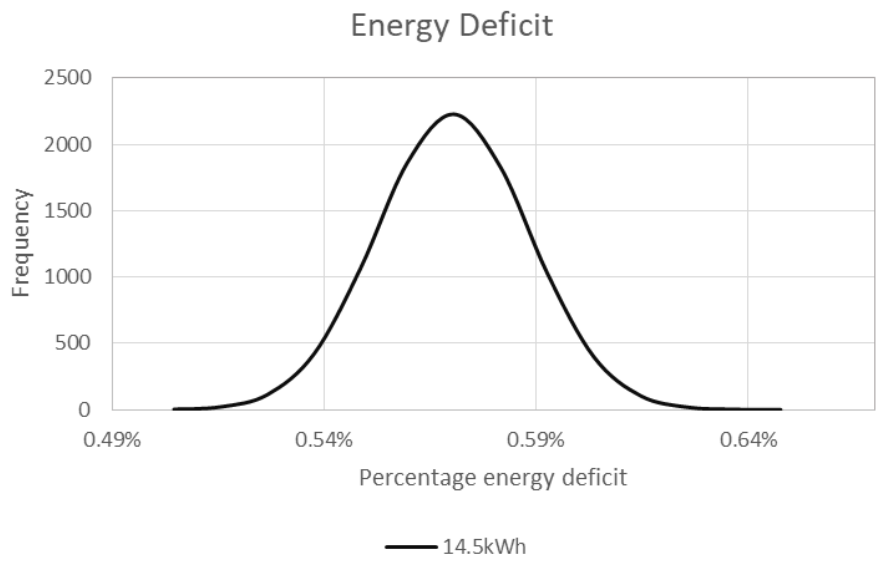

Source: Author

Figure 34 – Energy deficit cumulative distribution curve (Residential consumer)

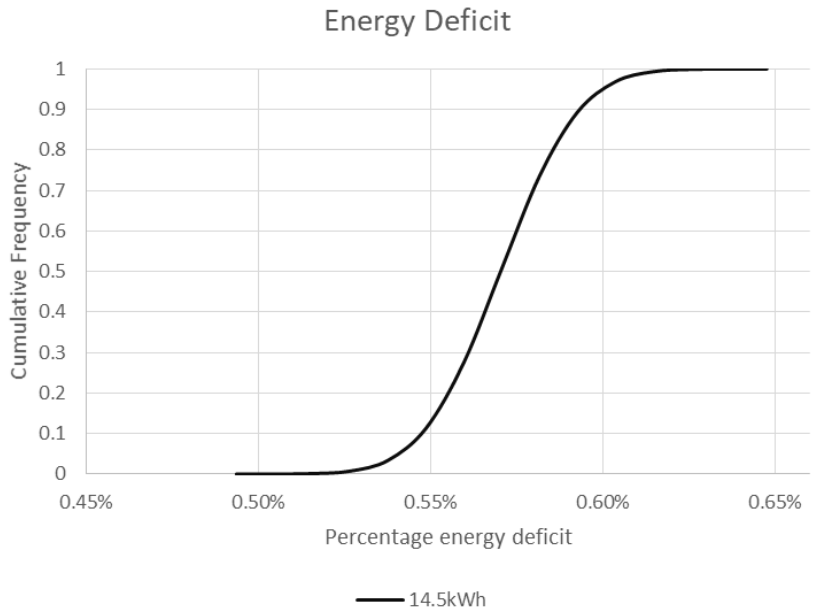

Source: Author

Figure 35 and Figure 36 are percentage supply interruption probability and cumulative distribution curves respectively of 7 different battery sizes for the commercial consumers (second case study).

Figure 35 – Supply Interruption probability distribution curves (Commercial consumer)

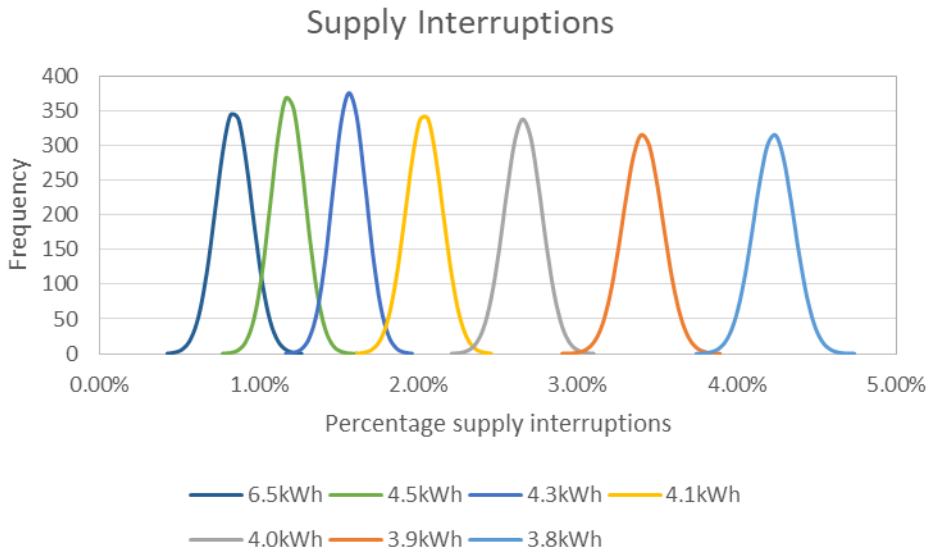

Source: Author

Figure 36 – Supply Interruption cumulative distribution curves (Commercial consumer)

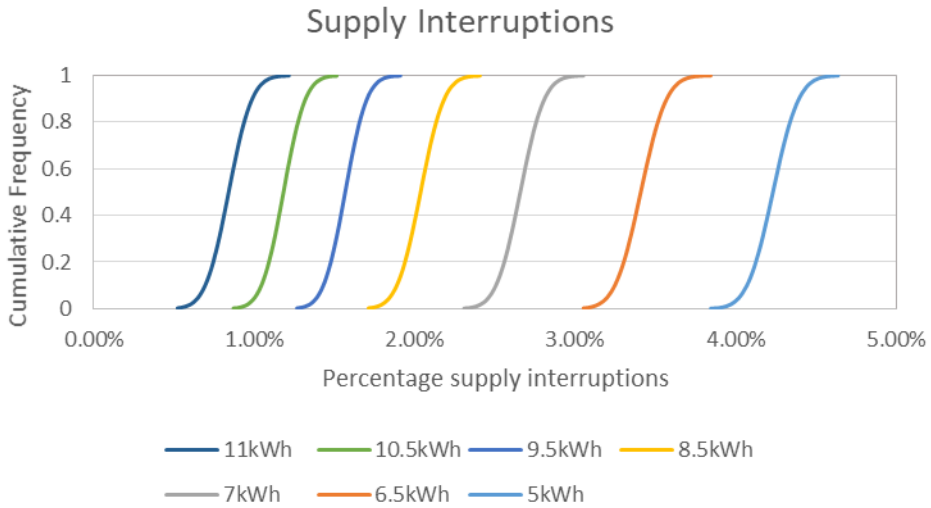

Source: Author

In Figure 37, the curve represents the probability distribution curve for a 4.1kWh battery with about 50% probability of achieving about 2.1% supply interruption for the year and Figure 38 is its cumulative distribution curve.

Figure 37 – Supply interruption probability distribution curve (Commercial consumer)

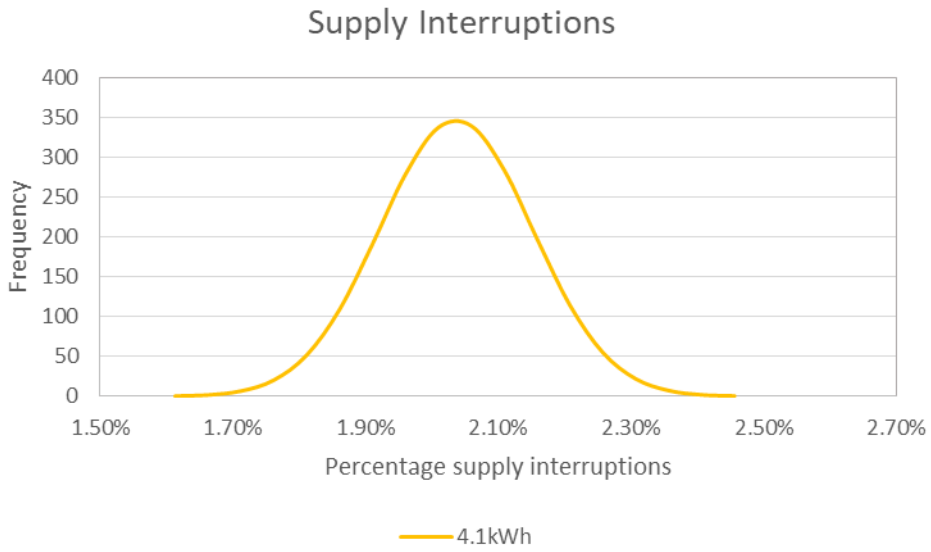

Source: Author

Figure 38 – Supply interruption cumulative distribution curve (Commercial consumer)

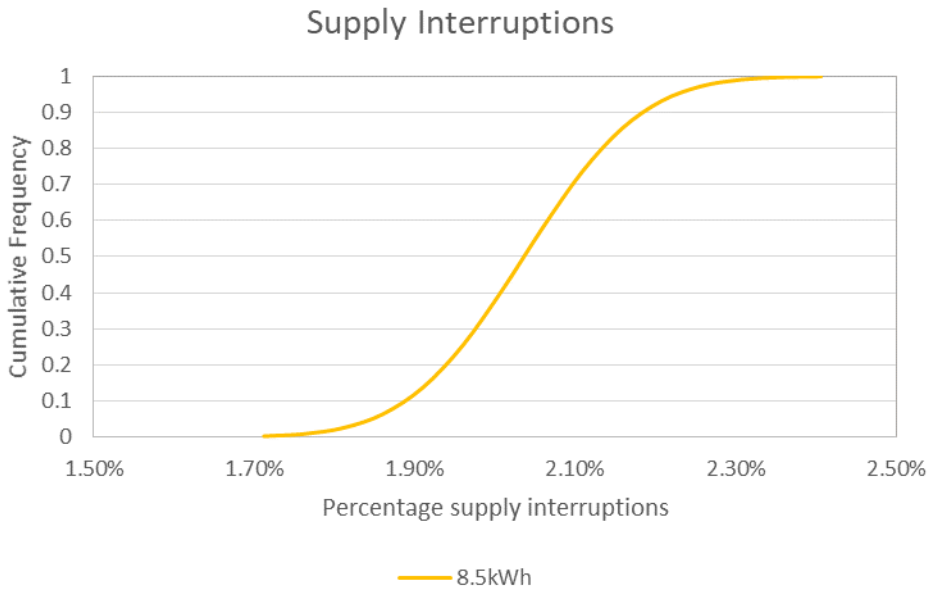

Source: Author

Figure 39 and Figure 40 are percentage energy deficit probability and cumulative distribution curves respectively of 7 different battery sizes for the commercial consumers (second case study).

Figure 39 – Energy deficit probability distribution curves (Commercial consumer)

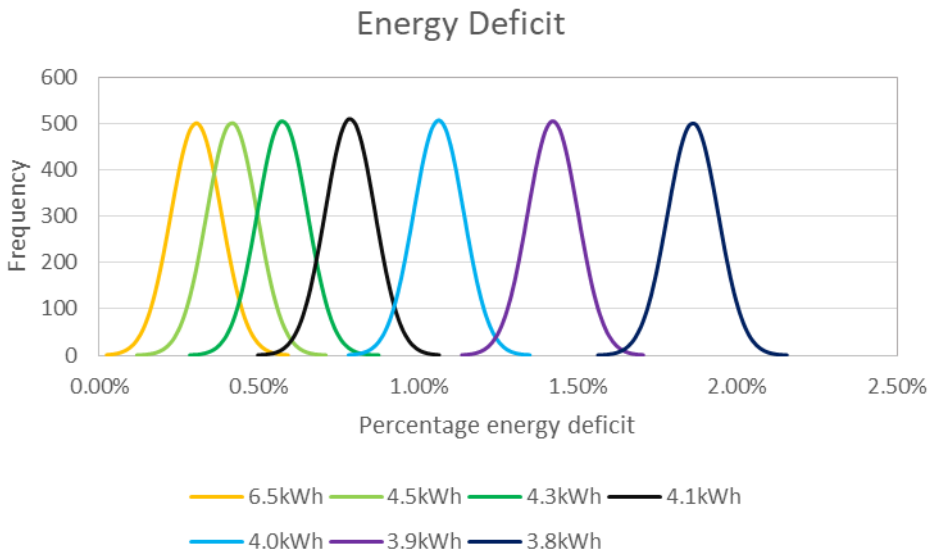

Source: Author

Figure 40 – Energy deficit cumulative distribution curves (Commercial consumer)

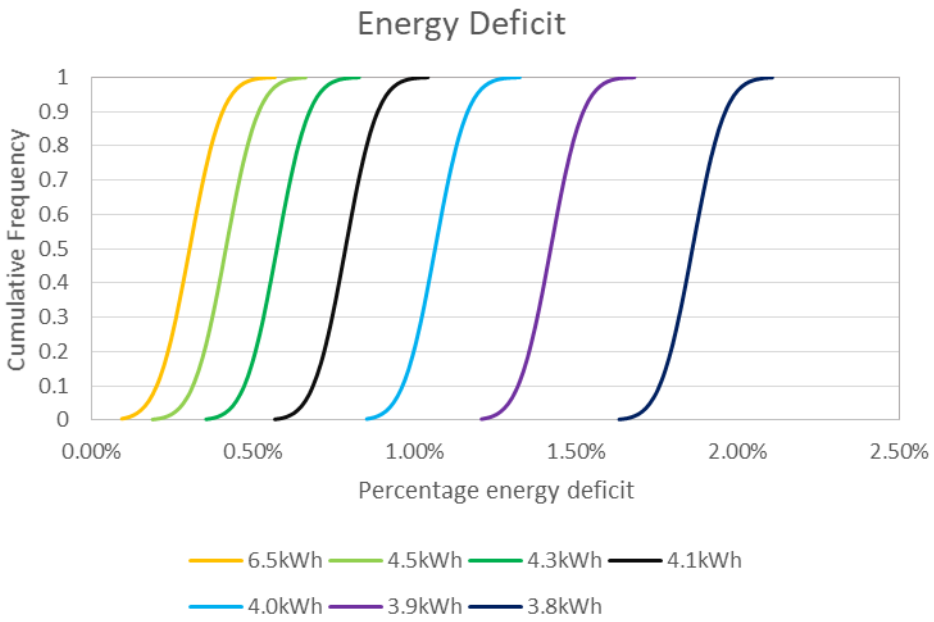

Source: Author

In Figure 41 represents the probability distribution curve for a 3.9kWh battery with 50% probability of getting about 1.4% energy deficit considering the whole year and Figure 42 is its cumulative distribution curve.

Figure 41 – Energy deficit probability distribution curve (Commercial consumer)

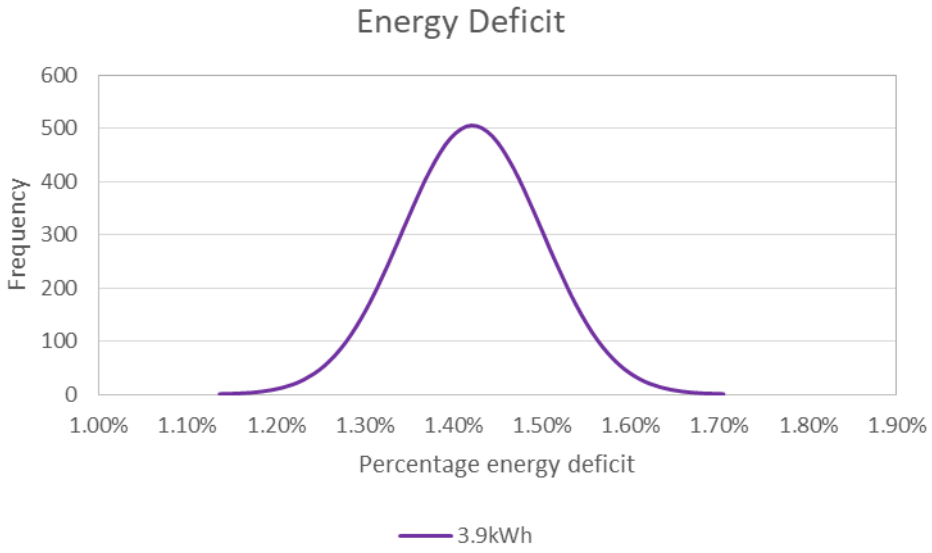

Source: Author

Figure 42 – Energy deficit cumulative distribution curve (Commercial consumer)

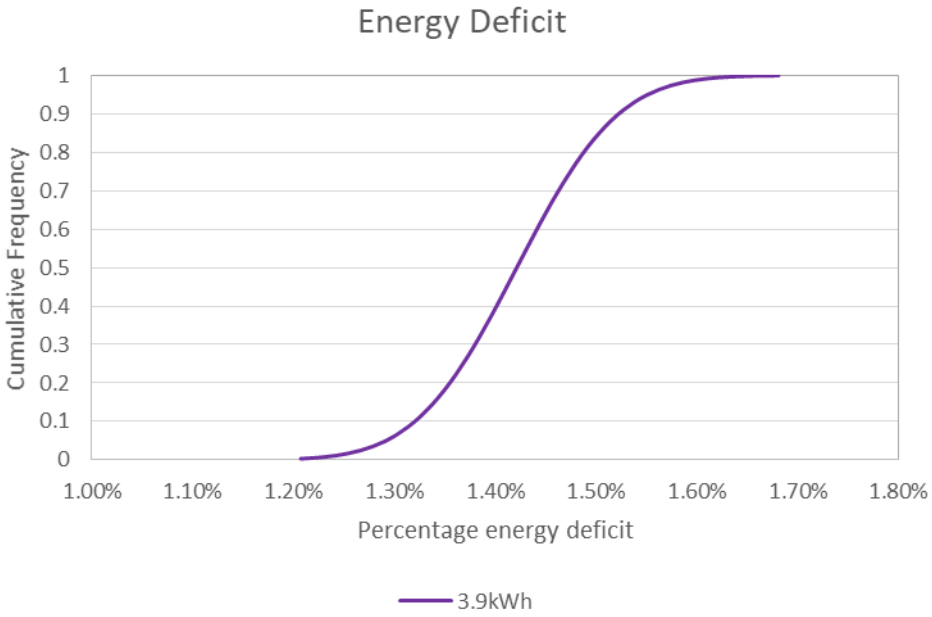

Source: Author

In order to optimally size and select the best BESS for each of the systems, the BESS sizing results obtained were evaluated economically considering BESS lifecycle of 15 years (MONGIRD et al., 2019) to determine the one with the best investment returns (benefit). Figure 43 and Figure 44 represent the cost analysis results (NPV and PBP) for the residential and commercial consumers respectively.

A positive NPV signifies that the investment is predicted to greater returns or benefits and the higher the NPV, the better the benefit. Following this logic, it can be observed in Figure 43 that the best BESS size for the residential consumer is the 16kWh lithium-ion battery. Notice the curve starts falling afterwards which signifies that investing beyond the 16kWh size will not yield more returns. All BESS sizes with positive NPV are predicted to yield great benefits therefore, depending on one's budget, one can decide to choose between BESS size 14.6kWh to 16kWh.

For the PBP, the lower the PBP, the lower the amount of time required to pay back on investment. From Figure 43, the 16kWh also has the best PBP of about 8 years which is good because it is less than the 15 years lifetime of the battery.

Figure 43 – NPV and PBP for various battery sizes (Residential consumer)

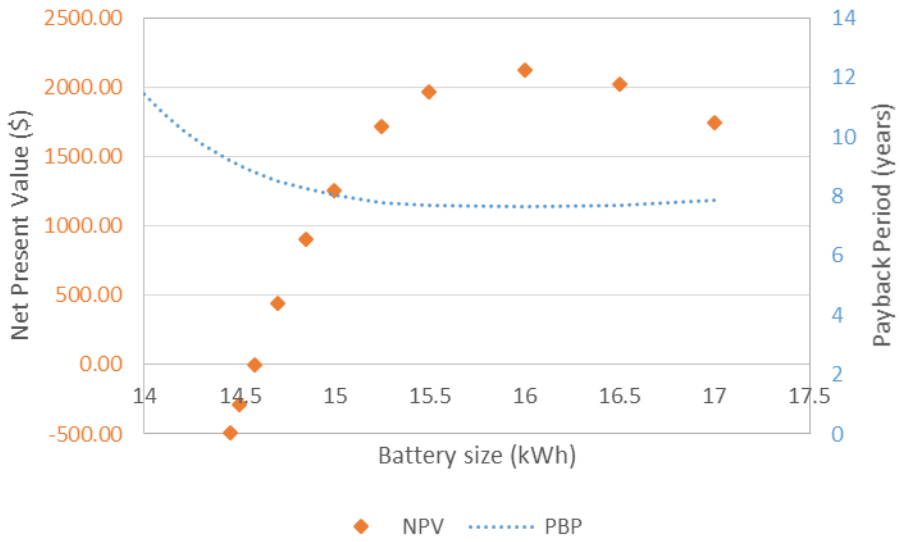

Source: Author

For the commercial consumer, it can be seen from Figure 45 that the 4.3kWh lithium-ion battery has the best NPV and PBP values signifying that it is the best battery to be invested in the system. However, depending on one's budget, BESS sizes between 4kWh and 4.3kWh are all considered good investments with different returns and payback periods.

Figure 44 – NPV and PBP for various battery sizes (Commercial consumer)

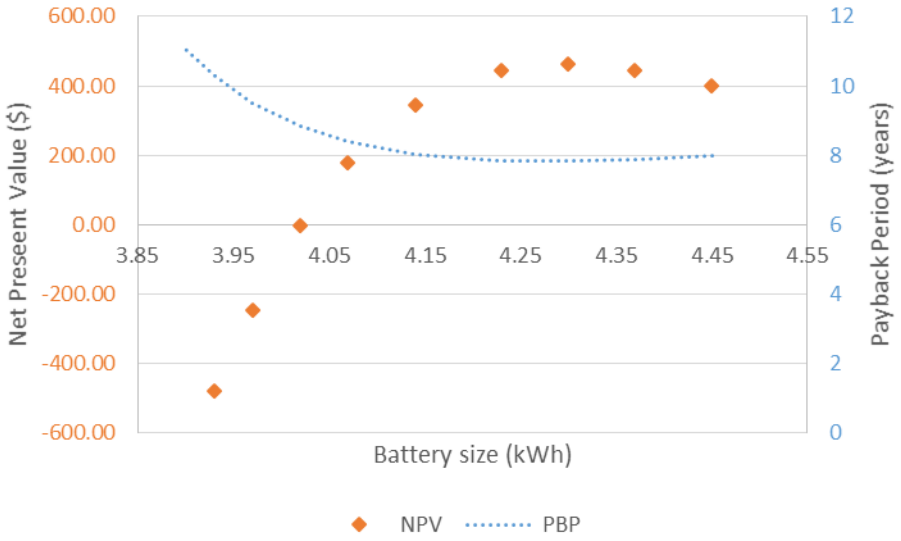

Source: Author

Table 18 presents the battery sizes for the residential and commercial consumers based on sizing methodology recommended by panel manufacturers. This methodology does not provide the flexibility in decision making like in the proposed methodology of this study. There is also the risk of unnecessarily oversizing BESS which occupies more space and can make PV system complex leading to high O&M costs. The oversizing in the methodology can be attributed to the choice of the value of days of autonomy which is usually between two to five days which in the case of this study, a value of three (3) was used. Selecting higher number of days of autonomy would result in a much higher BESS size and a lower value of days of autonomy could result in under-sizing of the BESS.

Table 18 – Battery size result for panel manufacturers' recommended methodology

Consumer	BESS size (kWh)
Residential	24.98
Commercial	8.57

Source: Author

6.0 CONCLUSION

This study presented a novel methodology to optimally size and select BESS in isolated PV systems using predicted hourly solar radiation data. The method assesses the performance of several possible BESS sizes indicating the risk of energy deficit and possible frequency of supply interruptions using 1000 predicted solar radiation scenarios each with equal probability of occurrence. The sized BESSs were then evaluated economically to determine the BESS with the best investment returns. Two case studies were considered in testing the methodology and the outcome was compared to the outcome of the conventional methodology recommended by panel manufacturers. The methodology potentially reduces the risk of energy shortage due to inadequate BESS sizing. It helps avoid the possibility of oversizing BESS thereby reducing unnecessary complexity of PV system and unnecessary installation and maintenance costs. The cost analysis which evaluates the economic performance of BESS is used in investment decision making. Depending on ones' budget, the cost analysis gives the flexibility of BESS size selection amongst various options each with its predicted investment returns.

The study found results of the proposed methodology to optimally size and select BESS in isolated PV systems considering hourly solar radiation data and cost analysis to be more robust and accurate than results of panel manufacturers' recommended methodology. The proposed method is considered to be more adequate owing to the fact that predicted solar radiation data generated from historical solar radiation data of where the PV system will be installed is utilized to estimate the amount of power to be generated by the PV system thereby making it possible to have an idea of the energy deficit to be expected with respect to the load demand and to size the BESS accordingly, as against days of autonomy recommended by panel manufacturers which is basically guessing number of consecutive days the BESS will go without being recharged and usually results in either oversizing or under-sizing of the BESS. The probability analysis using 1000 scenarios of solar synthetic series data carried out in the proposed methodology further increases the resolution of the result making the method more robust than panel manufacturers' recommended method.

Results of the proposed methodology also presents possible percentage energy deficit and supply interruption which makes decision making easier unlike in the method recommended by panel manufacturers where the details of possible energy deficit and supply interruption

cannot be obtained. Accuracy of the results of the proposed methodology can be observed in the graphs of Figures 20-23 where a comparison was made between measured and predicted solar radiations' percentage energy deficit and supply interruption outcomes. It can be seen that the difference when considering the two set of data is minimal and within accepted margins.

Observing the sizing results of both methodologies obtained in this study and presented in Table 14 and Table 16 for the proposed methodology, and Table 18 for the panel manufacturers' recommended methodology, it can be seen that BESS is unnecessarily oversized for both case studies in the recommended method of panel manufacturers. This ultimately leads to unnecessary over spending, complexity of the PV system, higher O&M costs and occupation of more space than necessary as large BESS size means more number of batteries to be installed.

The proposed methodology studied in this research has numerous advantages over the current conventional BESS sizing methodology recommended by panel manufacturers;

- The energy deficit and supply interruption outcomes of the methodology provides an insight into the performance of a BESS in the PV system. Therefore, one has an idea what to expect from the system even before it is installed and is able to make adjustments based on application requirements.

- Flexibility in BESS size selection: Considering the economic performance of different BESS sizes with different percentage energy deficits for the same PV system, one is able to make decision based on available budget.

- Flexibility in BESS technology selection: The methodology provides the luxury of comparing the performance of various BESS technologies when applied to the PV system.

- Reduces the risk of oversizing or under-sizing of BESS in PV system hence reduces the risk of complexity of the system and risk of power shortage in the system.

- Owing to the fact that the right size of BESS is used in the system, O&M costs are reduced.

This study therefore, concludes based on results obtained that the proposed methodology of BESS sizing and selection in isolated PV systems considering solar radiation data and cost analysis is more adequate than the methodology recommended by panel manufacturers. The methodology could also be used in the sizing of BESS in grid-connected and hybrid PV systems and in the sizing of BESS for wind turbine applications and other renewable energy sources.

6.1 Publications

Published

- "**Battery Storage System Sizing Using Synthetic Series Data**", presented at the 46th IEEE Photovoltaic Specialists Conference (2019)(ABUBAKAR; GEMIGNANI; MESCHINI ALMEIDA, 2019). Published in IEEE Xplore conference proceedings

Accepted for publication

- **"c-Si and Thin film Photovoltaic Penetration Scenarios in Kano State – Nigeria"**, submitted to EUPVSEC; RELVA, AHMAD, UDAETA, SILVA, GIMENEZ, ALMEIDA;

Submitted

- **"An Optimal Methodology for Sizing and Selection of BESS in Standalone PV systems",** submitted to CIRED 2021 conference; ABUBAKAR; MESCHINI ALMEIDA.
- **"Analysis of Battery Energy Storage System Sizing in Isolated PV Systems Considering A Novel Methodology and Panel Manufacturers Recommended Methodology",** submitted to IEEE T&D PES Conference and Exhibition Latin America 2020; ABUBAKAR; MESCHINI ALMEIDA

REFERENCES

ABBASSI, Abdelkader; DAMI, Mohamed Ali; JEMLI, Mohamed. A statistical approach for hybrid energy storage system sizing based on capacity distributions in an autonomous PV/Wind power generation system. **Renewable Energy**, *[S. l.]*, v. 103, p. 81–93, 2017. DOI: 10.1016/j.renene.2016.11.024. Disponível em: http://dx.doi.org/10.1016/j.renene.2016.11.024.

ABRADEE. Dados de Mercado das Empresas Distribuidoras Associadas à Abradee Número de Consumidores - Dezembro 2018 (Market Data of Distributing Companies Associated with Abradee Number of Consumers - December 2018). *[S. l.]*, p. 2019, 2019. Disponível em: http://www.abradee.org.br/planilhas-de-1996-a-2018-ref-2017/.

ABUBAKAR, Ahmad; GEMIGNANI, Matheus; MESCHINI ALMEIDA, Carlos Frederico. Battery Storage System Sizing Using Synthetic Series Data. *In*: CONFERENCE RECORD OF THE IEEE PHOTOVOLTAIC SPECIALISTS CONFERENCE 2019, **Anais** [...]. [s.l: s.n.] p. 1578–1583. DOI: 10.1109/PVSC40753.2019.8980615.

AGHAMOHAMMADI, Mohammad Reza; ABDOLAHINIA, Hajar. A new approach for optimal sizing of battery energy storage system for primary frequency control of islanded Microgrid. **International Journal of Electrical Power and Energy Systems**, *[S. l.]*, v. 54, p. 325–333, 2014. DOI: 10.1016/j.ijepes.2013.07.005. Disponível em: http://dx.doi.org/10.1016/j.ijepes.2013.07.005.

ALMEIDA, Marcelo Pinho; LAMIGUEIRO, Oscar Perpiñan; FERNÁNDEZ, Luis Narvarte. Using a nonparametric PV model to forecast AC power output of PV plants. **EU PVSEC Proceedings**, *[S. l.]*, p. 2227–2233, 2015. Disponível em: http://oa.upm.es/43686/.

ALTE STORE. **Off-grid Calculator**. [s.d.]. Disponível em: https://www.altestore.com/store/calculators/off_grid_calculator/. Acesso em: 13 abr. 2020.

ALTERNATIVE ENERGY. **Battery Bank Sizing**. 2020. Disponível em: http://www.altenergy.org/renewables/solar/DIY/battery-bank-sizing.html. Acesso em: 13 abr. 2020.

ÁLVARO, Daniel; ARRANZ, Rafael; AGUADO, José A. Sizing and operation of hybrid

energy storage systems to perform ramp-rate control in PV power plants. **International Journal of Electrical Power & Energy Systems**, *[S. l.]*, v. 107, n. October 2018, p. 589–596, 2019. DOI: 10.1016/j.ijepes.2018.12.009. Disponível em: https://linkinghub.elsevier.com/retrieve/pii/S0142061518311499.

BERNABÉ, Javier; MARTÍNEZ, Mohedano. BATTERIES IN PV SYSTEMS. *[S. l.]*, [s.d.].

BERNSTEIN, Lawrence. System sizing. **The Journal of Systems and Software**, *[S. l.]*, v. 8, n. 3, p. 253, 1988. DOI: 10.1016/0164-1212(88)90024-6.

BRACALE, Antonio; CARAMIA, Pierluigi; CARPINELLI, Guido; DI FAZIO, Anna Rita; FERRUZZI, Gabriella. A Bayesian method for Short-Term probabilistic forecasting of photovoltaic generation in smart grid operation and control. **Energies**, *[S. l.]*, v. 6, n. 2, p. 733–747, 2013. DOI: 10.3390/en6020733.

BUCCIARELLI, Martina; GIANNITRAPANI, Antonio; PAOLETTI, Simone; VICINO, Antonio; ZARRILLI, Donato. Sizing of energy storage systems considering uncertainty on demand and generation. **IFAC-PapersOnLine**, *[S. l.]*, v. 50, n. 1, p. 8861–8866, 2017. DOI: 10.1016/j.ifacol.2017.08.1543. Disponível em: https://doi.org/10.1016/j.ifacol.2017.08.1543.

BUCCIARELLI, Martina; PAOLETTI, Simone; VICINO, Antonio. Optimal sizing of energy storage systems under uncertain demand and generation. **Applied Energy**, *[S. l.]*, v. 225, n. March, p. 611–621, 2018. DOI: 10.1016/j.apenergy.2018.03.153. Disponível em: https://doi.org/10.1016/j.apenergy.2018.03.153.

CABELLO, Javier M.; ROBOAM, Xavier; JUNCO, Sergio; TURPIN, Christophe. Direct sizing and characterization of Energy Storage Systems in the Energy-Power plane. **Mathematics and Computers in Simulation**, *[S. l.]*, 2018. DOI: 10.1016/j.matcom.2018.04.002. Disponível em: https://doi.org/10.1016/j.matcom.2018.04.002.

CARLOS, J. S.; CORVACHO, H. Assessment of different correlation models for estimating solar irradiation on a non-horizontal surface. *[S. l.]*, v. 37, n. 3, p. 175–186, 2013.

CARPINELLI, Guido; FAZIO, Anna Rita Di; KHORMALI, Shahab; MOTTOLA, Fabio. Optimal sizing of battery storage systems for industrial applications when uncertainties exist.

Energies, *[S. l.]*, v. 7, n. 1, p. 130–149, 2014. DOI: 10.3390/en7010130.

CARPINELLI, Guido; MOTTOLA, Fabio; PROTO, Daniela. Probabilistic sizing of battery energy storage when time-of-use pricing is applied. **Electric Power Systems Research**, *[S. l.]*, v. 141, p. 73–83, 2016. DOI: 10.1016/j.epsr.2016.07.013.

CENTRE FOR SUSTAINABLE SYSTEMS UNIVERSITY OF MICHIGAN. Photovoltaic Energy Factsheet. **Science**, *[S. l.]*, 2019. DOI: 10.1126/science.228.4695.6-c.

CHEDID, Riad; SAWWAS, Ahmad. Optimal placement and sizing of photovoltaics and battery storage in distribution networks. **Energy Storage**, *[S. l.]*, v. 1, n. 4, p. 1–12, 2019. DOI: 10.1002/est2.46.

CHO, Kyeong-hee; KIM, Seul-ki; KIM, Eung-sang. Optimal Sizing of BESS for Customer Demand Management. **Journal of International Council on Electrical Engineering**, *[S. l.]*, v. 4, n. 1, p. 30–36, 2014. DOI: 10.5370/jicee.2014.4.1.030.

CHOICE. **How to buy the best solar battery storage**. 2020. Disponível em: https://www.choice.com.au/home-improvement/energy-saving/solar/buying-guides/battery-storage-buying-guide. Acesso em: 11 fev. 2020.

CORNEJO-BUENO, L.; CASANOVA-MATEO, C.; SANZ-JUSTO, S.; SALCEDO-SANZ, S. Machine learning regressors for solar radiation estimation from satellite data. **Solar Energy**, *[S. l.]*, v. 183, n. March, p. 768–775, 2019. DOI: 10.1016/j.solener.2019.03.079.

CRUZ, Anna Paula Soares. 済無No Title No Title. **Journal of Chemical Information and Modeling**, *[S. l.]*, v. 53, n. 9, p. 1689–1699, 2013. DOI: 10.1017/CBO9781107415324.004.

DAS, Bhaskarjyoti; KUMAR, Ashwani. A NLP approach to optimally size an energy storage system for proper utilization of renewable energy sources. **Procedia Computer Science**, *[S. l.]*, v. 125, p. 483–491, 2018. DOI: 10.1016/j.procs.2017.12.062. Disponível em: https://doi.org/10.1016/j.procs.2017.12.062.

DAS, Choton K.; BASS, Octavian; KOTHAPALLI, Ganesh; MAHMOUD, Thair S.; HABIBI, Daryoush. Overview of energy storage systems in distribution networks: Placement, sizing, operation, and power quality. **Renewable and Sustainable Energy Reviews**, *[S. l.]*, v. 91, n. November 2016, p. 1205–1230, 2018. DOI: 10.1016/j.rser.2018.03.068. Disponível em:

https://doi.org/10.1016/j.rser.2018.03.068.

DIORIO, Nicholas; DOBOS, Aron; JANZOU, Steven. Economic Analysis Case Studies of Battery Energy Storage with SAM. **Technical Report**, *[S. l.]*, n. November, 2015. DOI: 10.1109/PAHCE.2009.5158375.

DULOUT, Jeremy; JAMMES, Bruno; ALONSO, Corinne; ANVARI-MOGHADDAM, Amjad; LUNA, Adriana; GUERRERO, Josep M. Optimal sizing of a lithium battery energy storage system for grid-connected photovoltaic systems. **2017 IEEE 2nd International Conference on Direct Current Microgrids, ICDCM 2017**, *[S. l.]*, p. 582–587, 2017. DOI: 10.1109/ICDCM.2017.8001106.

ECN. End-use Metering Campaign for Residential Houses in Nigeria Metering Campaign Report Energy Commission of Nigeria Federal Ministry of Environment United Nations Development Programme Global Environment Facility. *[S. l.]*, n. September, 2013. Disponível em: http://www.ng.undp.org/content/dam/nigeria/docs/Sustainable Development/UNDP_NG_sustaindev_Metering_Campaign.pdf.

ECOWHO. **Solar Battery Storage Comparison**. 2020. Disponível em: https://www.ecowho.com/battery/. Acesso em: 12 fev. 2020.

EHNBERG, Jimmy S. G.; BOLLEN, Math H. J. Simulation of global solar radiation based on cloud observations. **Solar Energy**, *[S. l.]*, v. 78, n. 2, p. 157–162, 2005. DOI: 10.1016/j.solener.2004.08.016.

FILIPE, J. M.; BESSA, R. J.; SUMAILI, J.; TOMÉ, R.; SOUSA, J. N. A hybrid short-term solar power forecasting tool. **2015 18th International Conference on Intelligent System Application to Power Systems, ISAP 2015**, *[S. l.]*, 2015. DOI: 10.1109/ISAP.2015.7325543.

FOSSATI, Juan P.; GALARZA, Ainhoa; MARTÍN-VILLATE, Ander; FONTÁN, Luis. A method for optimal sizing energy storage systems for microgrids. **Renewable Energy**, *[S. l.]*, v. 77, p. 539–549, 2015. DOI: 10.1016/j.renene.2014.12.039.

FU, Ran et al. U . S . Solar Photovoltaic System Cost Benchmark : Q1 2017 U . S . Solar Photovoltaic System Cost Benchmark : Q1 2017. **National Renewable Energy Laboratory**,

[S. l.], n. September, p. 1–59, 2017. Disponível em: https://www.nrel.gov/docs/fy17osti/68925.pdf.

GAETAN, Masson.; SINEAD, Orlandi.; MANOEL, Rekinger. Global market outlook. **EPIA - European Photovoltaic Industry Association.**, *[S. l.]*, p. 60, 2018. DOI: 10.1787/key_energ_stat-2014-en. Disponível em: www.africa-eu-renewables.org.

GEMIGNANI, Matheus. Cenários sintéticos de radiação solar para estudos energéticos. *[S. l.]*, 2018.

GEMIGNANI, Matheus; ROSTEGUI, Guido J.; KAGAN, Nelson. Solar radiation synthetic sequences and bidding strategies for energy auctions. **2017 6th International Conference on Renewable Energy Research and Applications, ICRERA 2017**, *[S. l.]*, v. 2017-Janua, n. 1, p. 406–411, 2017. DOI: 10.1109/ICRERA.2017.8191094.

GHIMIRE, Sujan; DEO, Ravinesh C.; DOWNS, Nathan J.; RAJ, Nawin. Global solar radiation prediction by ANN integrated with European Centre for medium range weather forecast fi elds in solar rich cities of Queensland Australia. **Journal of Cleaner Production**, *[S. l.]*, v. 216, p. 288–310, 2019. DOI: 10.1016/j.jclepro.2019.01.158.

GOUDA, Shaban G.; HUSSEIN, Zakia; LUO, Shuai; YUAN, Qiaoxia. Model selection for accurate daily global solar radiation prediction in. **Journal of Cleaner Production**, *[S. l.]*, v. 221, p. 132–144, 2019. DOI: 10.1016/j.jclepro.2019.02.211.

HASSAN, Muhammed A.; KHALIL, A.; KASEB, S.; KASSEM, M. A. Potential of four different machine-learning algorithms in modeling daily global solar radiation. **Renewable Energy**, *[S. l.]*, v. 111, p. 52–62, 2017. DOI: 10.1016/j.renene.2017.03.083. Disponível em: http://dx.doi.org/10.1016/j.renene.2017.03.083.

HEIDER, Zulfiker. **Battery Sizing Calculation**. 2012. Disponível em: https://www.scribd.com/doc/97323800/Battery-Sizing-Calculation. Acesso em: 13 abr. 2020.

HIPEL, K. W.; MCLEOD, A. I. Time series modelling of water resources and environmental systems. **Time series modelling of water resources and environmental systems**, *[S. l.]*, p. 1994, 1994. DOI: 10.1016/0022-1694(95)90010-1.

IEEE 485. Battery Sizing. **Open electrical**, *[S. l.]*, 2019. Disponível em:

http://www.openelectrical.org/wiki/index.php?title=Battery_Sizing.

IEEE STANDARDS COORDINATING COMMITTEE. **IEEE Recommended Practice for Sizing Lead-Acid Batteries for Photovoltaic (PV) Systems**. [s.l: s.n.]. v. 2000

IRENA. Solar Photovoltaics. *[S. l.]*, v. 1, n. 4, 2012.

IRENA. **THE POWER TO CHANGE : SOLAR AND WIND COST REDUCTION POTENTIAL**. [s.l: s.n.].

JACOB, Ammu Susanna; BANERJEE, Rangan; GHOSH, Prakash C. Sizing of hybrid energy storage system for a PV based microgrid through design space approach. **Applied Energy**, *[S. l.]*, v. 212, n. November 2017, p. 640–653, 2018. DOI: 10.1016/j.apenergy.2017.12.040. Disponível em: https://doi.org/10.1016/j.apenergy.2017.12.040.

KERDPHOL, Thongchart; FUJI, Kiyotaka; MITANI, Yasunori; WATANABE, Masayuki; QUDAIH, Yaser. Optimization of a battery energy storage system using particle swarm optimization for stand-alone microgrids. **International Journal of Electrical Power and Energy Systems**, *[S. l.]*, v. 81, p. 32–39, 2016. DOI: 10.1016/j.ijepes.2016.02.006. Disponível em: http://dx.doi.org/10.1016/j.ijepes.2016.02.006.

LACHO, Pop. **Solar Batteries: The Definitive Guide**. 2019.

LAI, Kexing; WANG, Yishen; SHI, Di; ILLINDALA, Mahesh S.; JIN, Yanming; WANG, Zhiwei. Sizing battery storage for islanded microgrid systems to enhance robustness against attacks on energy sources. **Journal of Modern Power Systems and Clean Energy**, *[S. l.]*, v. 7, n. 5, p. 1177–1188, 2019. DOI: 10.1007/s40565-019-0501-1. Disponível em: https://doi.org/10.1007/s40565-019-0501-1.

LEONICS. **How to design solar PV system**. 2013. Disponível em: http://www.leonics.com/support/article2_12j/articles2_12j_en.php. Acesso em: 13 abr. 2020.

LI, Jiaming. Optimal sizing of grid-connected photovoltaic battery systems for residential houses in Australia. **Renewable Energy**, *[S. l.]*, v. 136, p. 1245–1254, 2019. DOI: 10.1016/j.renene.2018.09.099.

LIAO, Jian Tang; CHUANG, Yung Sheng; YANG, Hong Tzer; TSAI, Men Shen. BESS-

Sizing Optimization for Solar PV System Integration in Distribution Grid. **IFAC-PapersOnLine**, *[S. l.]*, v. 51, n. 28, p. 85–90, 2018. DOI: 10.1016/j.ifacol.2018.11.682. Disponível em: https://doi.org/10.1016/j.ifacol.2018.11.682.

LILIENTHAL, Peter. High Penetrations of Renewable Energy for Island Grids. *[S. l.]*, 2007.

LOADS, D. C. Battery sizing tips. **Energy**, *[S. l.]*, p. 48–51, 2009.

LOURENÇO, Luís Felipe Normandia; DE CAMARGO SALLES, Maurício Barbosa; GEMIGNANI, Matheus Mingatos Fernandes; GOUVEA, Marcos Roberto; KAGAN, Nelson. Time series modelling for solar irradiance estimation in northeast Brazil. **2017 6th International Conference on Renewable Energy Research and Applications, ICRERA 2017**, *[S. l.]*, v. 2017- Janua, p. 401–405, 2017. DOI: 10.1109/ICRERA.2017.8191093.

MARTINEZ-BOLANOS, Julio Romel; UDAETA, Miguel Edgard Morales; GIMENES, André Luiz Veiga; SILVA, Vinícius Oliveira Da. Economic feasibility of battery energy storage systems for replacing peak power plants for commercial consumers under energy time of use tariffs. **Journal of Energy Storage**, *[S. l.]*, v. 29, n. November 2019, p. 101373, 2020. DOI: 10.1016/j.est.2020.101373 no. Disponível em: https://linkinghub.elsevier.com/retrieve/pii/S2352152X19316251.

MARTINS, Rodrigo; HESSE, Holger C.; JUNGBAUER, Johanna; VORBUCHNER, Thomas; MUSILEK, Petr. Optimal component sizing for peak shaving in battery energy storage system for industrial applications. **Energies**, *[S. l.]*, v. 11, n. 8, 2018. DOI: 10.3390/en11082048.

MEJÍA-GIRALDO, Diego; VELÁSQUEZ-GOMEZ, Gregorio; MUÑOZ-GALEANO, Nicolás; CANO-QUINTERO, Juan Bernardo; LEMOS-CANO, Santiago. A BESS sizing strategy for primary frequency regulation support of solar photovoltaic plants. **Energies**, *[S. l.]*, v. 12, n. 2, p. 1–16, 2019. DOI: 10.3390/en12020317.

MEYBODI, Mehdi Aghaei; RAMIREZ SANTIGOSA, Lourdes; BEATH, Andrew C. A study on the impact of time resolution in solar data on the performance modelling of CSP plants. **Renewable Energy**, *[S. l.]*, v. 109, p. 551–563, 2017. DOI: 10.1016/j.renene.2017.03.024. Disponível em: http://dx.doi.org/10.1016/j.renene.2017.03.024.

MICHIORRI, Andrea; LUGARO, Jesus; SIEBERT, Nils; GIRARD, Robin; KARINIOTAKIS, George. Storage sizing for grid connected hybrid wind and storage power plants taking into account forecast errors autocorrelation. **Renewable Energy**, *[S. l.]*, v. 117, p. 380–392, 2018. DOI: 10.1016/j.renene.2017.10.070. Disponível em: https://doi.org/10.1016/j.renene.2017.10.070.

MONGIRD, K.; FOTEDAR, V.; VISWANATHAN, V.; KORITAROV, V.; BALDUCCI, P.; HADJERIOUA, B.; ALAM, J. Energy storage technology and cost characterization report. **Pacific Northwest National Laboratory**, *[S. l.]*, n. July, p. 1–120, 2019. Disponível em: https://www.energy.gov/sites/prod/files/2019/07/f65/Storage Cost and Performance Characterization Report_Final.pdf.

MORA-LÓPEZ, L.; MARTÍNEZ-MARCHENA, I.; PILIOUGINE, M. Machine learning approach for next day energy production forecasting in grid connected photovoltaic plants. **World Renewable Energy Congress**, *[S. l.]*, p. 2869–2874, 2011. DOI: 10.3384/ecp110572869. Disponível em: http://www.ep.liu.se/ecp/057/vol11/024/ecp57vol11_024.pdf.

MOZAW. **Best Solar Batteries ForYour Solar Power System**. 2019.

MÜLLER, Nicolás; KOURO, Samir; ZANCHETTA, Pericle; WHEELER, Patrick; BITTNER, Gustavo; GIRARDI, Francesco. Energy storage sizing strategy for grid-tied PV plants under power clipping limitations. **Energies**, *[S. l.]*, v. 12, n. 9, p. 1–17, 2019. DOI: 10.3390/en12091812.

NORTHERN ARIZON WIND AND SUN. **Batteries and Charging**. 2019.

OGUNLEYE, Eric Kehinde. Political Economy of Nigerian Power Sector Reform. *[S. l.]*, n. July 2019, p. 1–20, 2017. DOI: 10.1093/oso/9780198802242.001.0001.

OH, Eunsung; SON, Sung Yong. Energy-storage system sizing and operation strategies based on discrete Fourier transform for reliable wind-power generation. **Renewable Energy**, *[S. l.]*, v. 116, p. 786–794, 2018. DOI: 10.1016/j.renene.2017.10.028. Disponível em: https://doi.org/10.1016/j.renene.2017.10.028.

OPEN ELECTRICAL. **Battery Sizing**. 2017. Disponível em:

https://wiki.openelectrical.org/index.php?title=Battery_Sizing#Calculation_Methodology. Acesso em: 13 abr. 2020.

PERALTA, C. O.; SALLES, M. B. C. Advanced energy storage systems to increase the penetration of renewable energies in Fernando de Noronha Island. **Clean Electrical Power (ICCEP), …**, *[S. l.]*, v. 01, p. 0–4, 2017. Disponível em: http://ieeexplore.ieee.org/abstract/document/8004845/.

QUINTERO PULIDO, Diego Fernando; HOOGSTEEN, Gerwin; TEN KORTENAAR, Marnix V.; HURINK, Johann L.; HEBNER, Robert E.; SMIT, Gerard J. M. Characterization of storage sizing for an off-grid house in the US and the Netherlands. **Energies**, *[S. l.]*, v. 11, n. 2, 2018. DOI: 10.3390/en11020265.

RAMEDANI, Z.; OMID, M.; KEYHANI, A. A method based on neural networks for generating solar radiation map. *[S. l.]*, v. 3, n. 5, p. 775–786, 2012.

ROYER, Julio Cesar; WILHELM, Volmir Eugênio; TEIXEIRA JUNIOR, Luiz Albino; FRANCO, Edgar Manuel Carreño. Short-Term Solar Radiation Forecasting By Using an Iterative Combination of Wavelet Artificial Neural Networks. **Independent Journal of Management & Production**, *[S. l.]*, v. 7, n. 1, p. 271–288, 2016. DOI: 10.14807/ijmp.v7i1.393. Disponível em: http://www.ijmp.jor.br/index.php/ijmp/article/view/393.

SAENGER, Pierre; DEVILLERS, Nathalie; DESCHINKEL, Karine; PERA, Marie Cecile; COUTURIER, Raphael; GUSTIN, Frederic. Optimization of Electrical Energy Storage System Sizing for an Accurate Energy Management in an Aircraft. **IEEE Transactions on Vehicular Technology**, *[S. l.]*, v. 66, n. 7, p. 5572–5583, 2017. DOI: 10.1109/TVT.2016.2617288.

SINAPSIS. Avaliação dos custos de energia e suas implicações na regulação. *[S. l.]*, v. 1, p. 1–74, 2016.

SKH ARCHITECTS. **No Title**. 2017. Disponível em: http://www.skharchitects.com/photovoltaic-system-works/. Acesso em: 4 abr. 2020.

SOLAR QUOTES. **Lead Acid Batteries**. 2019a.

SOLAR QUOTES. **Lithium-ion Batteries Guide**. 2019b.

SOLAR STIK. **Calculating Battery Capacity**. 2020. Disponível em: https://www.solarstik.com/stikopedia/calculate-battery-capacity/. Acesso em: 13 abr. 2020.

SOLAR TOWN. **Choosing and Sizing Batteries, Charge Controllers and Inverters for Your Off-Grid Solar Energy System**. 2020. Disponível em: https://solartown.com/learning/solar-panels/choosing-and-sizing-batteries-charge-controllers-and-inverters-for-your-off-grid-solar-energy-system/. Acesso em: 13 abr. 2020.

TEITELBAUM, Brian. Designing a Battery-Based System. *[S. l.]*, 2016.

TROJAN BATTERY COMPANY. Battery sizing guidelines. *[S. l.]*, p. 0–1, [s.d.].

VENU, Chandu; RIFFONNEAU, Yann; BACHA, Seddik; BAGHZOUZ, Yahia. Battery storage system sizing in distribution feeders with distributed photovoltaic systems. **2009 IEEE Bucharest PowerTech: Innovative Ideas Toward the Electrical Grid of the Future**, *[S. l.]*, p. 1–5, 2009. DOI: 10.1109/PTC.2009.5282093.

VOYANT, Cyril; HAURANT, Pierrick; MUSELLI, Marc; PAOLI, Christophe; NIVET, Marie Laure. Time series modeling and large scale global solar radiation forecasting from geostationary satellites data. **Solar Energy**, *[S. l.]*, v. 102, p. 131–142, 2014. DOI: 10.1016/j.solener.2014.01.017. Disponível em: http://dx.doi.org/10.1016/j.solener.2014.01.017.

WANG, Libin; LI, CHunHui; WANG, JiaWei; ZHAO, Haibo; SHEN, ZeYuan. Optimal sizing of Battery Energy Storage System for household microgrid. *[S. l.]*, n. Iccmcee, p. 121–127, 2015. DOI: 10.2991/iccmcee-15.2015.25.

WEBB, K. Section 6 : Battery Bank Sizing Procedures. *[S. l.]*, [s.d.].

WENIGER, Johannes; TJADEN, Tjarko; QUASCHNING, Volker. Sizing of residential PV battery systems. *[S. l.]*, v. 46, p. 78–87, 2014. DOI: 10.1016/j.egypro.2014.01.160.

WHOLESALE SOLAR. **Off-grid battery bank sizing**. 2020. Disponível em: https://www.wholesalesolar.com/solar-information/battery-bank-sizing. Acesso em: 11 abr. 2020.

WONG, Ling Ai; RAMACHANDARAMURTHY, Vigna K.; TAYLOR, Phil; EKANAYAKE, J. B.; WALKER, Sara L.; PADMANABAN, Sanjeevikumar. Review on the optimal placement, sizing and control of an energy storage system in the distribution network. **Journal of Energy Storage**, *[S. l.]*, v. 21, n. December 2018, p. 489–504, 2019. DOI: 10.1016/j.est.2018.12.015. Disponível em: https://doi.org/10.1016/j.est.2018.12.015.

WORLD BANK GROUP. **Access to Electricity**. 2019. Disponível em: https://data.worldbank.org/indicator/eg.elc.accs.zs. Acesso em: 6 jul. 2019.

WU, Di; KINTNER-MEYER, Michael; YANG, Tao; BALDUCCI, Patrick. Analytical sizing methods for behind-the-meter battery storage $. *[S. l.]*, v. 12, p. 297–304, 2017. DOI: 10.1016/j.est.2017.04.009.

XIA, Shiwei; CHAN, K. W.; LUO, Xiao; BU, Siqi; DING, Zhaohao; ZHOU, Bin. Optimal sizing of energy storage system and its cost-benefit analysis for power grid planning with intermittent wind generation. **Renewable Energy**, *[S. l.]*, v. 122, p. 472–486, 2018. DOI: 10.1016/j.renene.2018.02.010. Disponível em: https://doi.org/10.1016/j.renene.2018.02.010.

XU, Guodong; SHANG, Ce; ZHANG, Xiaohu. Sizing battery energy storage systems for industrial customers with photovoltaic power. **Energy Procedia**, *[S. l.]*, v. 158, p. 4953–4958, 2019. DOI: 10.1016/j.egypro.2019.01.693.

YANG, Yuqing; BREMNER, Stephen; MENICTAS, Chris; KAY, Merlinde. Battery energy storage system size determination in renewable energy systems: A review. **Renewable and Sustainable Energy Reviews**, *[S. l.]*, v. 91, n. March, p. 109–125, 2018. a. DOI: 10.1016/j.rser.2018.03.047. Disponível em: https://doi.org/10.1016/j.rser.2018.03.047.

YANG, Yuqing; BREMNER, Stephen; MENICTAS, Chris; MENG, Ke; DONG, Zhao Yang; KAY, Merlinde. An economic optimization for BESS sizing in a hybrid PV and wind power plant. **2017 IEEE Innovative Smart Grid Technologies - Asia: Smart Grid for Smart Community, ISGT-Asia 2017**, *[S. l.]*, p. 1–6, 2018. b. DOI: 10.1109/ISGT-Asia.2017.8378353.

YUAN, Kaixin; YANG, Shanchao; WU, Kai; SHEN, Fang. Time Series Forecasting Based on Kernel Mapping and High-Order Fuzzy Cognitive Maps. **Economics Letters**, *[S. l.]*, p. 28, 2020. DOI: 10.1016/j.econlet.2020.109231. Disponível em:

https://doi.org/10.1016/j.econlet.2020.109231.

ZHANG, Chao; WEI, Yi-li; CAO, Peng-fei; LIN, Meng-chang. Energy storage system : Current studies on batteries and power condition system. **Renewable and Sustainable Energy Reviews**, *[S. l.]*, v. 82, n. July 2017, p. 3091–3106, 2018. DOI: 10.1016/j.rser.2017.10.030.

ZHANG, Yang; LUNDBLAD, Anders; ELIA, Pietro; BENAVENTE, F.; YAN, Jinyue. Battery sizing and rule-based operation of grid-connected photovoltaic-battery system : A case study in Sweden Level of Confidence State of Charge. **Energy Conversion and Management**, *[S. l.]*, v. 133, p. 249–263, 2017. DOI: 10.1016/j.enconman.2016.11.060.

ZHOU, Nan; LIU, Nian; ZHANG, Jianhua; LEI, Jinyong. Multi-objective optimal sizing for battery storage of PV-based microgrid with demand response. **Energies**, *[S. l.]*, v. 9, n. 8, 2016. DOI: 10.3390/en9080591.

ZOLFAGHARI, Morteza; GHAFFARZADEH, Navid; ARDAKANI, Ali Jahanbani. Optimal sizing of battery energy storage systems in off-grid micro grids using convex optimization. **Journal of Energy Storage**, *[S. l.]*, v. 23, n. March, p. 44–56, 2019. DOI: 10.1016/j.est.2019.02.027. Disponível em: https://doi.org/10.1016/j.est.2019.02.027.

ANNEX I: Graphical Representations of Monthly Residual a_t

Figure 45 – Residual a_t for February

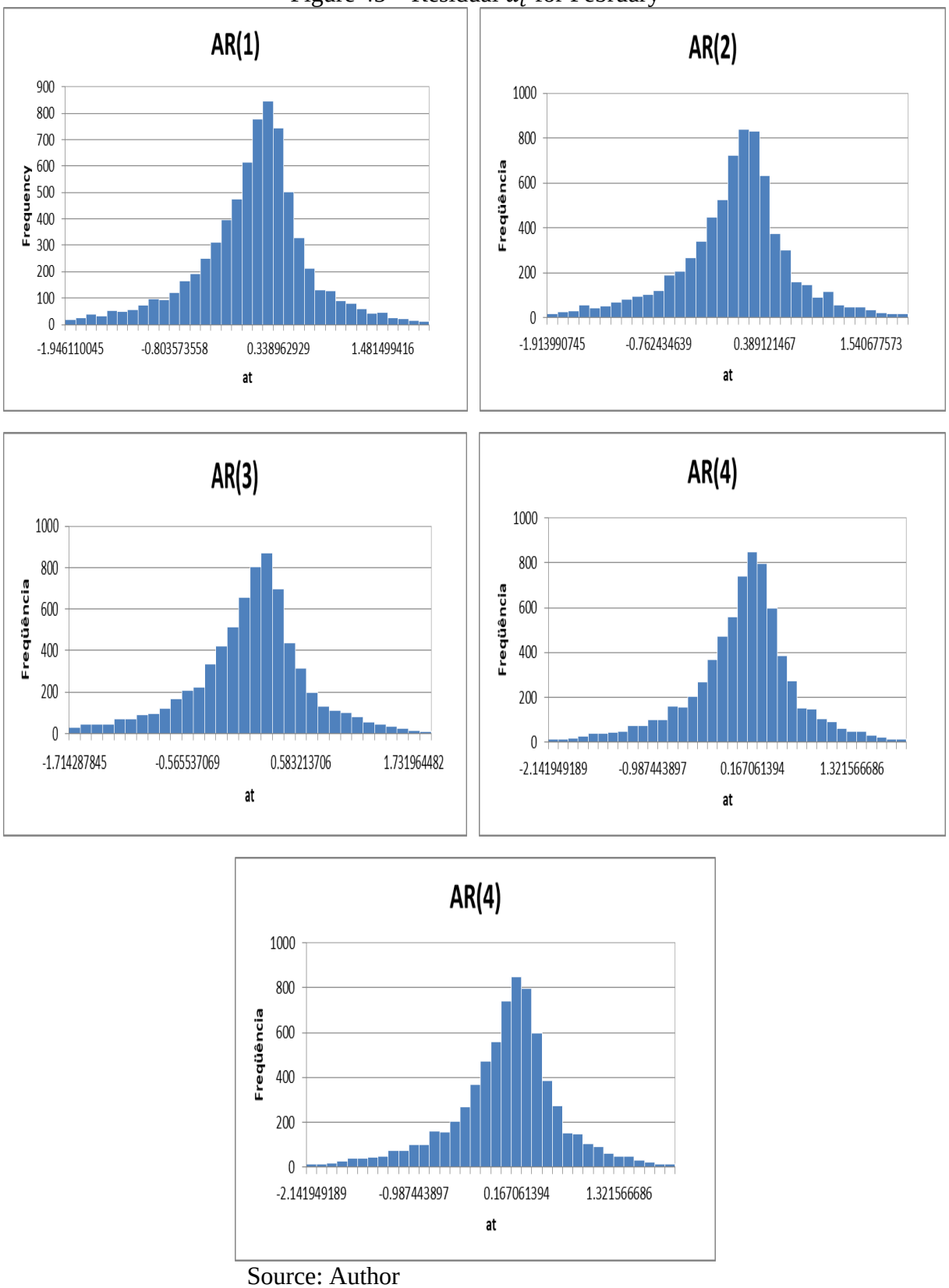

Source: Author

Figure 46 – Residual a_t for March

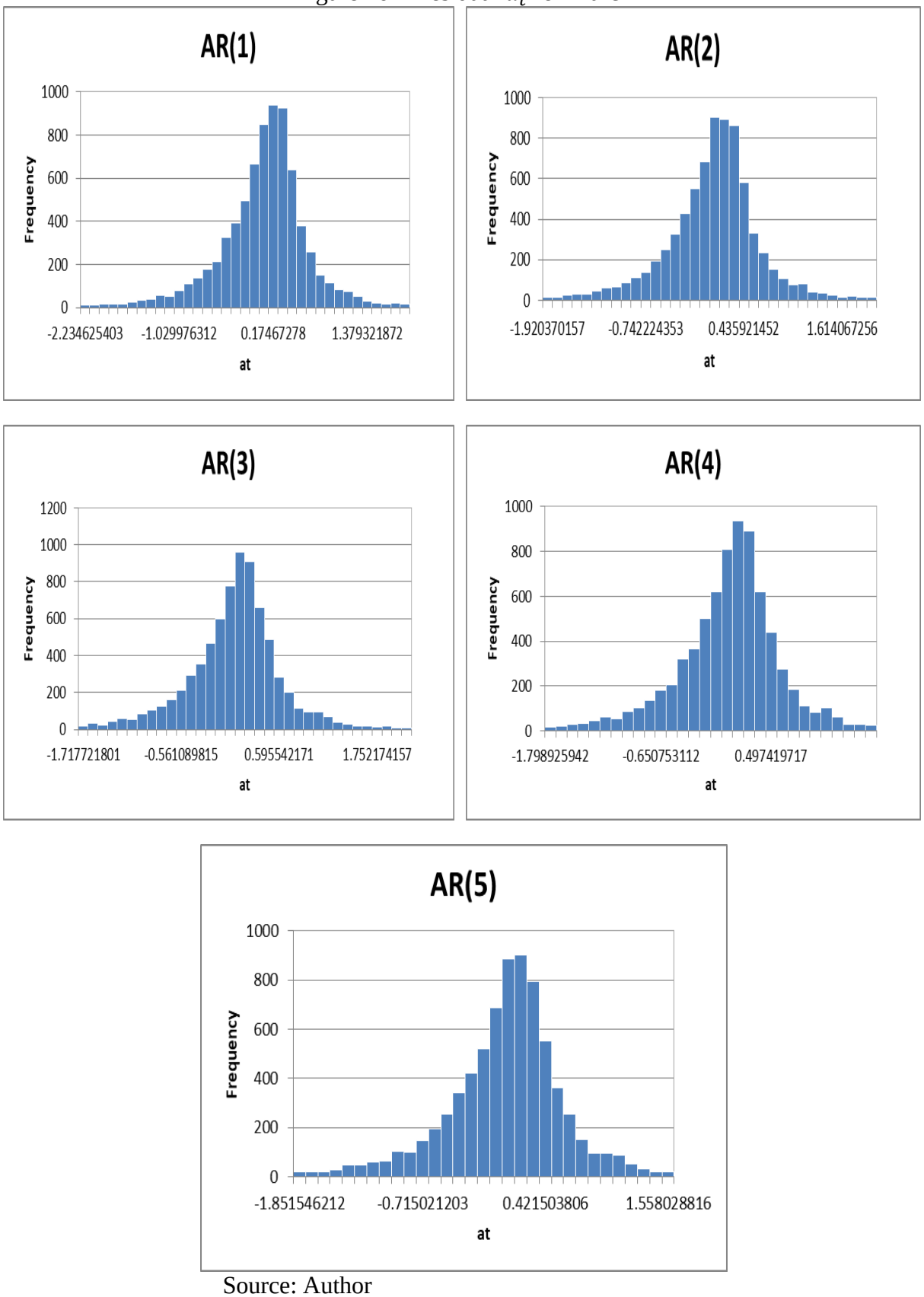

Source: Author

Figure 47 – Residual a_t for April

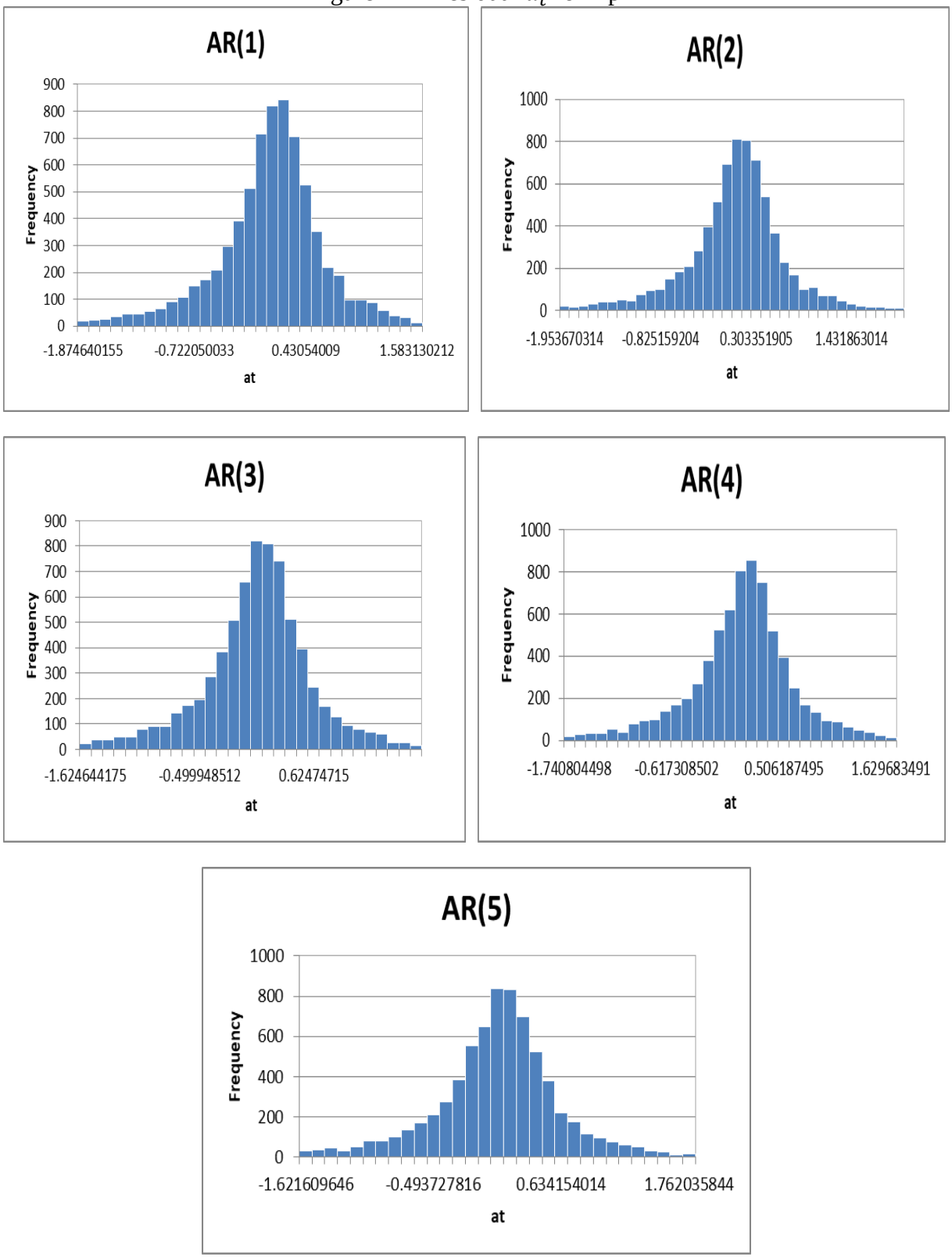

Source: Author

Figure 48 – Residual a_t for May

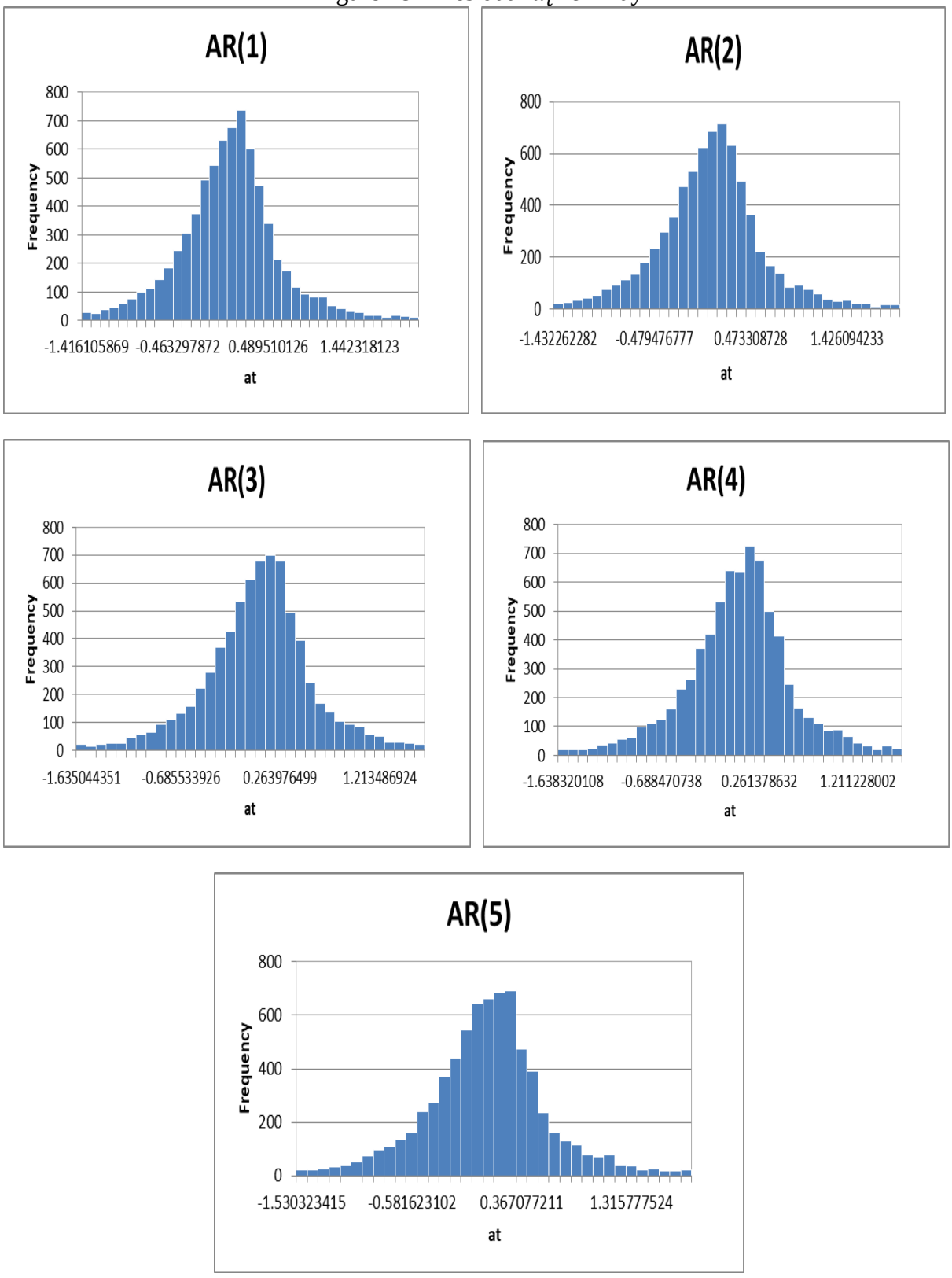

Source: Author

Figure 49 – Residual a_t for June

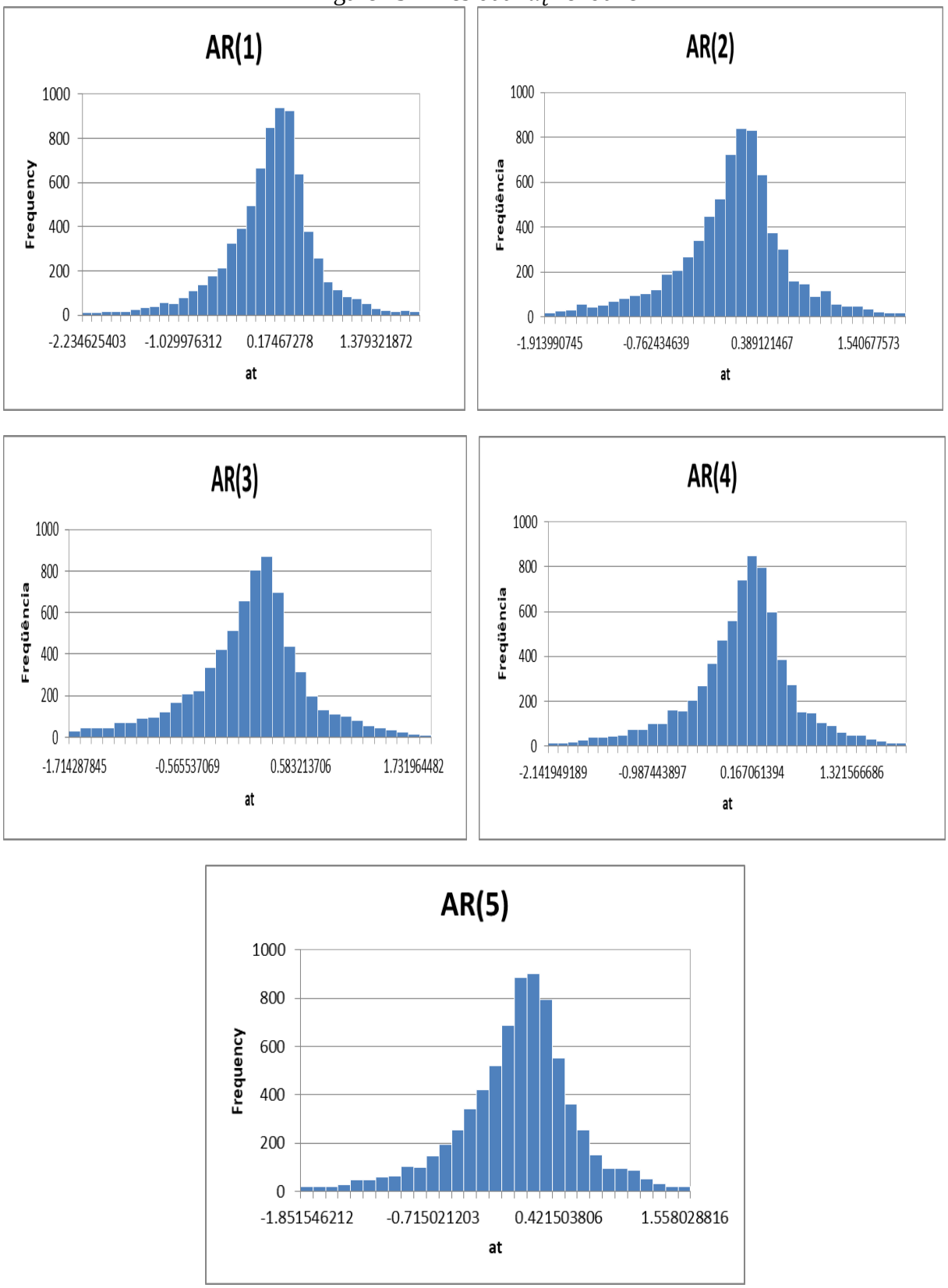

Source: Author

Figure 50 – Residual a_t for July

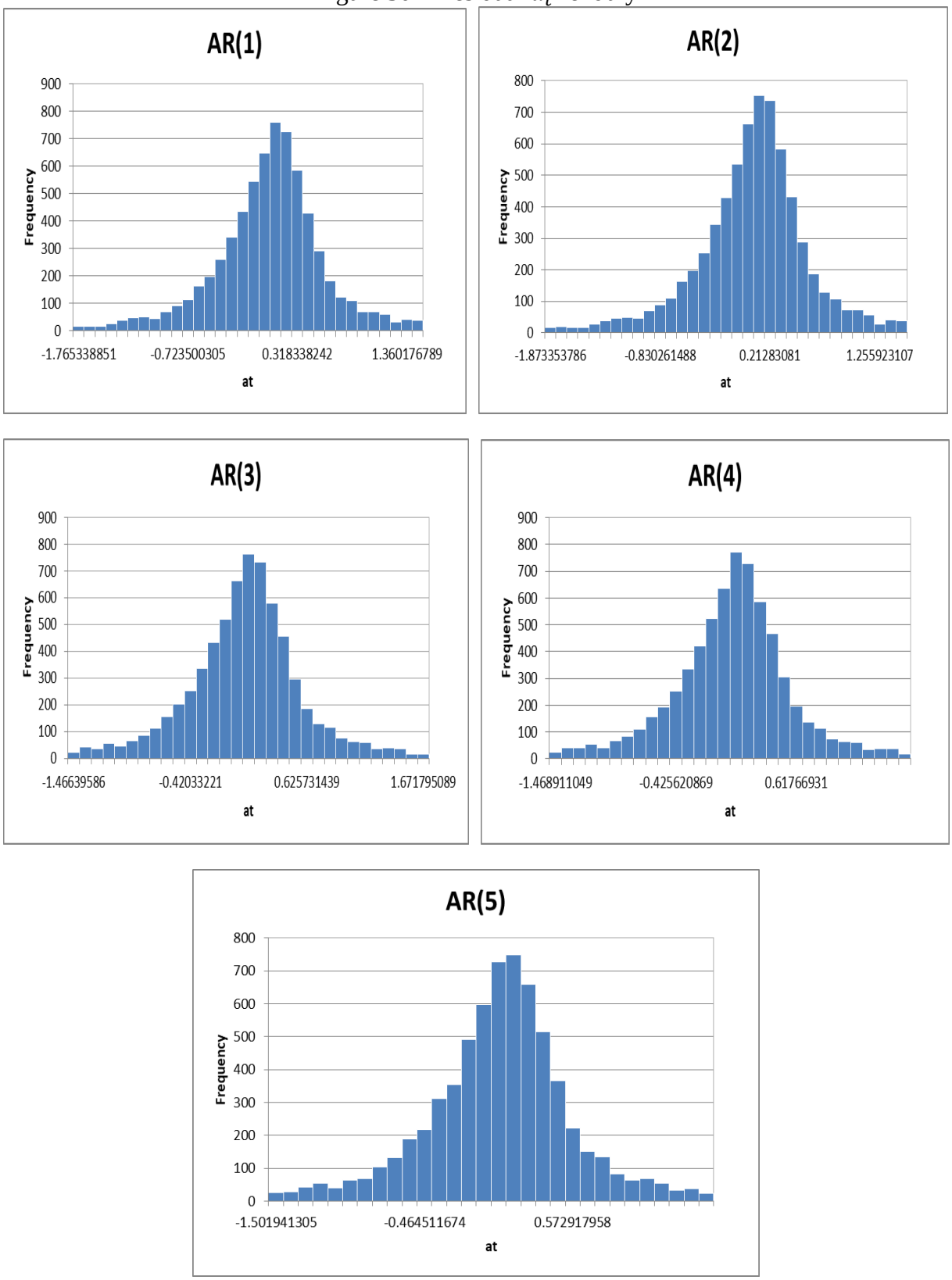

Source: Author

Figure 51 – Residual a_t for August

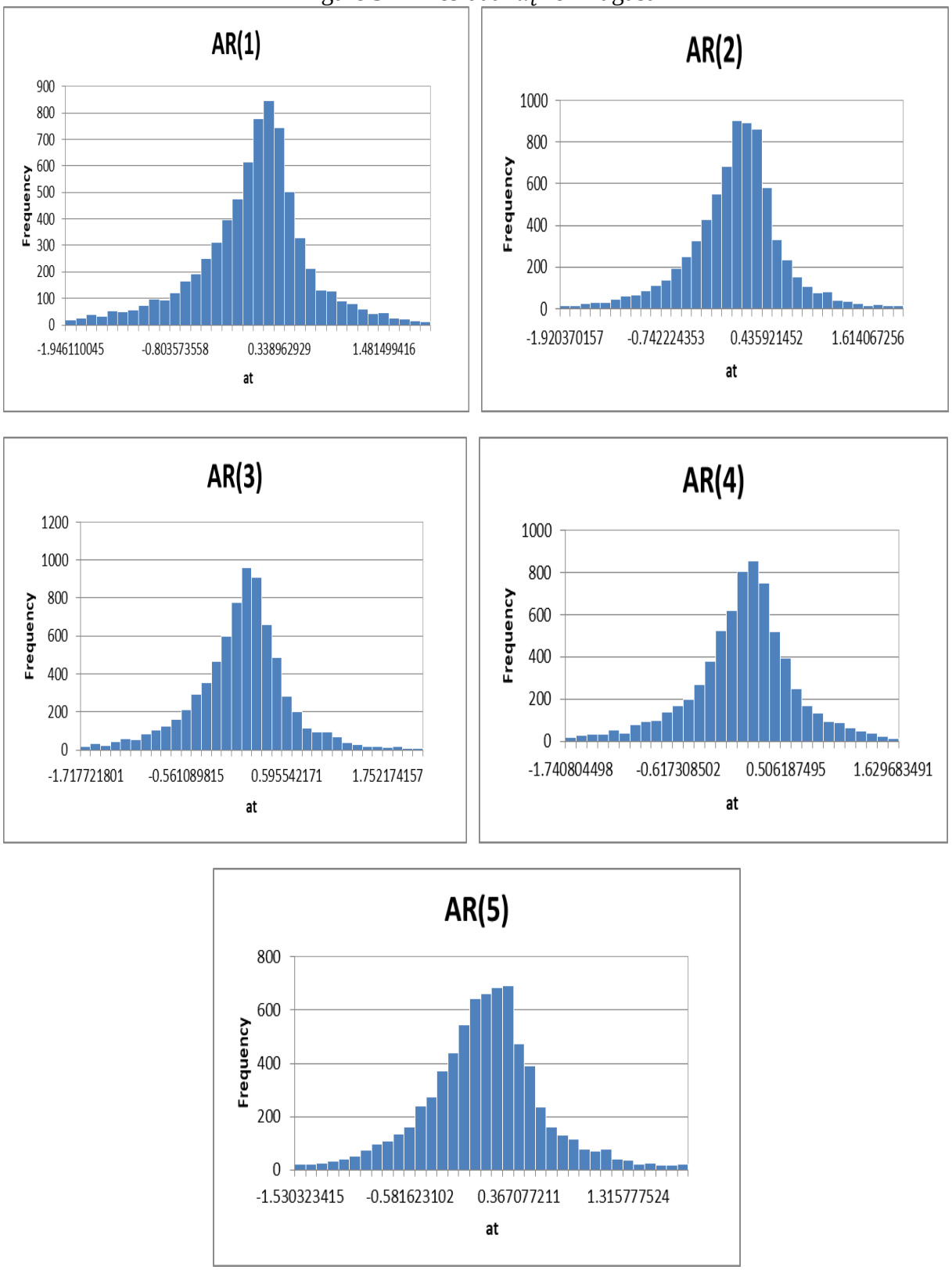

Source: Author

Figure 52 – Residual a_t for September

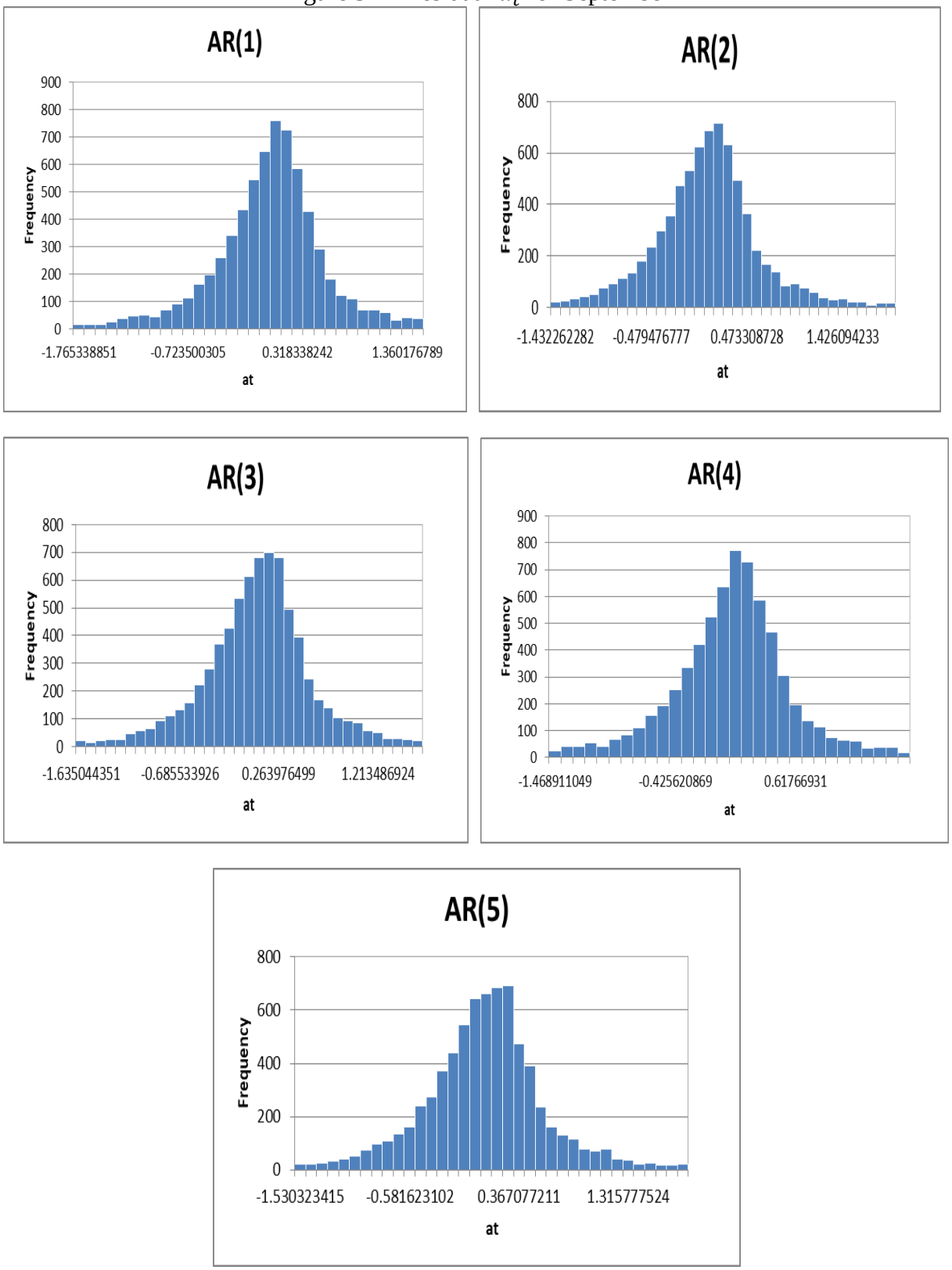

Source: Author

Figure 53 – Residual a_t for October

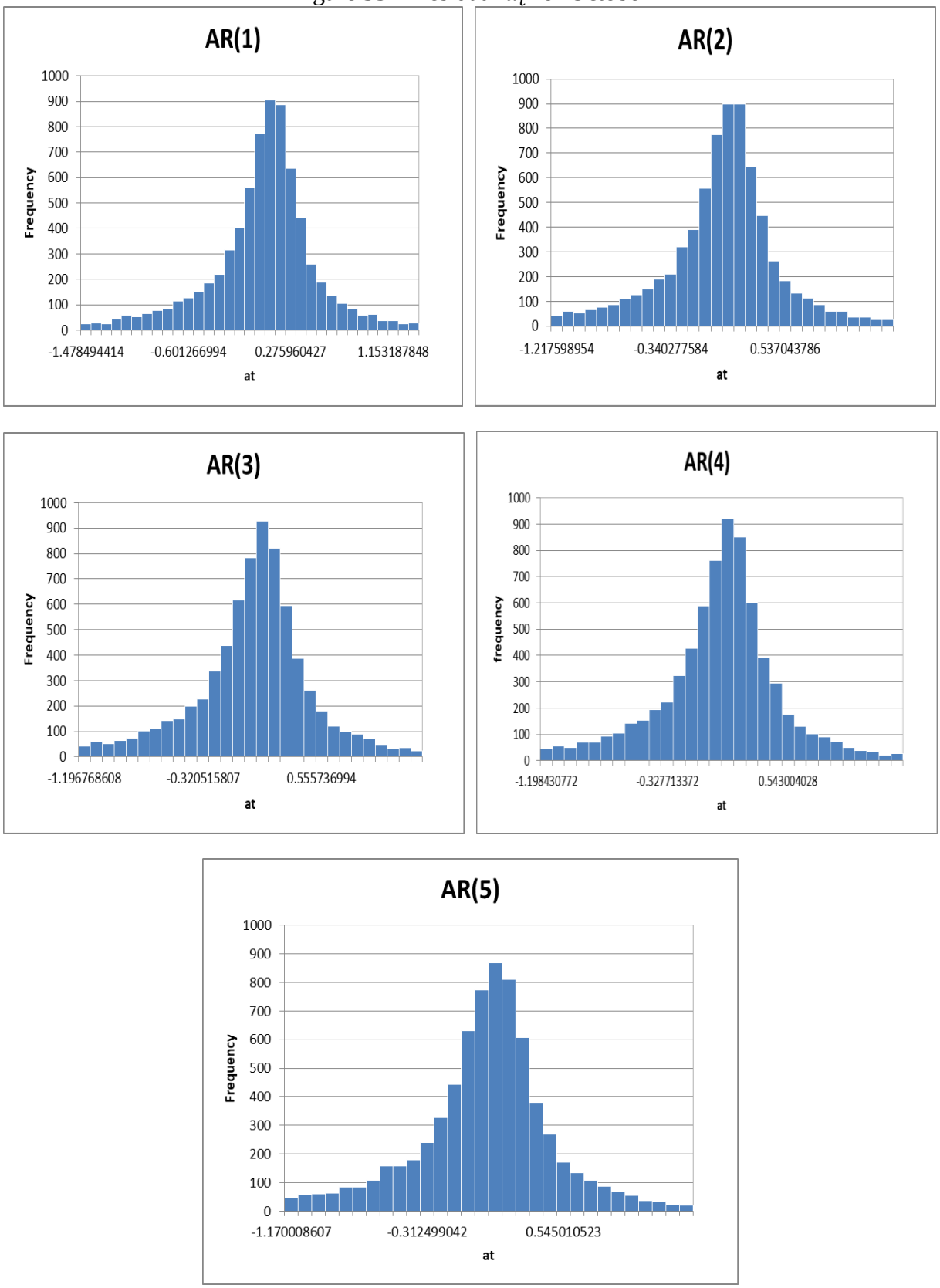

Source: Author

Figure 54 – Residual a_t for November

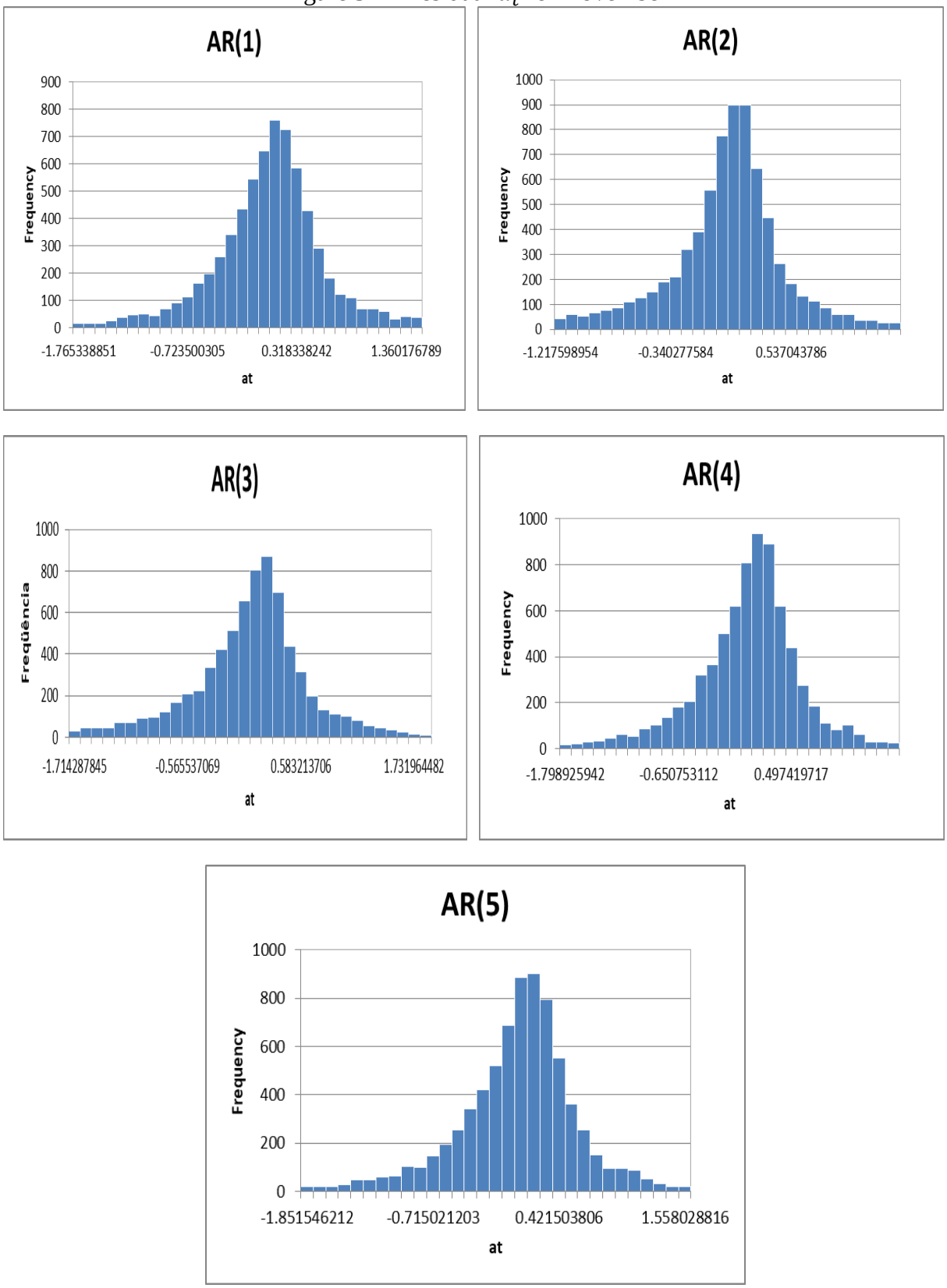

Source: Author

Figure 55 – Residual a_t for December

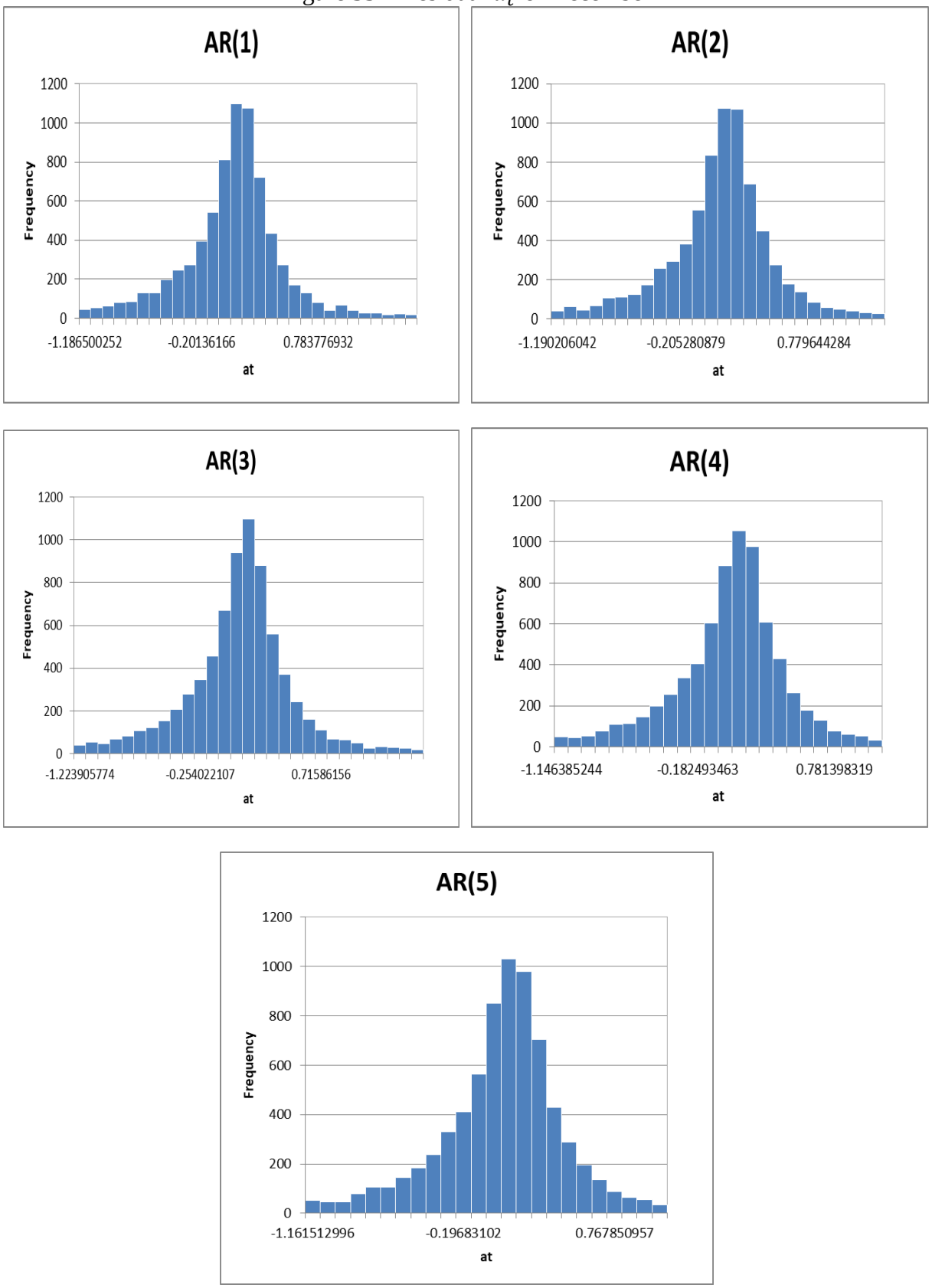

Source: Author

ANNEX II: Monthly Error Tables and Graphs

Table 19 – Error values by comparative method for February

	Error (pu)			
Models	**RMSE**	**AME**	**RMPE**	**PEmax**
AR(1)	1.0000	1.0000	0.9647	0.7496
AR(2)	0.9987	0.9975	0.9477	0.7212
AR(3)	0.9932	0.9907	0.9237	0.7403
AR(4)	0.9900	0.9872	0.9417	0.7369
AR(5)	0.9872	0.9838	1.0000	1.0000

Source: Author

Figure 56 – Graphical representation of errors for February

Source: Author

Table 20 – Error values by comparative method for March

	Error (pu)			
Models	**RMSE**	**AME**	**RMPE**	**PEmax**
AR(1)	1.0000	1.0000	0.9489	0.9089
AR(2)	0.9963	0.9956	1.0000	0.9280
AR(3)	0.9927	0.9913	0.9236	0.9066
AR(4)	0.9914	0.9898	0.9058	0.9439
AR(5)	0.9895	0.9885	0.9266	1.0000

Source: Author

Figure 57 – Graphical representation of errors for March

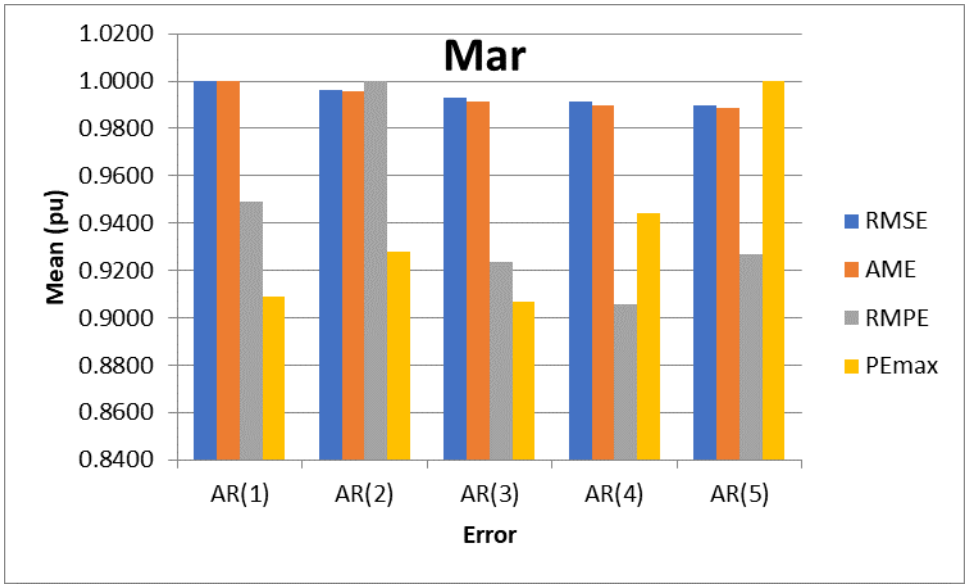

Source: Author

Table 21 – Error values by comparative method for April

	Error (pu)			
Models	**RMSE**	**AME**	**RMPE**	**PEmax**
AR(1)	1.0000	1.0000	0.9910	0.8907
AR(2)	0.9953	0.9953	0.9936	0.9287
AR(3)	0.9917	0.9908	0.9771	0.9578
AR(4)	0.9894	0.9885	1.0000	1.0000
AR(5)	0.9886	0.9870	0.9961	0.9863

Source: Author

Figure 58 – Graphical representation of errors for April

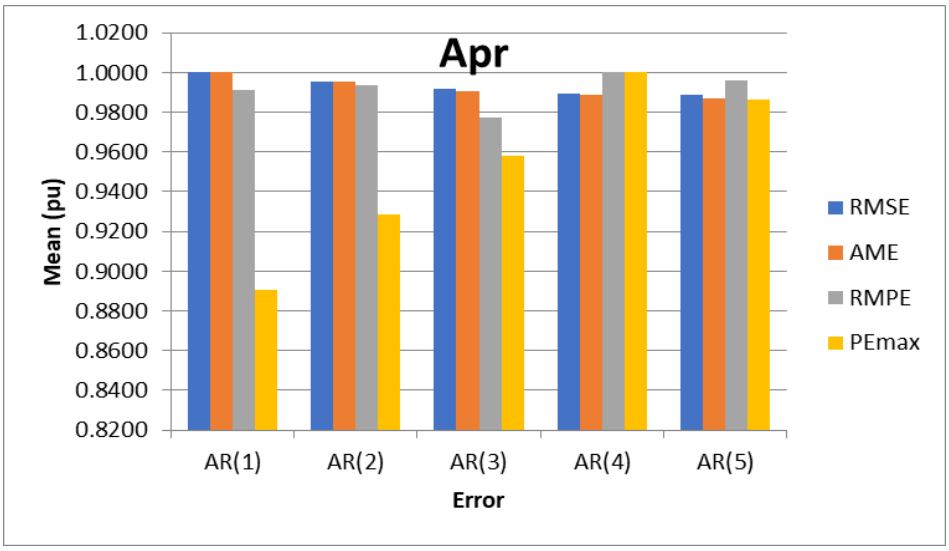

Source: Author

Table 22 – Error values by comparative method for May

	Error (pu)			
Models	**RMSE**	**AME**	**RMPE**	**PEmax**
AR(1)	1.0000	1.0000	0.9901	0.9755
AR(2)	0.9995	0.9988	0.9951	0.9892
AR(3)	0.9972	0.9957	1.0000	0.9863
AR(4)	0.9961	0.9950	0.9999	1.0000
AR(5)	0.9949	0.9931	0.9998	0.9939

Source: Author

Figure 59 – Graphical representation of errors for May

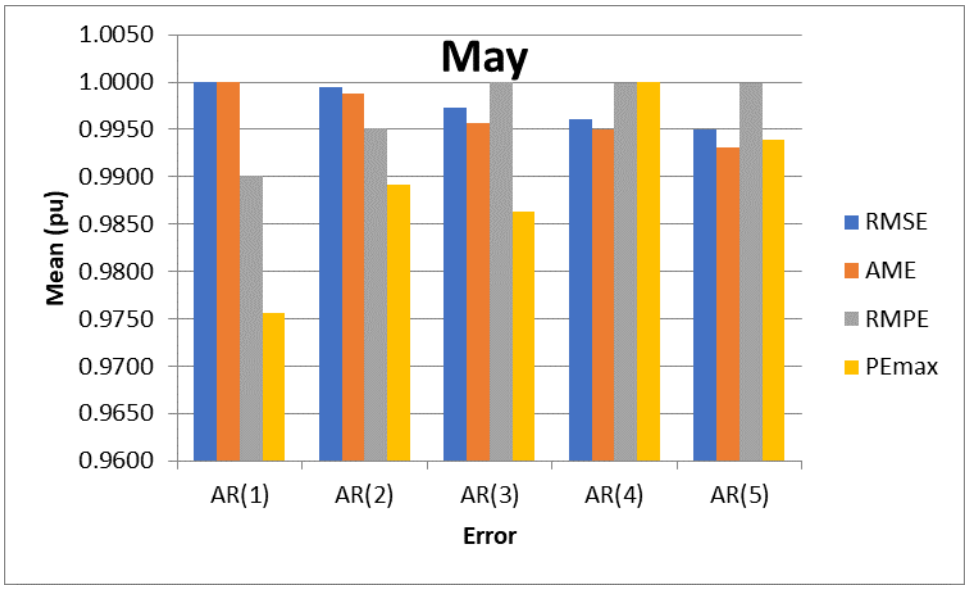

Source: Author

Table 23 – Error values by comparative method for June

	Error (pu)			
Models	**RMSE**	**AME**	**RMPE**	**PEmax**
AR(1)	1.0000	1.0000	0.9982	0.9648
AR(2)	0.9999	0.9997	1.0000	0.9661
AR(3)	0.9980	0.9977	0.9742	0.9883
AR(4)	0.9973	0.9968	0.9815	0.9982
AR(5)	0.9972	0.9963	0.9842	1.0000

Source: Author

Figure 60 – Graphical representation of errors for June

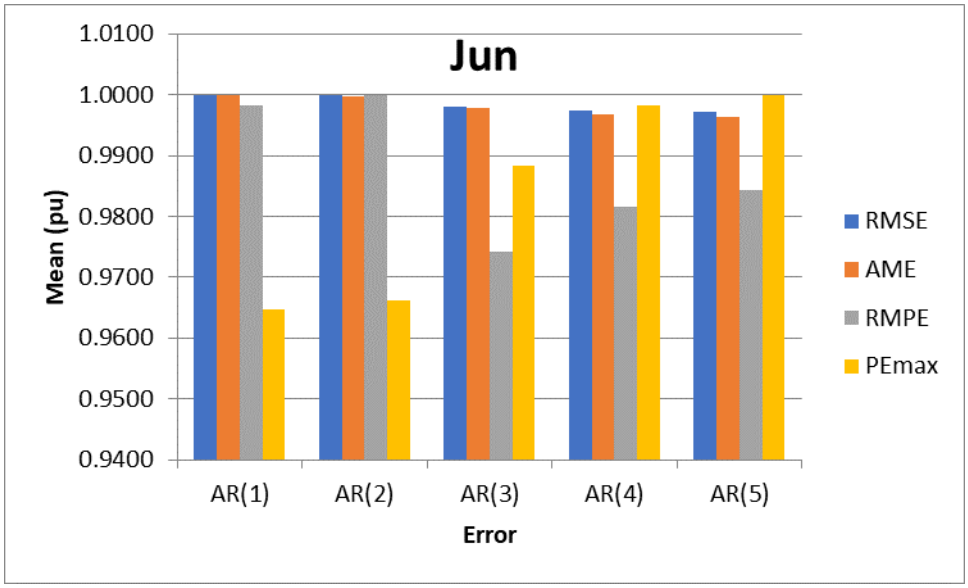

Source: Author

Table 24 – Error values by comparative method for July

	Error (pu)			
Models	**RMSE**	**AME**	**RMPE**	**PEmax**
AR(1)	1.0000	0.9996	0.9959	1.0000
AR(2)	0.9999	1.0000	0.9878	0.9748
AR(3)	0.9979	0.9982	0.9941	0.9693
AR(4)	0.9978	0.9983	0.9898	0.9468
AR(5)	0.9970	0.9978	1.0000	0.9098

Source: Author

Figure 61 – Graphical representation of errors for July

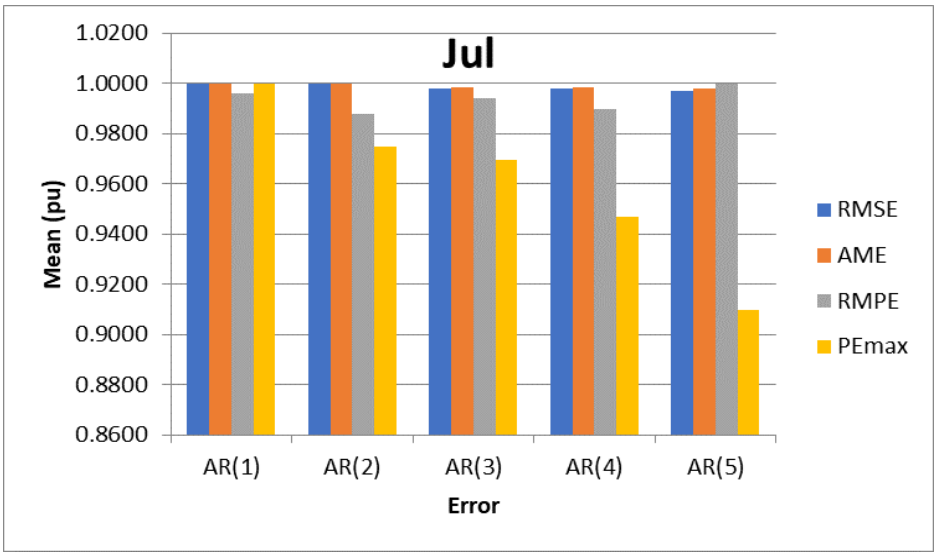

Source: Author

Table 25 – Error values by comparative method for August

	Error (pu)			
Models	**RMSE**	**AME**	**RMPE**	**PEmax**
AR(1)	1.0000	1.0000	1.0000	1.0000
AR(2)	0.9996	0.9987	0.9947	0.9426
AR(3)	0.9974	0.9970	0.9949	0.9391
AR(4)	0.9967	0.9965	0.9930	0.9427
AR(5)	0.9959	0.9947	0.9888	0.9330

Source: Author

Figure 62 – Graphical representation of errors for August

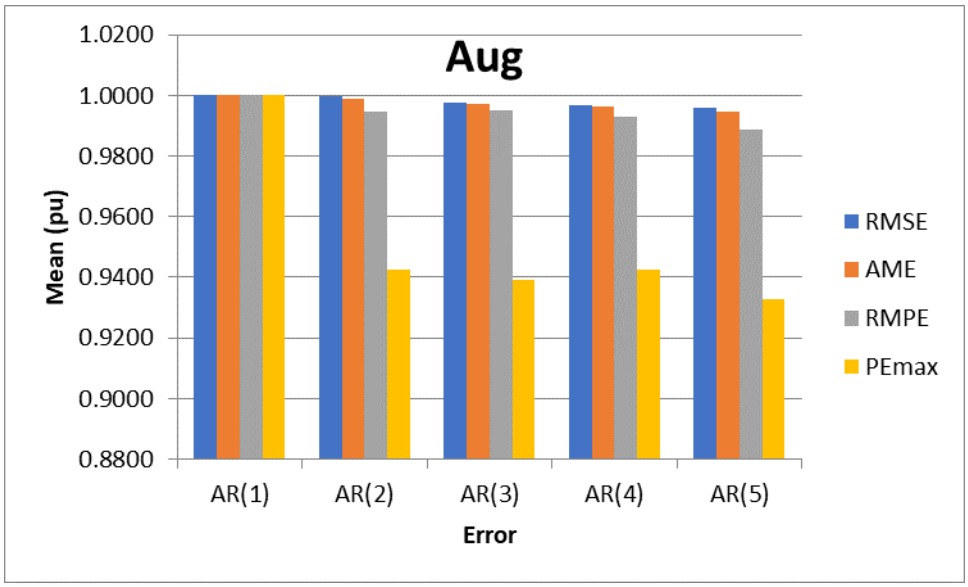

Source: Author

Table 26 – Error values by comparative method for September

	Error (pu)			
Models	**RMSE**	**AME**	**RMPE**	**PEmax**
AR(1)	1.0000	0.9986	0.9847	0.9961
AR(2)	0.9999	0.9984	0.9850	1.0000
AR(3)	0.9960	0.9999	0.9930	0.9576
AR(4)	0.9958	1.0000	0.9910	0.9620
AR(5)	0.9945	0.9994	1.0000	0.9918

Source: Author

Figure 63 – Graphical representation of errors for September

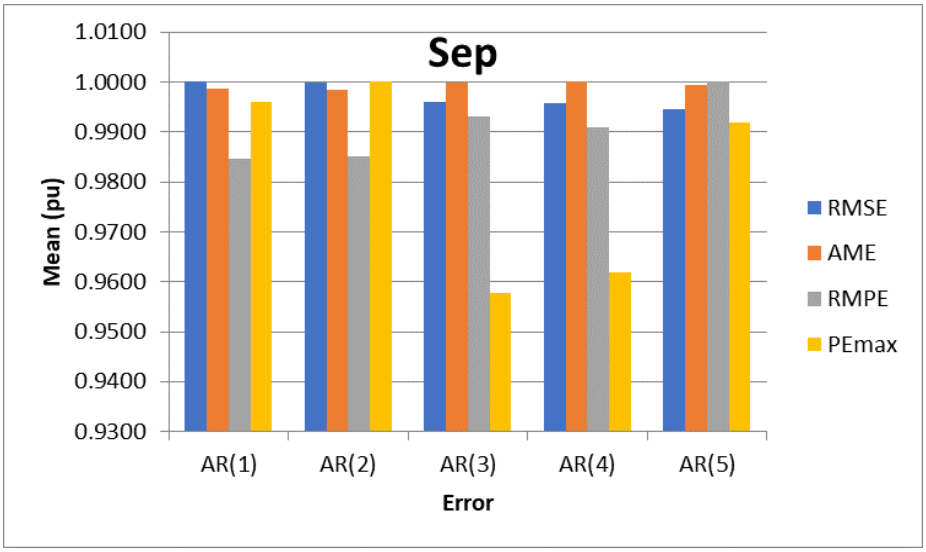

Source: Author

Table 27 – Error values by comparative method for October

	Error (pu)			
Models	**RMSE**	**AME**	**RMPE**	**PEmax**
AR(1)	0.9999	1.0000	0.9625	0.9050
AR(2)	1.0000	0.9999	0.9624	0.9059
AR(3)	0.9961	0.9997	1.0000	0.9265
AR(4)	0.9959	1.0000	0.9997	0.9326
AR(5)	0.9935	0.9999	0.9956	1.0000

Source: Author

Figure 64 – Graphical representation of errors for October

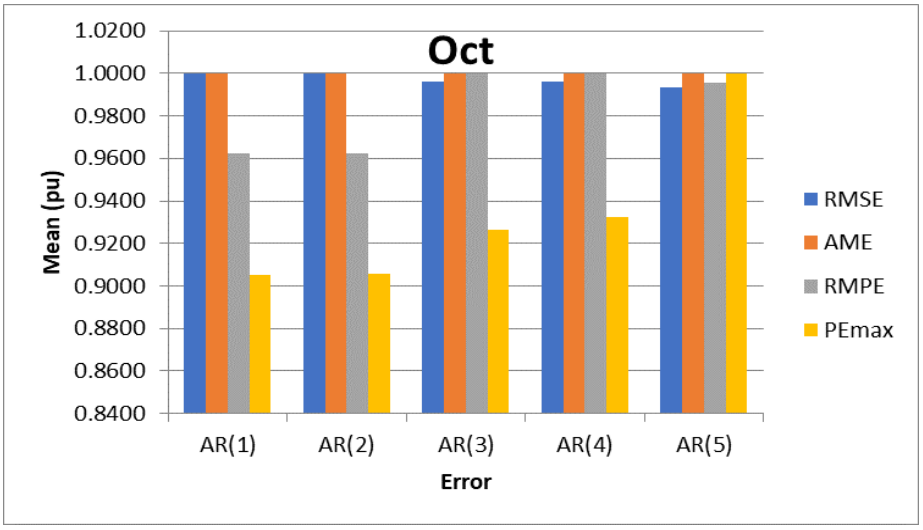

Source: Author

Table 28 – Error values by comparative method for November

	Error (pu)			
Models	**RMSE**	**AME**	**RMPE**	**PEmax**
AR(1)	1.0000	0.9998	1.0000	1.0000
AR(2)	1.0000	1.0000	0.9964	0.9303
AR(3)	0.9982	0.9970	0.9664	0.8979
AR(4)	0.9970	0.9954	0.9490	0.9228
AR(5)	0.9955	0.9949	0.9286	0.8697

Source: Author

Figure 65 – Graphical representation of errors for November

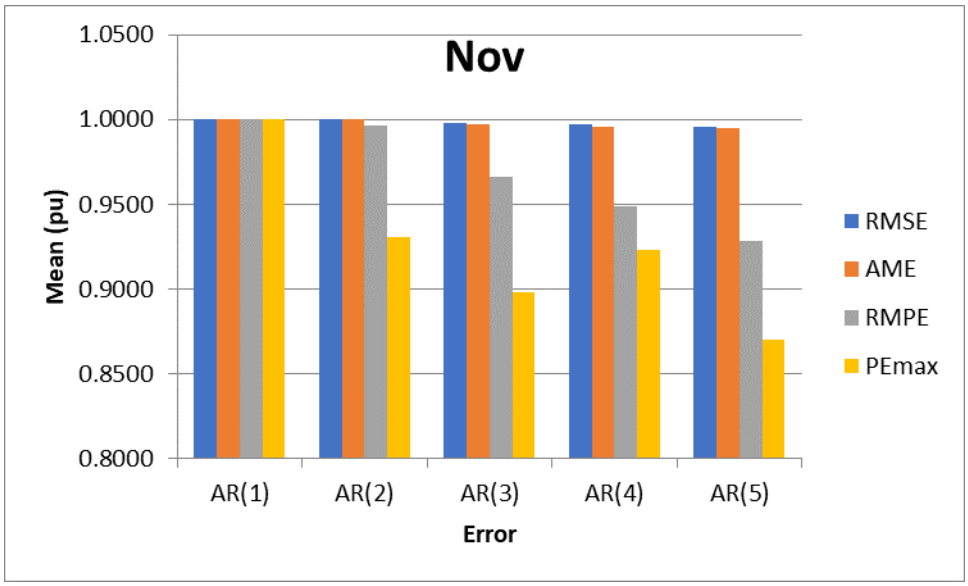

Source: Author

Table 29 – Error values by comparative method for December

	Error (pu)			
Models	**RMSE**	**AME**	**RMPE**	**PEmax**
AR(1)	1.0000	1.0000	0.9519	0.9265
AR(2)	0.9957	0.9975	0.9822	1.0000
AR(3)	0.9908	0.9966	0.9997	0.9620
AR(4)	0.9882	0.9955	1.0000	0.9442
AR(5)	0.9871	0.9952	0.9734	0.7643

Source: Author

Figure 66 – Graphical representation of errors for December

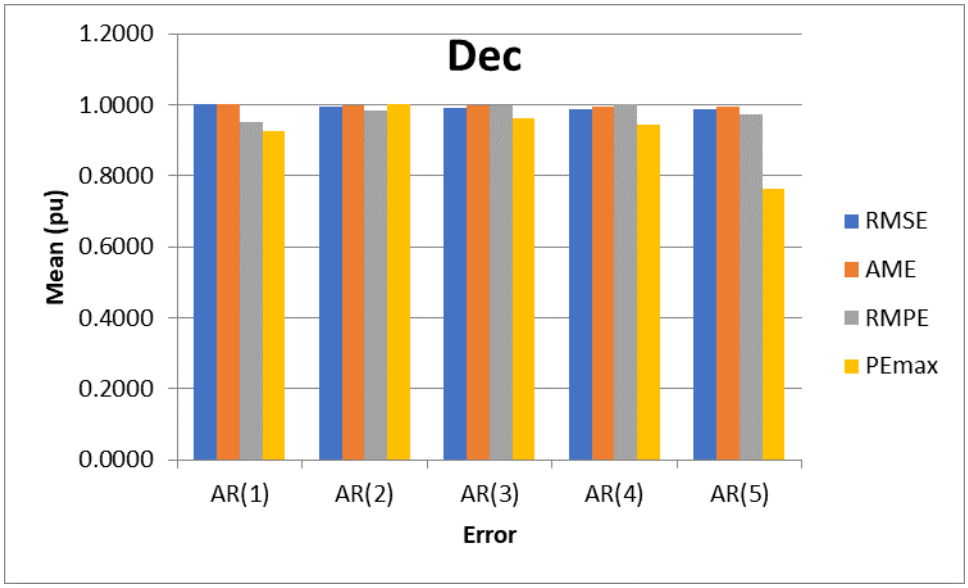

Source: Author

ANNEX III: Monthly Confidence Interval Graphs

Figure 67 – Confidence interval graph for February

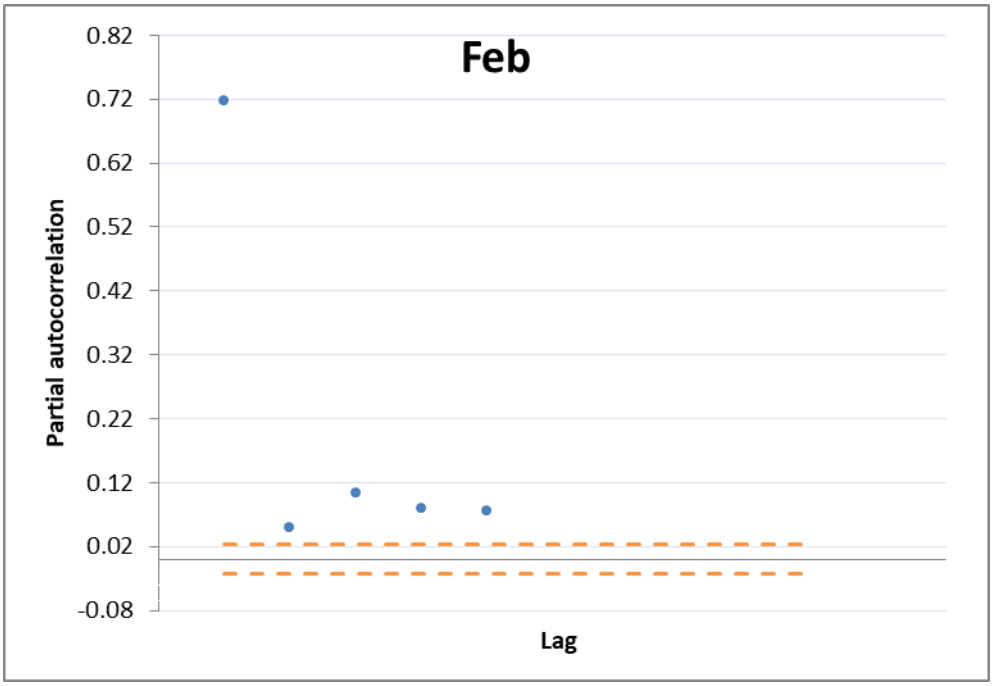

Source: Author

Figure 68 – Confidence interval graph for March

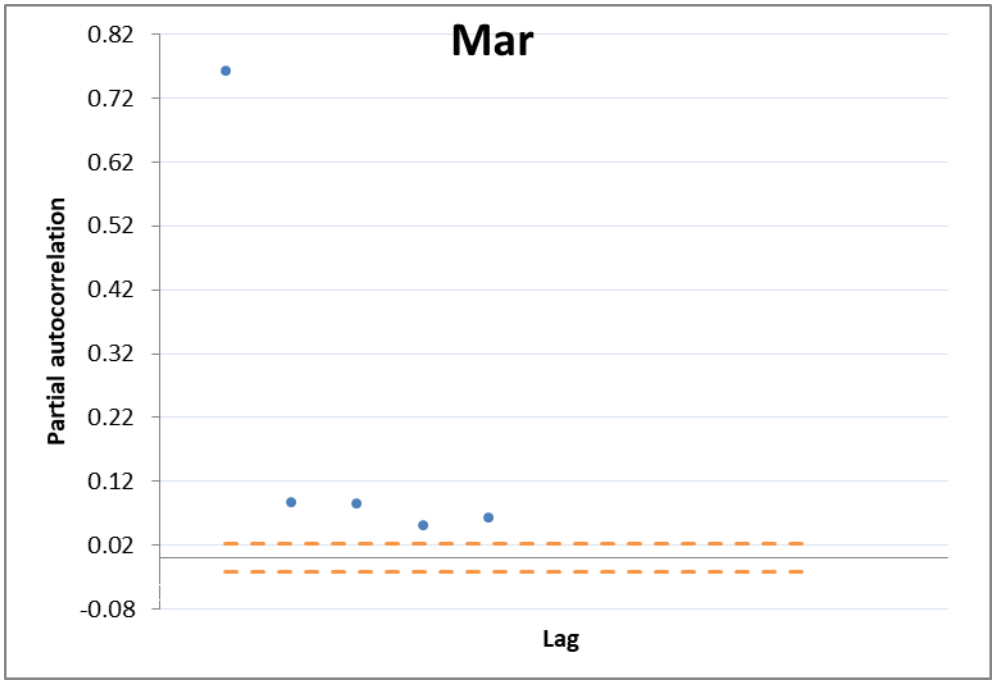

Source: Author

Figure 69 – Confidence interval graph for April

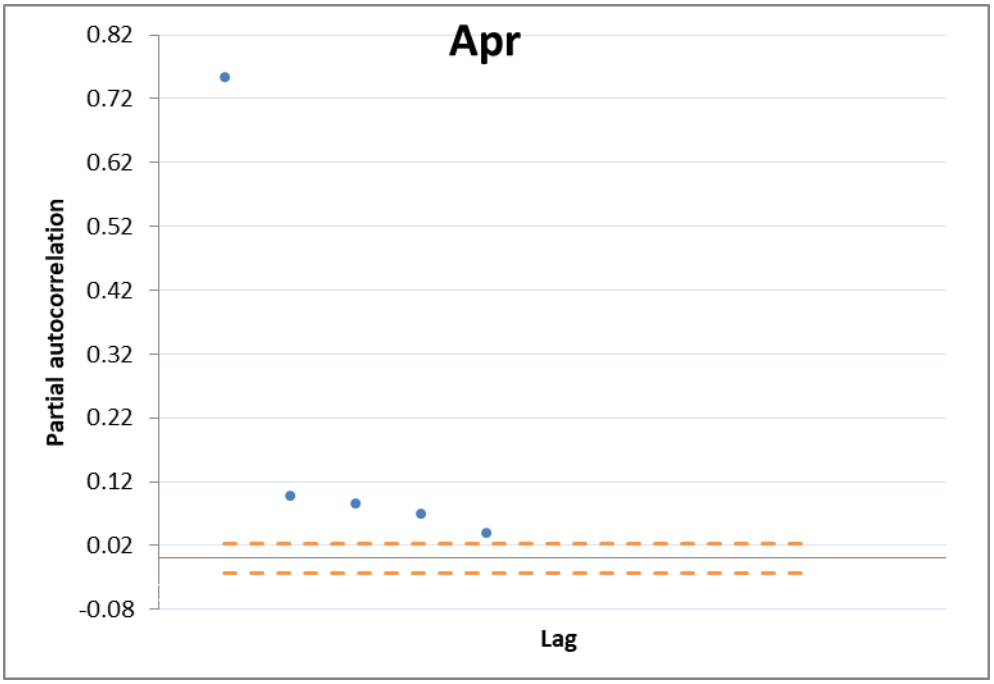

Source: Author

Figure 70 – Confidence interval graph for May

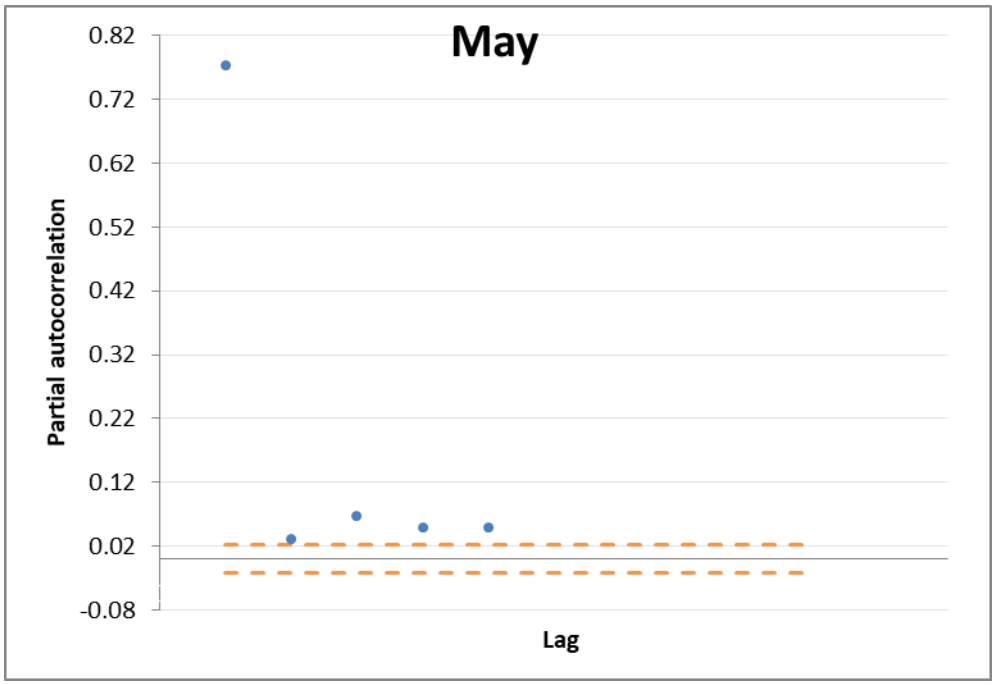

Source: Author

Figure 71 – Confidence interval graph for June

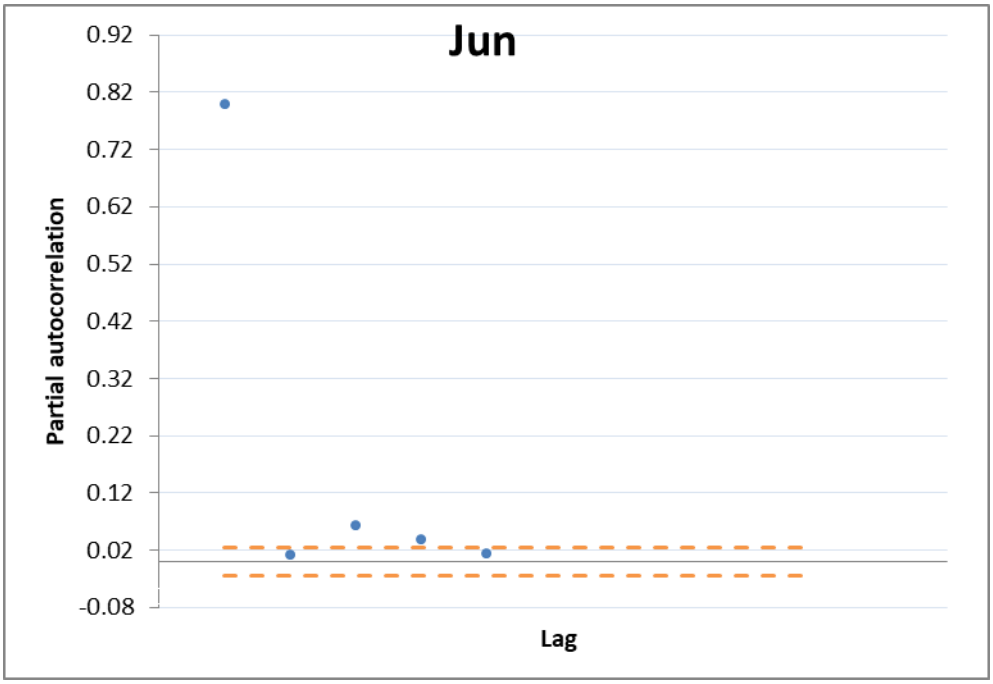

Source: Author

Figure 72 – Confidence interval graph for July

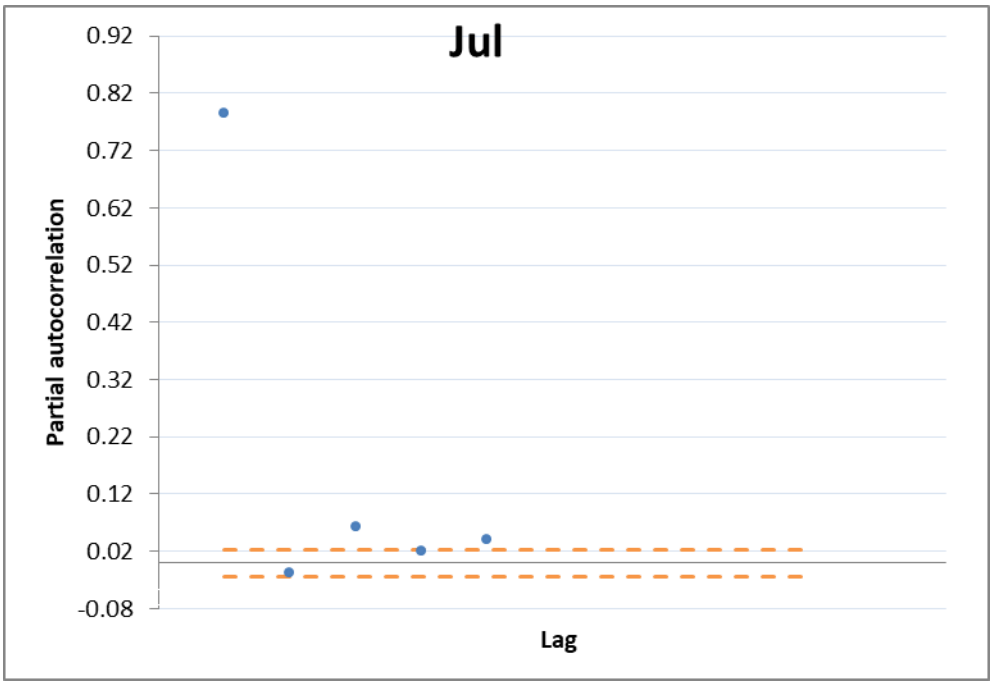

Source: Author

Figure 73 – Confidence interval graph for August

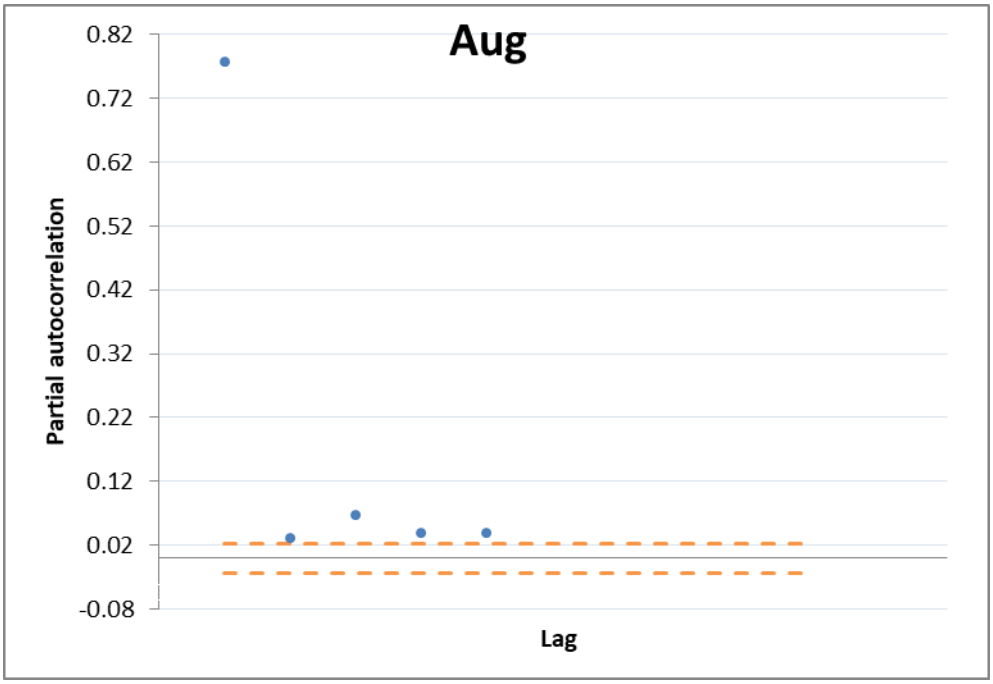

Source: Author

Figure 74 – Confidence interval graph for September

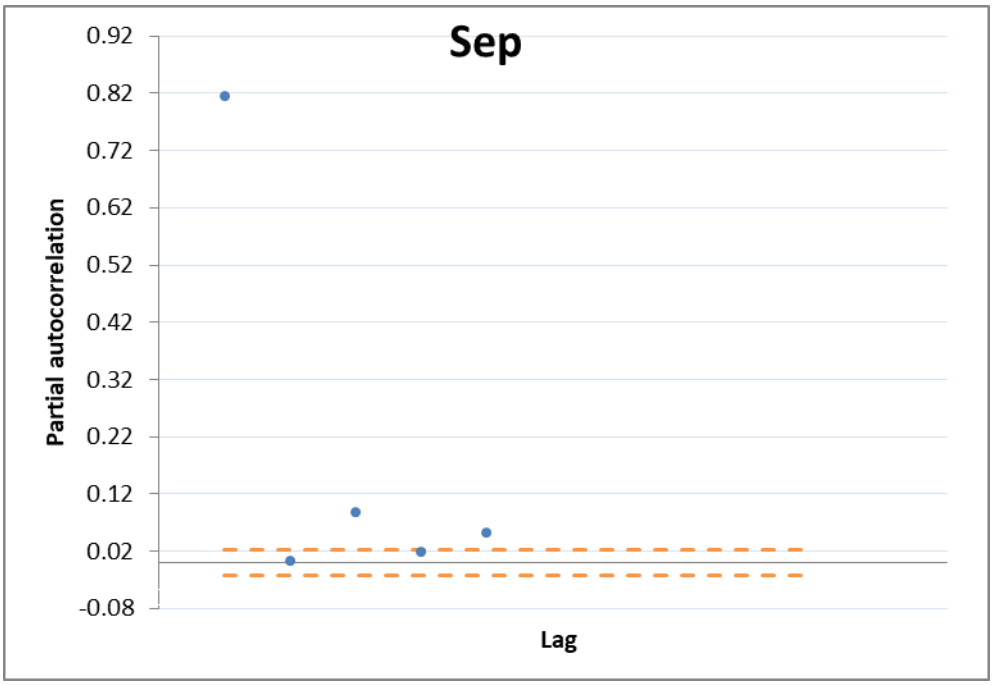

Source: Author

Figure 75 – Confidence interval graph for October

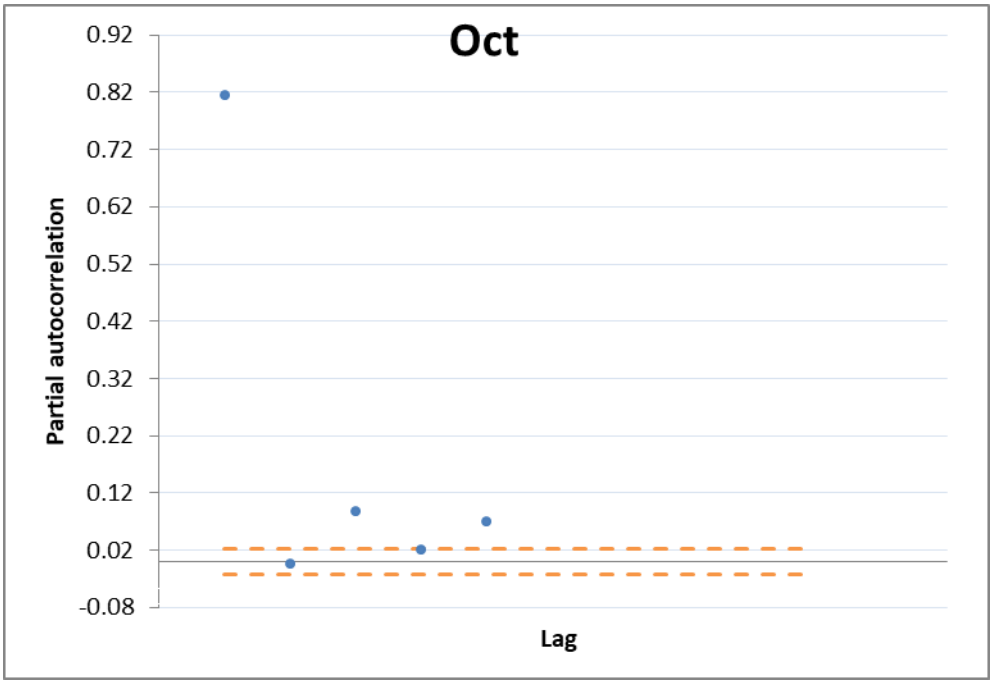

Source: Author

Figure 76 – Confidence interval graph for November

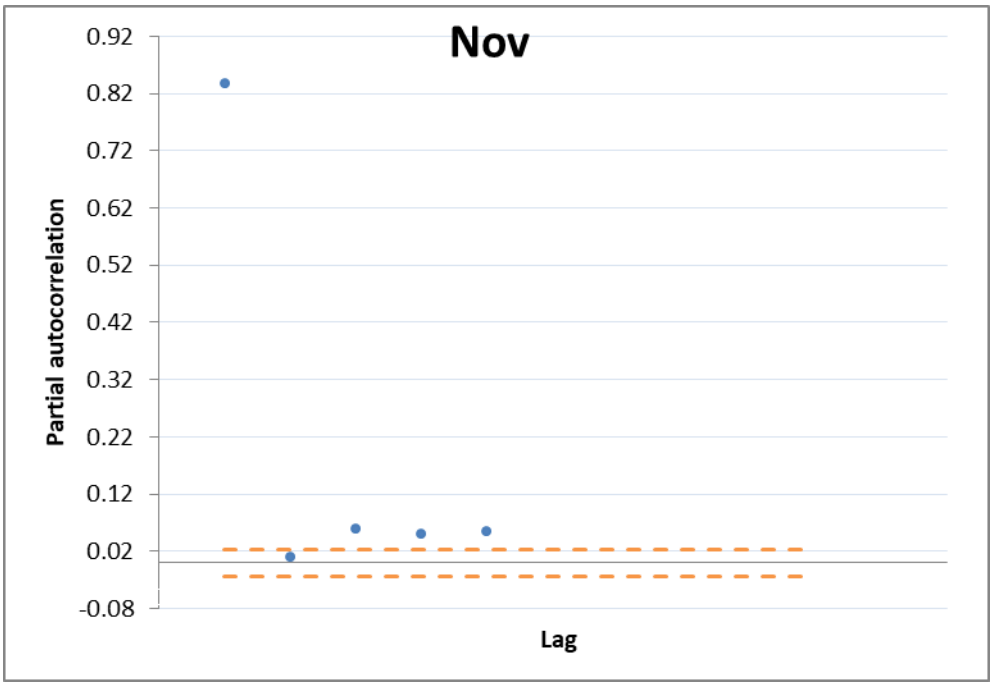

Source: Author

Figure 77 – Confidence interval graph for December

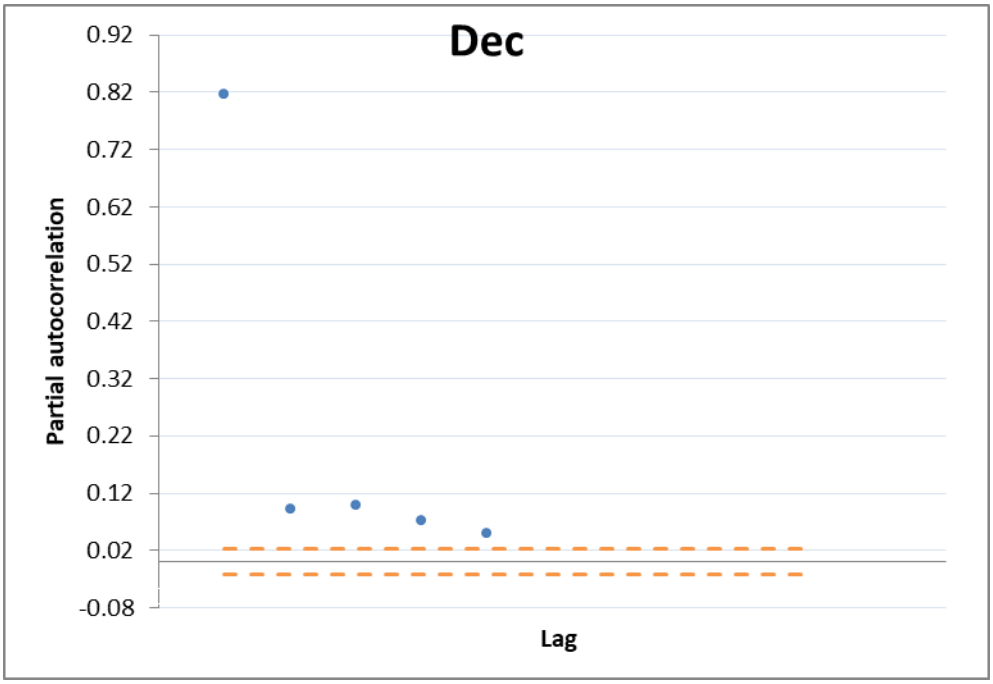

Source: Author